Advanced Control of Upper-Limb Prostheses with

Time-Synchronized Distributed Wireless Electrodes

by

Jianan Li

A Thesis

Submitted to the Faculty

of the

WORCESTER POLYTECHNIC INSTITUTE

in partial fulfillment of the requirements for the

Degree of Doctor of Philosophy

in

Electrical and Computer Engineering

Dec 2022

APPROVED:

Professor Edward A. Clancy, Major Advisor, WPI ECE

Professor Xinming Huang, Committee Member, WPI ECE

Todd Farrell, Ph.D., Committee Member, Liberating Technologies, Inc., Holliston, MA

Abstract

The human hand is the most powerful tool for human beings to sense and manipulate the world about them. The loss of one or both hands significantly impairs these abilities. Upper-limb prostheses help reproduce absent hand function. The electromyogram (EMG) generated by remnant muscle tissue is used as the control source in myoelectric prostheses. This thesis first describes a method for rapid calibration of hand-wrist EMG-force, as a basis for myoelectric prosthesis control, with performance evaluated via virtual real-time testing. Second, aspects of a distributed wireless electrode system are described. Such a system is needed to replace socket-based wired electrodes which do not fit into evolving osseointegrated prosthetics. Rather, electrodes need instead be placed inside of a liner without a wired connection to the prosthesis.

The first part of the thesis studied a real-time rapid prosthesis calibration method based on hand-wrist EMG-force modeling, evaluated using both able-bodied and limb-absent subjects. Both 1-DoF (degree of freedom) and 2-DoF simultaneous, independent and proportional (SIP) control tasks were tested with three main control methods: conventional 2-site control ("sequential" mode switching via co-contraction) using 2 electrodes, intuitive 2-DoF SIP control (using EMG-force from muscles that typically activate the relevant DoFs), and mapping 2-DoF SIP control (using EMG-force from muscles that typically do *not* activate the relevant DoFs). The number of electrodes (6 or 12) was also tested for the 2-DoF SIP controllers. Performance on dynamic virtual target tracking tasks in 2-DoFs and a fixed virtual target stability task were evaluated. For all subjects, both 2-DoF SIP controllers with 6 optimally-sited electrodes had statistically better target matching performance than sequential control in number of matches (average of 4–7 vs. 2 matches, $p < 0.001$) and throughput (average of 0.75–1.25 vs. 0.4 bits/s, $p < 0.001$), but not overshoot rate and path efficiency. There were no statistical differences between 6 and 12 optimally-sited electrodes for both 2-DoF SIP controllers.

The second part of the thesis investigated two aspects of wireless electrodes: power consumption when transmitting using a Bluetooth Low Energy (BLE) microcontroller and clock synchronization methods in distributed BLE systems. Using a Texas Instruments (TI) BLE microcontroller, power consumption was measured in different condition combinations. Results found that with the built-in ADC (which consumed 0.8–0.9 mA), total power consumption ranged from 0.9–3.0 mA, which satisfies the requirements of daily usage when powered by a coin cell battery. We additionally developed a low latency, BLE-based time synchronization algorithm and data alignment method. The method was implemented on

two BLE platforms (TI, Nordic) to demonstrate the portability of the algorithm. We found time synchronization errors between two independent peripheral nodes of, on average, 69 ± 71 μs with 0.56 ms 90th percentile error for a TI platform and 477 ± 490 μs with 1.21 ms 90th percentile error for a Nordic platform. Total end-to-end latency was less than three connection intervals (i.e., <30 ms for Nordic, <45 ms for TI).

Acknowledgement

First and most, I am greatly thankful to my academic advisor, Dr. Edward A. Clancy. He not only guided me through my academic years at WPI, but also provides life experiences guidance and support for my life. I am honored to be a PhD student of the teacher like him.

Thanks to my committee members, Dr. Xinming Huang and Dr. Todd Farrell. Dr. Xinming Huang provides a lot of guidance on wireless area which is new to me. Dr. Todd Farrell gives a lot of advice and feedback on prosthesis related project which helps a lot for me.

Thanks for the whole LTI team for the technical support when we switch the testing platform. Without their help, the project would not proceed as expected.

Thanks to my senior alumnus Ziling Zhu. He helped me get familiar with research area and worked together to go through all the difficulties. Thanks to my senior alumnus Berj Bardizbanian. The previous project he did is the foundation of my work.

Thanks to my beloved parents Mei Xie and Jianke Li. The most important persons for me, love and support me with all their hearts. Thanks for my grandparents Congyi Xie and Guiying Sun. They love me unconditionally.

Thanks to all the partners in the lab: He Wang, Haopeng Wang, William J. Boyd and Kiriaki J. Rajotte who gave me a lot of help on my research.

Contents

Chapter 1: Introduction

This introduction includes two main parts: background and a description of the contributions of my Ph.D. work. The background part initially describes the history of upper limb prostheses and the biomedical knowledge of EMG and related signal processing techniques for myoelectric prosthesis control. The background then describes the history of wireless communications and related time-synchronization algorithms for distributed wireless electrode development. The contribution part describes the current research field and my related contributions presented in the remaining thesis chapters.

1.1 History of Upper Limb Prostheses

A prosthesis is an artificial device that substitutes for a missing part of the body. Upper limb amputations are defined by limb absence at anatomical levels at or distal to the forequarter. An upper limb prosthesis helps to mitigate the effects of impairments due to absent limbs.

1.1.1 Causes of Limb Absence

There are about 57.7 million people living with limb amputations worldwide (Ziegler-Graham, MacKenzie et al. 2008). There are an estimated 1.6 million individuals who experienced limb loss, of which 41,000 people experienced upper limb loss at levels at or above the wrist in 2005 in the United States (Ziegler-Graham, MacKenzie et al. 2008, Limb Loss Task Force/Amputee Coalition 2012). Traumatic amputations comprise 68.6% of upper limb amputations (McDonald, Westcott-McCoy et al. 2020). During a 5-year national trauma databank analysis from 2000 to 2004, 8910 amputations were performed. Of these amputations, 6155 (69.1%) involved a finger and 782 (8.7%) were upper extremity (Barmparas, Inaba et al. 2010).

The most common reason for upper limb amputation is trauma. Other reasons included cancer and infection. Also about 1 in 1900 babies are congenital absence for either upper or lower limb defects. In 2005, an estimated 500,000 people were affected by amputation of the hand or fingers (Dillingham, Pezzin et al. 2002, Burger and Vidmar 2016). Compared to the lower limb, which is responsible for locomotion (walking, running, climbing), the upper limb completes sophisticated and complex tasks. Multiple degrees of freedom (DoF) tasks are conducted through the combination of fingers, hand, wrist, elbow and shoulder movement. Also, the large proportion of the brain related to upper limb movement and sensing indicates the sophistication of hand and finger motions (Schieber 2001). Upper limb loss can reduce quality of life (Ahmadizadeh, Merhi et al. 2017).

1.1.2 Upper Limb Prosthesis Categories

  A.   Passive prosthesis

  The earliest record of a prosthetic hand is from 77 AD (Zuo and Olson 2014). The Roman scholar Pliny the Elder recorded in his encyclopedia Naturalis Historia. Most passive prostheses allow no movement at any of the joints and are light weight with a fixed pose. Simple tasks can be achieved such as holding items, stabilizing objects, and carrying items. The most famous ancient prosthetic hand was the iron hand of Götz von Berlichingen known as *Götz of the Iron Hand.* He lost his right arm at the wrist during the war of the
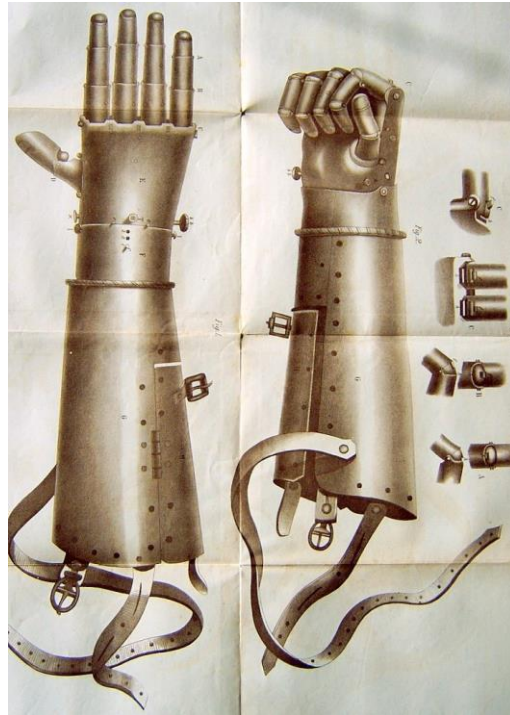
Figure 1.1 The second Götz of the Iron Hand. (Image from en.wikipedia.org/wiki/Götz_von_Berlichingen)

Succession of Landshut and the local blacksmith built a prosthetic hand with the mechanism changing the position of the finger, wrist and even thumb interphalangeal joint. His prosthetic hand gave him the ability to hold a shield or reins, or even to write.

  B.   Body-powered prosthesis

  A body-powered prosthesis moved by the individual's remaining body was first pointed out by German dentist Peter Baliff in 1818 (Meier 2004). He introduced a device using leather straps that interacted with the shoulder area and attached to the residual limb. Due to World War I, the number of upper limb amputees increased. To serve the need for amputee rehabilitation, the Association of Limb Manufacturers of America (now the American Orthotic & Prosthetic Association) was founded in 1917. World War II resulted

in 3475 U.S. upper limb amputees, as antibiotics saved their lives(Petri and Aguila 2002). This huge demand for artificial upper limbs led to the advancement of the body-powered prosthesis. The most common body-powered type was a harness with a strap that lies over the scapula connected to a cable that operates a hook-like prosthetic terminal device. In 1948, the Bowden cable body-powered prosthesis was introduced (Figure 1.2) (O'Keeffe, 2011). Most of today's body-powered prostheses are variants of the cable body-powered
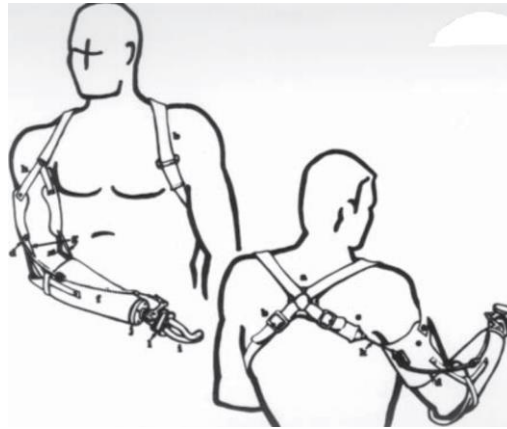
Figure 1.2 Bowden cable Body-powered prosthesis.
Figure from (O'Keeffe 2011).

design. The most important improvement from prior systems using cables or harnesses to control the limb was that users could operate both hands simultaneously and finish more complex tasks.

C.   Myoelectric prosthesis

A myoelectric prosthesis is an externally powered artificial limb that is controlled by the electrical signals generated by remnant muscles. The primary differences between body-powered prostheses and myoelectric prostheses are power methods and control methods. In 1948, Munich University physics student Reinhold Reiter first created a myoelectric prosthesis using amplified surface EMG to control the prosthesis(Reiter 1948). Modern myoelectric prostheses use two-site EMG signal control, using two antagonist muscle contractions to control prosthesis hand open and close. More advanced proportional control can be achieved by using EMG to control the speed of prosthesis movement. Silicone sleeves are often used to secure EMG electrodes to the residual limb.

A myoelectric prosthesis provides several advantages, such as comfortable attachment, non-invasive signal detection and no unsightly cables. Some drawbacks still exist, including robustness, high cost, the latency between muscle activation and prosthesis movement, difficulty in securing electrodes to the skin,

difficulty controlling multiple DoF motions (e.g., combined hand and wrist motions), and no feedback of the control motions forcing users to rely highly on visual feedback.

1.2 EMG and Related Signal Processing Techniques

1.2.1 EMG Background

EMG (electromyogram) is the electrical signal generated by muscles. When muscle cells activate and contract, an electric potential is generated. This electrical potential can be recorded and used to detect motions or for medical uses.

Skeletal muscle comprises 30 to 40% of total body mass. Other muscle types include cardiac muscle and smooth muscle. Skeletal muscle fundamentally allows a human to perform movements and to function(Robertson, Caldwell et al. 2013). Fig. 1.3 shows the structure of skeletal muscle and connective tissues. Tendons attach the skeletal muscle tissue to bone throughout the body. The epimysium is the outermost layer of tissue surrounding the entire muscle. The perimysium is the middle layer surrounding bundles of muscle fibers. A fascicle is a bundle of muscle fibers. In between the fascicles, there are blood vessels, sensory tissues, and connective tissues which support muscle movement. The endomysium is the innermost layer surrounding individual muscle fibers. The smallest unit of skeletal muscle is the muscle fiber, of which there are two types: Type I (slow twitch) fiber and Type II (fast twitch) fiber. Type I fibers can sustain low forceful contraction and avoid fatigue for long periods (Linssen, Stegeman et al. 1991). Type II

Fig. 1.3 Structure of a skeletal muscle from https://en.wikipedia.org/wiki/Muscle_fascicle

fibers can generate more powerful and fast contraction but are fast to fatigue. All fibers are innervated by a

motor neuron which controls the timing of its respective fiber's contraction. Motor neurons are a specialized type of cell which originate in the spinal cord and brain. There are two types of motor neurons, upper motor neurons originating from the brain and connecting with lower motor neurons, and lower motor neurons which originate from the spinal cord and directly connect with muscle fibers. When the brain sends a motor command, an electrical signal will transmit through the motor neurons and cause an electro-chemical activation of the muscle fibers. Then, the fibers depolarize leading to muscle contraction. Muscle depolarization and repolarization are membrane potential changes that create an electromagnetic field. This field can be recorded as the EMG signal. Surface EMG and indwelling EMG are EMG recording methods. Indwelling EMG can record an individual motor unit's activity, but requires electrical needles (or wires) to penetrate the skin and be placed near the muscle. Surface EMG records the signal on the skin surface, which is non-invasive.
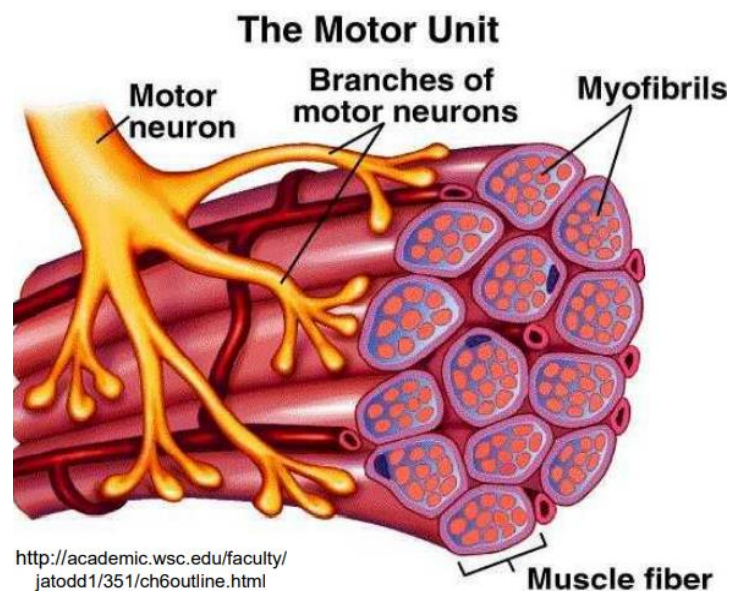
Fig. 1.4 Motor Unit

1.2.2 Surface EMG Recording

The basic functional unit for EMG recording is the motor unit, which is defined as one motor neuron and all surrounding muscle fibers that it innervates. Each motor neuron only contains one type of the muscle fiber. Each single motor unit's muscle fibers contract in unison. Fig 1.5 shows an individual motor unit's depolarization and repolarization voltage, as measured with respect to the extracellular space. The resting potential for the motor unit is about -70 mV, which is due to the cellular concentration of ions inside and
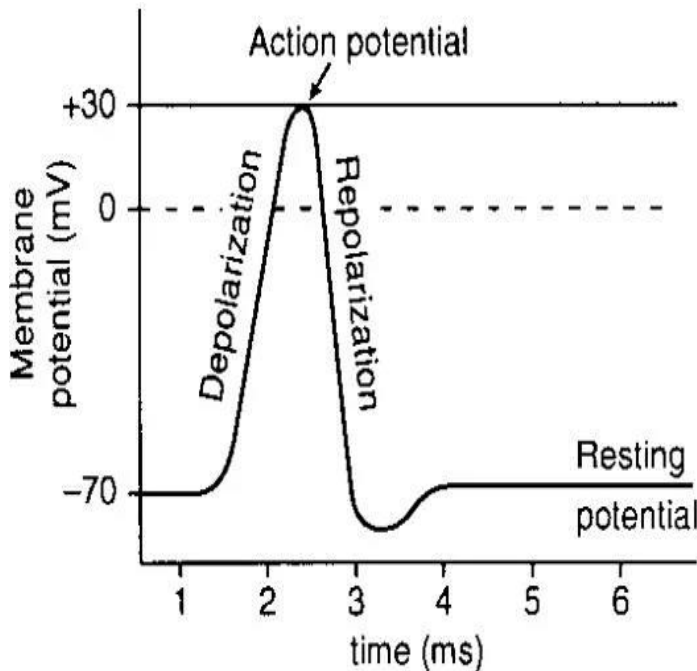
Fig. 1.5 Motor Unit's depolarization and repolarization from https://www.physicsforums.com/threads/action-potential-of-a-skeletal-muscle-fibre-where-is-calcium.473984/

Fig 1.6 From motor unit's potentials to surface EMG .Figure from (Konrad 2005)

outside of the cell. When the muscle fiber is activated, the action potential reaches +30 mV, followed by repolarization back to the resting potential. Each action potential lasts 2–4 ms. During slowly-varying increasing force contractions, most motor units have initial firing rates of 5–10 pulses/sec and increase to 20 pulses/sec or even 60 pulses/sec as contraction increases. Different motor units fire at random times and different rates. Increases in muscle tension are the result of increases in firing rate and/or the number of active motor units (recruitment). The summation of all the motor unit's potentials is the recorded surface EMG (Fig 1.6). Most surface EMG is recorded from a large area of the skin surface which combines multiple motor units' potentials, thus the combination signals looks like an amplitude-modulated random signal.

1.2.3 Surface EMG Signal Processing

For surface EMG, the most common signal processing method is EMG amplitude estimation, i.e., estimation of the signal's time-varying standard deviation (EMGσ). As the surface EMG signal is the combination of multiple individual motor units randomly firing at different times and rates, the sum of all
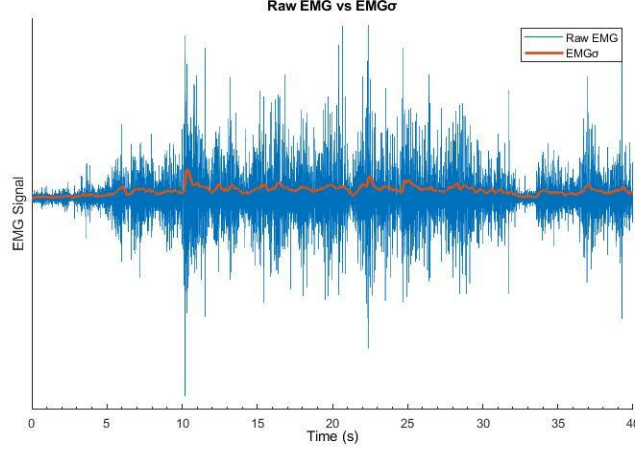
Fig. 1.7 Raw EMG and pre-processed EMGσ at 1000Hz sampling rate.

these potentials can be modeled as an amplitude modulated, zero-mean, random signal(Clancy 1991). Common surface EMG signal processing stages include: highpass filtering to remove DC offsets and motion artifacts, 50/60 Hz notch filtering to remove powerline noise, lowpass filtering to remove noise in the higher frequencies, and then taking the moving average root mean square (RMS) or moving average mean absolute value (MAV). For constant-force, non-fatiguing contractions, the noise-free surface EMG signal can be modeled as Gaussian distributed. Thus, the surface EMG signal m[n] can be written as (Parker, Stuller et al. 1977, Hogan and Mann 1980, Clancy and Hogan 1994):

$$m[n] = s \cdot x[n] + v[n], 0 \leq n \leq N$$

where n is the discrete-time sample index, s is EMGσ, $s \cdot x[n]$ is the noise-free EMG where $x[n]$ is zero mean, unit-variance, wide-sense stationary and correlation-ergodic, and $v[n]$ is the additive noise with variance of q^2. As we assume the samples are independent, the probability density function (PDF) of a vector formed from N consecutive values of m is (Clancy 1991, Clancy 2019, Wang, Rajotte et al. 2019):

$$p_{m|s}(M|s) = \frac{1}{(2\pi(s^2 + q^2))^{N/2}} e^{\frac{-\sum_{n=0}^{N-1} M^2[n]}{2(s^2 + q^2)}}, -\infty \leq M_n \leq \infty$$

Thus, the optimal maximum likelihood, real-valued solution for $\hat{s}$ is (Clancy 2019, Wang, Rajotte et al. 2021):

$$\hat{s}[n] = \left[(\frac{1}{N}\sum_{i=0}^{N-1} M^2[N-i]) - q^2\right]^{1/2}$$

Several assumptions/limitations are used in the above estimate. Sample independence is not true for real EMG signals, but can be approximated via signal whitening. And, real time EMG signals are never strictly constant force. More advanced processing methods can be used to solve related problems for different distribution estimates and for non-constant EMG signals.

Other EMG features such as waveform length, zero crossing rate and slope sign change rate also show good performance in EMG-force models (Hasson, Williams et al. 1989, Dai, Bardizbanian et al. 2016). The waveform length feature is the sum of the absolute difference between two adjacent samples, which can be written as: $\Delta m[n] = |m[n+1] - m[n]|$. The zero crossing rate feature counts the rate at which the signal crosses zero. The slope sign change rate feature indicates the rate of local peaks of the EMG signal.

1.2.4 EMG-force Modeling

Surface EMG signals can be used to estimate related limb activation, for example from amputees. For most upper limb amputations, forearm tissue remains, with remnant nerves and muscles still functioning. Using EMG from the remnant tissue to estimate hand-wrist activations for prosthesis control can improve daily activity functions. A general polynomial nonlinear EMG-force model can be written as(Press, Flannery et al. 1994, Bardizbanian, Keating et al. 2020):

$$F[n] = \sum_{d=1}^{D}\sum_{q=0}^{Q}\sum_{e=1}^{E} c_{q.d} EMG\sigma_e^d[n-q], \qquad q \le n \le N$$

where F is the estimated force, n is the sample index, D is the polynomial nonlinear order, Q is the number of time lags, $EMG\sigma$ is the processed EMG, and subject-specific coefficients $c_{q.d}$ are calculated by a least-squares fit procedure.

1.2.5 Osseointegration and Targeted Motor and Sensory Reinnervation

Recently, osseointegration technology (Branemark 1983, Albrektsson and Johansson 2001, Mavrogenis, Dimitriou et al. 2009, Parithimarkalaignan and Padmanabhan 2013) to directly attach a titanium rod into living bones, to serve as a prosthesis mount, has been introduced (Fig 1.8). It eliminates the use of sockets that historically were used to attach the prosthesis, and can provide increased stability and comfort for amputees. In addition, even when using a socket, patients enjoy the use of liners for comfort and suspension. However, securing wired electrodes through a liner presents a challenge. Another technology used in prosthesis control is targeted motor reinnervation (TMR), which reroutes motor nerves to target muscles, such as the pectoralis muscles of the chest. This technique gives amputees an ability to use the newly

controlled pectoralis EMG signals to control the prosthesis. Targeted sensory reinnervation technology is reattaching sensory nerves to main peripheral nerve trunks, giving a new way to provide feedback and generate a closed loop between the amputee and the prosthesis (Jonsson, Caine-Winterberger et al. 2011).
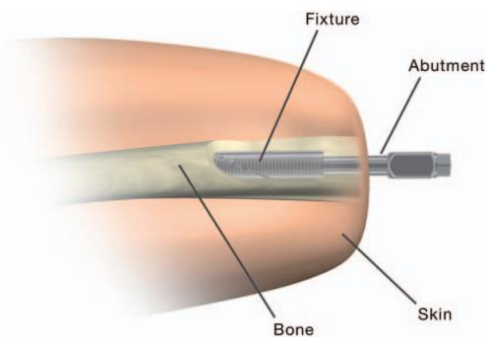
Fig 1.8 Implant system for prosthesis osteointegration (Jonsson, Caine-Winterberger et al. 2011)

These techniques are expensive and not currently covered by insurance, limiting their worldwide usage. Even with the latest implant technology. The most common control methods is still using surface EMG. But, without a socket to support the prosthesis, there is no place to mount electrodes. Thus, the second part of this thesis develops wireless electrodes for the general purpose of acquiring biosignals at distinct locations which could take both advantage of osteointegration and surface EMG technology.

1.3 Wireless Techniques History and Applications

1.3.1 History of Wireless Communications

Wireless communication is defined as an information transfer method between two or more points that does not use an electrical conductor as a medium for the transfer. There are several wireless technologies such as sonic, optical, and radio waves. The sonic method is the most used wireless communication method where most creatures developed the ability to generate and hear the specific frequency sound for communication purposes. Smoke signals are one of the oldest forms of long-distance optical communication; the smoke color and interval could transmit different information. In 1880, the first modern wireless photophone was invented by Alexander Graham Bell and Charles Summer Tainter using a beam of light to transmit audio. The radio communication method carries information by modulating properties of electromagnetic waves transmitted through space. In 1888, Heinrich Hertz proved the existence of radio waves. Guglielmo Marconi developed a wireless telegraph system in 1894 and was awarded the 1909 Nobel Prize in Physics. Invention of the cellular telephone in 1973 led to the rapid development and revolution of wireless technology. In 1997, local area network technical standard IEEE 802.11 (WIFI) was established for

wireless local area network computer communication. In the next year (1998), IEEE 802.15.1 (Bluetooth) was standardized by IEEE.

1.3.2 Internet of Things and Wearable Sensor-based Wireless System

Nowadays, developing wireless sensing technologies have drawn a lot of attention from both research and industry. Additionally, people also care more about their own health condition, which has led to the latest wireless mobile health monitoring research area: body sensor networks (BSNs) (Gravina, Allinia et al. 2017). A BSN is a miniaturized network based on Internet of Things technology and sensor technology, using various physiological parameters of the human body as the data source and wireless data communication within the range of the human body as the carrier. A body sensor network can be used to manage chronic diseases, monitor special populations such as elderly people living alone, and provide fast and real-time health guidance in community hospitals. Multiple wireless protocols are used in BSN research, such as WIFI, Bluetooth, BLE, ZigBee, NFC (near-field communication) and RFID (Cao, Leung et al. 2009). But, for wearable sensor networks, the protocol used should not only satisfy flexibility, and provide seamless and easy communication; but also be low powered (Pantelopoulos and Bourbakis 2010). Within all these protocols, BLE (Bluetooth low energy) (Omre and Keeping 2010) satisfies both high transmitting rate and low power. Also, BLE can use a single central device to communicate with multiple peripheral nodes with low latency which can benefit distributed wireless biosensor systems.

1.3.3 History of Bluetooth Technology

Bluetooth (Marquess 2010) is an open specification for short-range wireless voice and data communications that was originally developed for short distance cable replacement. It uses the 2.402 GHz to 2.480 GHz frequency band in personal area networking and operates all over the world. Recently IEEE no longer maintains the standard and Bluetooth SIG (Special Interest Group) oversees development of the specification, including BLE (which has lower power consumption and higher transmitting rate).

BLE is derived from the Bluetooth standard and mainly focused on lower power consumption for its first version (BLE 4.0). BLE decreased the average power from 1 W to 0.01–0.5 W by reducing the number of channels to 40 2-MHz wide channels instead of the 79 1-MHz wide channels used with classic Bluetooth technology, depending on the use case. And, compared to the standard Bluetooth latency of 100 ms, BLE has a latency of 6 ms latency from a non-connection state.

However, there are some limitations to BLE 4.0(Šolić, Leoni et al. 2020). The most important one is the data packet size. In wireless transmission, all data are assembled into a packet first and then transmitted at the next connection event. For BLE 4.0, the maximum data packet size is limited to 27 bytes. Then, BLE 4.2 (Marquess 2014) increased the data packet size limitation to 251 bytes per packet, which makes higher data

rate transmitting possible. And, the latest BLE 5.0 (Marquess 2016) improves the physical layer transmitting rate from 1 Mbps to 2 Mpbs, which reduces each full 251 byte packet transmit time from 2.12 ms to 1.06 ms.

1.3.4 BLE Architecture

BLE devices can be classified into two types: single-mode and dual-mode devices. Single-mode devices can only communicate with BLE devices, where dual-mode devices can support BLE and classic Bluetooth. BLE is designed in a modular fashion. The protocol stack is separated into three main blocks, Application, Host and Controller. The Application layer differs between BLE devices and user cases. The Host and Controller structures are illustrated in Fig. 1.9. The Host includes 5 main parts: Generic Access Profile (GAP), Generic Attribute Profile (GATT), Attribute Protocol (ATT), Security Manager (SM) and the Logical Link Control and Adaptation Protocol (L2CAP). The Controller includes 2 parts: Physical Layer (PHY) and the Link Layer (LL). Communication between the Host and Controller is handled by the Host-Controller Interface (HCI).
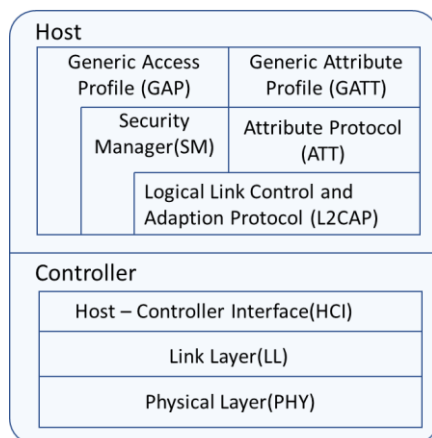
Fig. 1.9 BLE Protocol Stack.

Physical Layer (PHY): The Physical layer is the lowest layer of the protocol stack; it determines the data value and how data bits transmit over the air. BLE works in the 2.4 GHz ISM frequency band divided into 40 channels, where each channel is 2 MHz wide (Fig. 1.10). Three channels (37, 38, 39) are used for advertising and the other channels are used for data transmitting. Adaptive frequency hopping (AFH) algorithms are used for channel hopping to minimize the interference from other devices within the same band. Gaussian frequency shift keying is used for frequency modulation. BLE 4.2 and earlier versions provide a raw data rate of 1 Mbps uncoded modulation where BLE 5.0 introduced 2 Mbps, which uses less time for transmit and receive. The 2 Mbps PHY uses less energy, but the transmit range is only 80% of the 1 Mbps PHY (Marquess 2016). To achieve a larger transmit range, Coded PHY was also introduced in BLE 5.0. Using the core 1 Mbps transmit speed with two possible error correction coding schemes yields raw data

rates of 500 kbps and 125 kbps, gaining up to double and quadruple range, respectively, compared to the default 1 Mbps PHY.
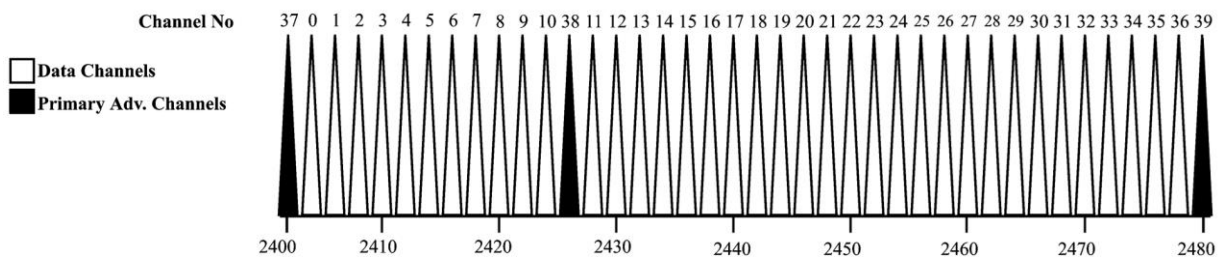
Fig. 1.10 BLE Channel division.

Link Layer (LL):   The Link layer defines the basic BLE state machine, transitions, packet format and connection management. Link layer also controls encrypted data encoding and decoding for Coded PHY. The BLE state machine defines 5 different states: **Standby** is the LL initial state until instructions are given by the Host layer. The **Advertising** state can only be entered from Standby state and it will start transmitting advertising packets and listen for the response packet. **Scanning:** a device in scanning mode will listen to the advertise packet. This state can only be entered from standby state. **Initiating:** once the scanning state receives an advertiser requesting a connection packet, it will enter initiating state and move to connect state. Or, it returns to standby state if it fails to receive a packet. **Connection:** this is the state established when two devices are connected. The device enters connection state from initiating state named as Central (Master). The device enters connection state from advertising state named as Peripheral (Slave).

Host-Controller Interface (HCI):   HCI manages communication between Host and Controller. Four different transport layers are used between Host and Controller: UART, three-wire UART, USB, and Secure digital. Different layers can be chosen based on different application scenarios. Separation of Host and Controller most benefits software development (Richards 2015).

Logical Link Control and Adaption Protocol (L2CAP):   L2CAP is defined by the standard Bluetooth protocol. The main roles of L2CAP are responses for quality of service, routing, segmentation, fragmentation and reassembly of packets for higher level protocols. The Maximum Transmission Unit (MTU) is defined in the L2CAP layer. MTU defines the maximum data packet size that it can receive. Any packet larger than MTU will send back a reject message. The minimum MTU is 23 bytes.

Security Manager (SM):   SM not only encrypts and decrypts data packets, but also handles device pairing and authentication.

Attribute Protocol (ATT):   BLE devices use a server-client architecture to control data transmission. The server needs to define and send the attributes to the client. Each attribute can be set to either notify or indicate

mode. The client can discover, read and write attributes. Each attribute includes three properties: attribute type, attribute handle, and attribute permission. The attribute type is a universally unique 128-bit identifier. The attribute handle references the specific attribute. The permission defines if it can be read and/or write.

Generic Attribute Profile (GATT):   GATT define the types of attributes and how they can be used. GATT contains several Services, and each Service contains one or more related Characteristics. Characteristics are defined using attributes, which is the table of the services, characteristics, and descriptors.

Generic Access Profile (GAP):   GAP is the highest layer of the Host; it directly interacts with the application layer. GAP defines the procedures related to transport profiles during communication. Also, GAP controls the transmit-receive state of the device as one of five states: Standby, Advertising, Scanning, Initiating and Connected. Fig. 1.11 shows the relations of all five states. For each BLE device, its GAP layer must run in one of four roles: Broadcaster (the device is an advertiser that is non connectable), Observer (the device scans for advertisements but cannot initiate connections), Peripheral (the device is an advertiser that is connectable and operates as slave in a single link-layer connection), or Central (the device scans for advertisements, initiates connections and operates as a master in single or multiple link-layer connections).
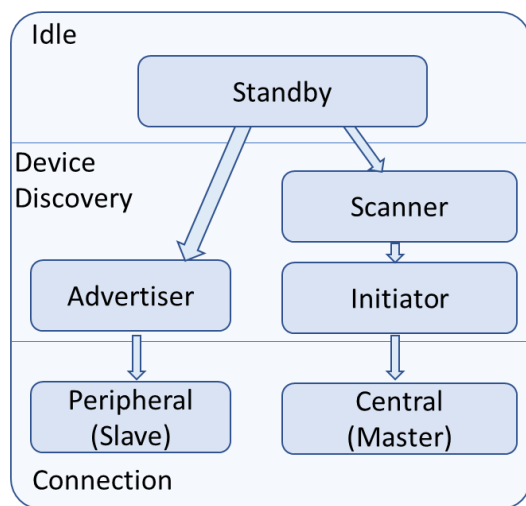
Fig. 1.11 BLE Generic Access Profile (GAP) State.

1.3.5 BLE Data Transmitting

The basic BLE data transmitting block is called a packet. Each packet includes 4 parts: Preamble (a fixed sequence of alternating 0 and 1 bits used for frequency synchronization, symbol timing estimation, and automatic gain control training, containing 8 bits for 1 Mbps PHY and 16 bits for 2 Mbps PHY), access address (32 bit correlation code used to avoid sending packets to unrelated BLE devices on the same RF

channel), protocol data unit (PDU is a 2 to 257 byte data packet or advertising packet), and cyclic redundancy check (a 24 bit checksum for bit-error checking during packet transmission).

The PDU packet can be separated into two types: advertising packet and data channel packet. The advertising packet contains a 2 byte header and 255 bytes of payload. The data channel packet contains a 2 byte header, 251 bytes of payload and a 4 byte MIC (message integrity check).

Two different data transmit modes are used in BLE: connected mode and connectionless mode. The connectionless mode (broadcasting or advertising) can transmit data to more than one peer at the same time. However, the payload is limited to 31 bytes and a connection interval larger than 100 ms is preferred. Therefore, the throughput for connectionless mode is limited to <500 bytes per second. Even after BLE 5.0 introduced extended advertisements which can send out up to 255 bytes following the 31 bytes, the total throughput is still limited to <3000 bytes per second (Pantelopoulos and Bourbakis 2010). Also, connectionless mode cannot exchange data packets from the receiver side to devices using broadcasting or advertising. Connected mode is based on establishing a dedicated connection between devices to exchange data packets periodically. It still follows the advertising, scan, and reply connection request packet procedures. Once the connection is established, the peripheral device stops advertising and becomes the slave, and the central device becomes the master. A connection event interval is used between master and slave to control how often data packets are exchanged. The connection event interval is an integer multiple of 1.25 ms with the range of 7.5 ms to 4 seconds.

1.3.6 Time Synchronization Issues in Wireless Systems

Within BSN (body sensor network) research, time synchronization is a vital feature for some high precision multi-channel body sensors such as ECG, EMG and EEG(Brunelli, Farella et al. 2016). These applications typically need multiple channels for data analysis. However, the standard time synchronization only using the most recent received central clock used in BLE systems via connect mode is not precise enough for high sampling rates used in these applications (Asgarian and Najafi 2017). Hence, our interest in time synchronization methods within BLE. Since improved BLE wireless protocols are being issued nearly every year, it is not wise to modify the standard BLE protocol layer. Instead, an application layer time synchronization method is needed that satisfies both the ability to synchronize multiple sensors with high precision and easily migrate in-between different versions of the wireless protocols.

In wired (centralized) systems, all the peripherals have access to the microcontroller's common clock or can easily receive precise timestamps to achieve time synchronization. However, in wireless (distributed) systems, there is no accessible global clock—each node has its own clock. And, conditions such as different temperatures, clock drift, and oscillator error (Sundararaman, Buy et al. 2005, Tirado-Andres and Araujo

2019) contribute to synchronization error. Even if the devices could be precisely synchronized at power-up, they would not remain synchronized over time. Thus, a method is needed to synchronize time between the various wireless devices, and then use that time synchronization to align multiplexed data at the central node.

1.4 Current State of My Research Field and My Contribution

This section describes the main research works I completed during my Ph.D. study. The first part followed the outline of the PsiCon (proportional, simultaneous and independent control) project supported by the U.S. Eunice Kennedy Shriver National Institute of Child Health & Human Development. The project had 4 phases, and I was the lead student researcher on phase C. Phase C focused on real-time virtual prosthesis control with rapid calibration. The second part followed the outline of the Asterisk project supported by the US Army Medical Research and Materiel Command. The project had 2 phases, and I was the lead student researcher on both phases. The first phase focused on using wireless electrodes to replace current wired electrodes and testing the different wireless protocols. The second phase implemented a distributed wireless electrode system and solved related time synchronization problems. Both of these phases were completed in collaboration with Liberating Technologies, Inc. (Holliston, MA)

1.4.1 Real-time Virtual Prostheses Control

Current research field: There are millions of limb amputations worldwide. The human hand is the most sophisticated and powerful tool for humans to sense and interact with the environment. Thus, limb loss can reduce quality of life (Ahmadizadeh, Merhi et al. 2017). Currently, most commercial prostheses only allow users to control one movement at a time, which does not satisfy most activities of daily living such as handling a door knob (to twist and pull a door open). Typical 2-site myoelectric control requires co-contraction mode switching in order for the prosthesis to switch between distinct DoFs (e.g., between hand control and wrist control). With this approach, many complex daily tasks are difficult to perform.

To achieve more complex motion control, an advanced human-machine interface is needed which allows users to better control prosthetic devices. Two major EMG-based methods are being studied. One method is classification (a.k.a. pattern recognition). Several groups have demonstrated excellent performance higher than 95% accuracy for more than 10 classes (Englehart and Hudgins 2003, Farrell 2008, Hahne, Graimann et al. 2012, Kuiken, Miller et al. 2016, Farina, Vujaklija et al. 2017). Another frequently studied method is regression. An advantage of regression methods is their ability to achieve multiple DoF simultaneous, independent and proportional control. Other methods, including convolutional neural networks and transfer learning show the possibility of controlling multiple DoF prosthesis motions (Prahm, Schulz et al. 2019, Wang, Fang et al. 2020). However, for these simultaneous, independent and proportional control methods,

model training generally requires a force feedback (Zhu, Martinez-Luna et al. 2020) which is not available in prosthesis users. Also, the calibration contraction time increases drastically for multiple DoF control.

My contribution to this field: We experimentally tested, in virtual real time tasks, a regression based simultaneous, independent, and proportional 2-DoF hand-wrist myoelectric prosthesis controller, calibrated without force feedback and with reduced calibration time. Different numbers of electrodes (6 or 12) were tested, with the electrode sites selected from a superset of 16 electrode sites using backward stepwise selection. Two, 2-DoF control methods were considered, wrist radial-ulnar & extension-flexion (Mapping control) and hand pronation-supination & open-close (Intuitive control), and compared with the conventional 2-site sequential control method. A subject's real-time myoelectric signal controlled the cursor on the screen to reach different random-generated, two-dimensional target positions. Also, subjects were asked to hold constant 2-DoF force efforts for a period of time. The count of properly acquired targets, overshoot rate, path efficiency of target tracking, and stability when holding a constant force for each DoF pair were tested to evaluate the performance of real-time 2-DoF control.

1.4.2 Distributed Wireless Electrodes Development

Current research field: In recent years, the development of wireless technologies and low power wireless transmission protocols have paved the way for using wireless bio-sensors to continuously monitor human biosignals, benefiting both medical research and personal health care. Most biosignal applications require multiple signal channels for data analysis such as conventional two-site myoelectric prosthesis control. Currently, most wireless sensor systems either use one combined peripheral data sender hard-wired to multiple sensors or use custom wireless protocols to achieve high throughput and low latency. Combining sensors at a peripheral node does not eliminate wires locally attached across the body (thus, not really wireless) and can make it hard to site all electrodes at their desired positions due to the wires. Custom protocols make it hard to migrate from one platform to another, in particular to take advantage of ongoing electronic device improvements.

For a fully distinct wireless data acquisition system, each ADC is controlled via its local clock. Due to temperature differences, manufacturer tolerance error, or other circumstances, these local clocks run at slightly different rates and experience drift. Thus, a method is needed to synchronize time between the various wireless devices, and then use that time synchronization to align multiplexed data from the various peripheral nodes. Several groups achieved clock synchronization based on Bluetooth beacon role, but this role does not permit reception of data packets at the same time, thus interrupting the data stream. Other groups use extra hardware or modify the lower level of the BLE protocol to achieve high precision synchronization ($9\pm17\mu s$)

(Rheinlander and Wehn 2016). But, those methods either consume more power or make it hard to migrate to newer BLE versions, which gives up some of the advantages of using BLE.

My contribution to this field: My Ph.D. work developed a time synchronization algorithm and data alignment method that operates at the BLE application layer, with low-latency. The method is easily transferred from one BLE platform to another and was demonstrated herein on two platforms. The method separately synchronizes each peripheral to the central, which gives the ability to expand to multiple peripheral nodes. As a result, multiple peripherals are mutually synchronized. The 95th percentile absolute errors for both the TI and Nordic platforms were less than 1.8 ms and 90th percentile absolute errors both less than 1.2 ms, which is appropriate for use by most ECG, EEG and EMG applications. The 95th percentile results were not particularly sensitive to the timestamp update interval or the number of timestamp pairs used in the time synchronization model.

1.5 Collaborative Projects During my Ph.D.

During my Ph.D. study, I was also involved in other collaborative projects that were led by other students in my laboratory. The projects listed herein each led to a jointly authored publication in which I was a secondary/contributing (i.e., not first) author. For project "PsiCon Phase A," we improved EMG-force modeling by reducing the training duration and generated a universal filter as a substitution for subject-specific EMG-force models. For Phase B, we tested the characteristics of EMG and force in bilateral mirror tasks with or without force feedback. For Phase D, we experimentally tested, in physical real time tasks using a prosthesis emulator, prosthesis control to complete several daily tasks and compared different control methods.

1.5.1 Efficient EMG-Force Training Project

Current research field: A growing number of researchers have studied dynamic system models relating surface EMG signals to muscle force. These supervised EMG-force models are used in a variety of applications, including ergonomic assessment, clinical biomechanics, and motor control research (Li, Zhang et al. 2020). Several groups use 1-DoF mode switching, with and without proportional control (Solomonow, Guzzi et al. 1986). Recently, this research was extended from 1-DoF to multiple joint applications. They have studied multifunctional pattern recognition (Kuiken, Miller et al. 2016). Some researchers use a large number of specialized electrodes (64–192) and acquire multi-degree-of-freedom data. Large electrode arrays are primarily intended to extract more information and reduce errors in EMG force/kinematic estimation. However, these arrays are not practical for 1-DoF and 2-DoF commercial prosthetics.

Project team contribution to this field: A rapid calibration method was introduced for dynamic EMG-force models. The number of electrodes and different training durations of calibration data were examined. Time durations of 14, 22, 30, 38, 44, 52, 60, 68 and 76 seconds of calibration data from 2 to 16 electrodes were tested. Results found that training duration can be reduced to 44 seconds for open-close with flexion-extension contractions, or 60 seconds for open-close with radial-ulnar contractions. Electrode numbers no smaller than 4 produced reasonable error.

1.5.2 EMG Mirrored-Force Project

Current research field: System identification models relating EMG signals to force are now used in myoelectric upper-limb prostheses research. For able-bodied subjects, both EMG and force can be measured and used for model training. In this case, the EMG-estimated force can be compared with the ground truth force to evaluate model accuracy. However for limb-absent subjects, we cannot directly measure the force from the missing limb. Thus, ground truth force is either taken as the target force trajectory, or taken from the sound (contralateral) limb during bilaterally symmetric contractions. There are no studies which have examined the accuracy of either of these two alternatives.

Project team contribution to this field: To assess the problem that we cannot directly measure force in limb-absent subjects, we studied three alternative output sources during dynamic and static force hand-wrist tasks in able-bodied subjects. (1) Contralateral force during bilaterally symmetric movement. (2) Target movement when tracking the target without visual feedback. (3) Target movement in bilateral tracking with mirror visual feedback from the contralateral side. For *tracking* accuracy, we found that, within a task, any visual force feedback decreased both bilateral and unilateral *tracking* RMSE (by a factor of 2–3), with feedback from the dominant side being slightly preferred. Across both *tracking and matching* tasks, the more complex 2-DoF tasks produced higher RMSE than 1-DoF tasks, with most of the increase in error attributed to hand open-close. Perhaps subjects focused more feedback attention on the other DoF. Overall, the *matching* RMSEs were rather large (~10 %MVC for tasks that ranged to ±30 %MVC), suggesting that high-fidelity EMG-force models calibrated to forces from the sound side may be no more accurate than simpler models.

1.5.3 Real-time Prostheses Control Project

Current research field: The human hand is the most powerful tool for humans to perceive and interact with the environment and can perform complex and precise tasks. Consequently, limb loss can reduce quality of life. Millions of people in the US suffer from limb-absence (Ziegler-Graham, MacKenzie et al. 2008). A prosthetic hand is the most common solution for upper limb amputations. For decades, most commercial prosthetics have used two bipolar EMG electrodes fixed in sockets for two-site control of hand opening and

closing or wrist rotation. The co-contraction toggle is used to switch between these two functions. Essentially, this is still 2-site, sequential 1-DoF control (Cordella, Ciancio et al. 2016). In addition, some prior lab-based prostheses testing of multi-DoF control used a large number of electrodes, which is not feasible in existing commercial prostheses. Thus, new system identification algorithms such as regression-based 2-DoF control with a small number of electrodes are necessary.

Project team contribution to this field: This study was a real-time virtual prostheses control experiment. We investigated a simultaneous, independent and proportional 2-DoF prosthesis real-time control system based on a regression algorithm. Different numbers of electrodes (6 or 12) were tested (Bardizbanian, Zhu et al. 2020). Two, 2-DoF control methods were considered, Intuitive control (hand open-close and wrist pronation-supination controlled virtual target size and rotation, respectively) and "Mapping" control (wrist flexion-extension and ulnar-radial deviation controlled virtual target left-right and up-down movement, respectively), then compared with the conventional 2-site sequential control method. Both able-bodied and limb-absent subjects were enrolled in this research. Three tasks were tested and analyzed. In the 1-DoF box-block test, conventional 2-site control had twice the number of blocks transported than 2-DoF methods, but this difference was not statistically significant. In the 2-DoF clothespin refined test and the 2-DoF door-knob test, each of Mapping and Intuitive control used shorter time to complete the task than conventional 2-site control.

1.6 Introduction of Remaining Chapters

The remaining chapters introduce all my Ph.D. projects in detail according to their completion order. Each chapter is a published or submitted paper to a journal or conference.

1.6.1 Primary Projects and Their Related External Publications (First-Authored Papers)

Chapter 2 describes the real-time virtual prostheses control method using no force feedback and rapid regression model calibration. This chapter is in revision.

Chapter 3 discusses an application-layer time synchronization method and related data alignment method for multichannel biosignal sensors using the BLE protocol. This chapter will be submitted as a journal paper.

Chapter 4 focuses on power consumption tests while transmitting biosignals using the BLE protocol. This chapter was published as a conference paper in the *2018 IEEE Signal Processing in Medicine and Biology Symposium (SPMB), Temple University, Philadelphia, PA, 1 December 2018*.

1.6.2 Collaborative Projects and Their Related External Publications (Secondary-Authored Papers)

Chapters 5–8 describe related works about real-time prostheses control.

Chapter 5 discusses real-time prostheses control on both able-bodied and limb-absent subjects, led by Ziling Zhu. This chapter was published as a journal paper in *IEEE Transactions on Neural Systems & Rehabilitation Engineering*.

Chapter 6 shows EMG-force performance using alternative feedbacks for limb-absent subjects, led by Ziling Zhu. This chapter was published as a conference paper in the *2019 IEEE Signal Processing in Medicine and Biology Symposium*.

In Chapter 7, we present off-line tests on different EMG-force and EMG-target models for limb-absent subjects, led by Ziling Zhu. This chapter was published as a journal paper in *IEEE Transactions on Neural Systems and Rehabilitation Engineering*.

Chapter 8 discusses efficient EMG-force training with different testing conditions, led by Bardizbanian Berj. This chapter is published as a conference paper in the *2020 42nd Annual International Conference of IEEE Engineering in Medicine & Biology Society*.

Chapter 2: Virtual Regression-based Myoelectric Hand-wrist Prosthesis Control and Electrode Site Selection using No Force Feedback

This chapter is in development as a journal paper submission. Jianan Li , Ziling Zhu, William J. Boyd, Carlos Martinez-Luna, Chenyun Dai, Haopeng Wang, He Wang, Xinming Huang, Todd R. Farrell, Edward A. Clancy.

Abstract—**Most transradial prosthesis users with conventional "Sequential" myoelectric control have two electrode sites which control one degree of freedom (DoF) at a time. Rapid EMG co-activation toggles control between DoFs (e.g., hand and wrist), providing limited function. We implemented a regression-based EMG control method which achieved simultaneous and proportional control of two DoFs in a virtual task. We automated electrode site selection using a short-duration (90 s) calibration period, without force feedback. Backward stepwise selection located the best electrodes for either six or 12 electrodes (selected from a pool of 16). We additionally studied two, 2-DoF controllers: "Intuitive" control (hand open-close and wrist pronation-supination controlled virtual target size and rotation, respectively) and "Mapping" control (wrist flexion-extension and ulnar-radial deviation controlled virtual target left-right and up-down movement, respectively). In practice, a Mapping controller would be mapped to control prosthesis hand open-close and wrist pronation-supination. Eleven able-bodied subjects and 4 limb-absent subjects completed virtual target matching tasks (fixed target moves to a new location after being "matched," and subject immediately pursues) and fixed (static) target tasks. For all subjects, both 2-DoF controllers with 6 optimally-sited electrodes had statistically better target matching performance than Sequential control in number of matches (average of 4–7 vs. 2 matches, p< 0.001) and throughput (average of 0.75–1.25 vs. 0.4 bits/s, p< 0.001), but not overshoot rate and path efficiency. There were no statistical differences between 6 and 12 optimally-sited electrodes for both 2-DoF controllers. These results support the feasibility of 2-DoF simultaneous, proportional myoelectric control.**

Index Terms— **EMG signal processing, Electromyogram, Myoelectric control, Electrode site selection.**

2.1 Introduction

Approximately 1.9 million individuals were experiencing limb loss in 2012 in the United States (Limb Loss Task Force/Amputee Coalition 2012), with 41,000 people affected in the upper limb (Ziegler-Graham, MacKenzie et al. 2008). Limb loss is expected to double by 2050. There are about 57.7 million limb amputations worldwide (Dillingham, Pezzin et al. 2002, Burger and Vidmar 2016, McDonald, Westcott-McCoy et al. 2020).

The human hand is the most powerful tool for human beings to sense and operate in their environment and can perform sophisticated and precise tasks (Jones and Lederman 2006). Accordingly, limb loss can reduce quality of life (Ahmadizadeh, Merhi et al. 2017). The major task for upper limb prostheses is to substitute the function of the real hand. As the human hand-wrist has 27 degrees of freedom (DoF)—including 3 rotational DoFs for the wrist (Hirt, Seyhan et al. 2017)—it is difficult to create a prosthesis capable of fully replacing the movement and function of the hand (Biddiss, Beaton et al. 2007).

Electromyography (EMG) is one of the most widely used biosignals for controlling upper limb prostheses (Urbanek and van de Smagt 2016, Li, Zhang et al. 2020). For decades, most commercial prostheses have used two bipolar EMG electrodes secured within the socket for two-site control of either hand open-close or wrist rotation (Cordella, Ciancio et al. 2016). Co-contraction mode switching is used to toggle between these two functions (Fougner, Stavdahl et al. 2012). However, such sequential 2-DoF control is not readily compatible with many daily tasks requiring simultaneous joint movement, such as rotating a doorknob while opening a door or holding a bottle for water drinking (Kestner 2006). To achieve more natural motion control, an advanced human-machine interface is needed. Within interface development, the most important need is for more advanced user intention recognition so that a prosthesis can better produce the desired movement (Vujaklija, Farina et al. 2016, Ahmadizadeh, Khoshnam et al. 2021).

Pattern recognition/classification analysis is one of the most studied advanced prosthesis control methods. Several groups have demonstrated accuracy higher than 95% for more than 10 classes (Englehart and Hudgins 2003, Farrell 2008, Hahne, Graimann et al. 2012, Kuiken, Miller et al. 2016, Vidovic, Hwang et al. 2016, Farina, Vujaklija et al. 2017). Some advanced commercial prostheses automatically identify different motions based on classification methods (http://www.coaptengineering.com, https://www.ottobock.com/en-us/product/8E70, https://www.i-biomed.com/sense.html) (Bates, Fergason et al. 2020). However, all current pattern recognition methods face the limitation that only one motion can be selected at a time. The only way that motion combination can be achieved is by training all different combinations of primary motions as their own distinct classes. However, doing so dramatically increases the

number of classes, causing lower accuracy performance (Toledo-Perez, Rodriguez_Resendiz et al. 2019). Accordingly, commercial solutions limit the number of classes selected.

Regression-based methods are another commonly studied advanced prosthesis control method. In contrast to classification-based control, it aims to provide intuitive simultaneous, independent and proportional control of multiple DoFs. Offline and online study has introduced different regression model approaches (Early, Hargrove et al. 2016, Hahne, Schweisfurth et al. 2018, Igual, Igual et al. 2019, Bardizbanian, Zhu et al. 2020, Piazza, Rossi et al. 2020, Zhu, Li et al. 2022). Also, recent work has tested several real-time scenarios, showing some advantages and robustness of the regression method over that of classification (Hahne, Markovic et al. 2017, Hahne, Schweisfurth et al. 2018, Dai, Zhu et al. 2019, Igual, Igual et al. 2019, Piazza, Rossi et al. 2020, Olsson, Malesevic et al. 2021). The training data set needed for regression can be smaller than that needed for pattern recognition of a large number of classes. But, training duration is still problematic in general. Clearly, shorter calibration durations are more suitable for commercial prosthetic fitting procedures (Hahne, Biessmann et al. 2014, Mozaffarian, Benjamin et al. 2016, Clancy, Martinez-Luna et al. 2017).

Additionally, the number of electrodes needed for 2-DoF control may be smaller than other advanced control approaches, which simplifies clinical prosthetic systems (Ameri, Scheme et al. 2014, Bardizbanian, Zhu et al. 2018). Evidence from prosthesis control and EMG-force studies suggests that a minimum of four electrodes for simultaneous, independent and proportional 2-DoF control seems necessary, with some additional electrodes showing improvements (Parker, Englehart et al. 2006, Peerdeman, Boere et al. 2011, Dai, Zhu et al. 2019). While fewer electrodes are more feasible for embedding within a socket (Iqbal, Subramaniam et al. 2018), the optimal number of electrodes and repeatable methods for selecting their sites have received little study (Cavanaugh, Clancy et al. 1983, Huang, Zhou et al. 2008, Kendell, Lemaire et al. 2012, Clancy, Martinez-Luna et al. 2017, Dai, Zhu et al. 2019). Clinical EMG site selection is presently a trial and error process (Sturma, Hruby et al. 2018) (https://coaptengineering.com/clinician-manual/electrode-site-planning).

There is some evidence that regression methods may be more robust to muscle fatigue and different arm postures (Hwang, Hahne et al. 2017, Igual, Igual et al. 2019). However, regression-based controllers also have their own challenges. The first and most important is that model training generally requires force feedback, which is not available to prosthesis users (Wang, Jiang et al. 2017). Second, for multi-DoF control, calibration duration increases when including all DoFs (Cipriani, Sassu et al. 2011, Smith, Kuiken et al. 2016). Third, once calibrated, all model parameters are fixed, thus it's hard to adapt the controller when electrodes shift, leading to a drop in accuracy (Hwang, Hahne et al. 2017). Fourth, while the extrinsic muscles of the fingers (e.g., for use in hand open-close) are located at the surface of the forearm (Smith, Tenore et al. 2008,

Jiang, Englehart et al. 2009, Jiang, Huang et al. 2018), and thus readily available for EMG acquisition in many limb-absent subjects, muscles which control wrist rotation are located deeper (e.g., supinator) or alongside the finger muscles (e.g., pronator teres), making them harder to distinctly record with surface EMG electrodes (Mao, Lee et al. 2009). Independent control (e.g., hand vs. wrist), therefore, becomes more challenging. Several groups instead "map" wrist rotation to other related contractions, such as radial-ulnar contraction (Hahne, Biessmann et al. 2014). Performance comparison between these various control strategies has been limited.

Machine learning control methods have recently been introduced, such as convolutional neural networks and transfer learning, using 8 to 64 EMG channels (Prahm, Schulz et al. 2019, Wang, Fang et al. 2020). The laboratory-based results for this research still have several practical drawbacks such as high computation cost, subject specific training processes, and robustness (including the difficulty of successful operation of large-count electrode systems within a commercial prosthesis socket) (Iqual, Pardo et al. 2019).

A substantial technology gap exists between desired commercial prostheses and advanced technologies studied in the literature (Connolly 2008, Harris, Katyal et al. 2011). Fundamental concerns include: (1) the need for long training and calibration times for most control methods, which are not acceptable for most prosthesis users; (2) the need for force feedback during calibration, which is not available for some myocontrol methods; and (3) not knowing the optimal number of electrodes to utilize or where to site them in either an automated or repeatable manner. Furthermore, a large portion of prior studies only include control participants and, perhaps, a small limb-absent sample size (e.g., as few as one) (Barnett, Heinemann et al. 2012, Hafner and Sawers 2016). In this study, we evaluated a regression-based simultaneous, independent and proportional 2-DoF hand-wrist virtual myoelectric prosthesis controller calibrated with substantially reduced calibration time, and without force feedback. We compared the use of 6 vs. 12 electrodes (automatically selected via backward stepwise selection from a pool of 16 electrodes). We tested this method on both able-bodied and limb-absent subjects in real time using a virtual task. Three control methods, two 2-DoF regression-based methods, plus traditional two-site sequential control were compared in this study. Overall, our primary contributions to the literature are in methods to reduce calibration training time, calibrate EMG-force models without the use of force feedback, and optimal selection and siting of the minimum number of electrodes.

2.2 Methods

2.2.1 Experimental Apparatus

Eleven able-bodied subjects (aged 18–55 years, 6 males and 5 females, all right-handed) and 4 trans-radial limb-absent subjects (aged 39–66 years, 3 males and 1 female, 2 congenital and 2 traumatic limb absence) participated, as approved by the Worcester Polytechnic Institute IRB (IRB Protocol 17-155). Each limb-absent subject had prior myoelectric prosthesis experience. Each subject provided written informed consent. All limb-absent subjects had at least 5 cm of residual limb with functional muscle for electrode placement, and all able-bodied subjects had no physical limitations of their dominant forearm muscles. All recruited subjects completed the experiment.
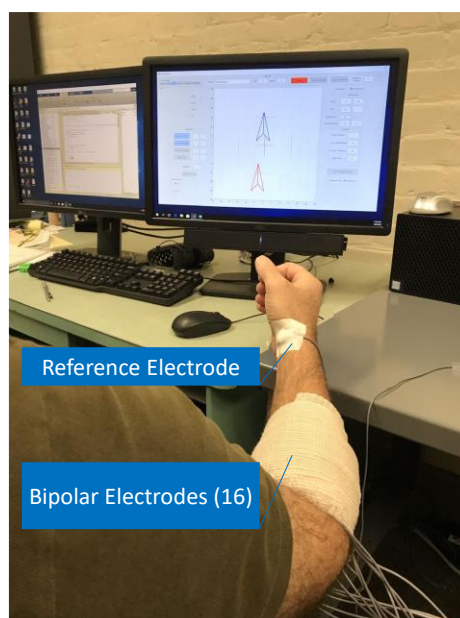
Fig. 2.1 Experimental apparatus for able-bodied subject. Sixteen electrodes were secured around the dominant forearm to collect EMG signals. Reference electrode was attached over the styloid process of the radius. The forearm moved freely while resting on a plastic arm rest.

Subjects sat at the experimental apparatus (Fig. 2.1). Their arm (dominant for able-bodied subjects, affected for limb-absent) was in a neutral position with the elbow resting on a plastic arm rest. Subjects faced a computer screen which showed a virtual target (blue arrowhead) and a red arrowhead cursor controlled by the subject (Fig. 2.2). Target/cursor up-down movement corresponded to wrist radial-ulnar (Rad-Uln) effort, respectively [±30% maximum voluntary contraction (MVC) display range]; right-left movement to extension-flexion (Ext-Flx) effort, with Ext corresponding to right cursor movement for right handedness (±30% MVC display range); rotation to pronation-supination (Pro-Sup), with clockwise cursor rotation corresponding to right handed supination (±30% MVC mapped to ±90o); and target/cursor size to hand open-

close (Opn-Cls), with larger target corresponding to open (±30% MVC mapped to 5–50% of the full screen size).

One of two cursor control methods was used. First, velocity control was used in the dynamic target tracking tasks, as this method best mimics current prosthesis control methods. The cursor's speed was the EMG-estimated force level (in %MVC) per second. Thus, at a constant effort of 30% MVC, it took subjects 1 s to translate the cursor from the origin to the 30% MVC display range. The cursor would remain at its current position when no contraction was made. Second, position control was used in fixed target tracking tasks, as this method requires continuous muscle effort to maintain the cursor in a fixed position. The cursor location corresponded to the EMG-estimated force level (in %MVC). The cursor returned to the origin when no contraction was made. In either control mode, the cursor position was updated every 10 ms (100 Hz update rate) (Boyd 2018).
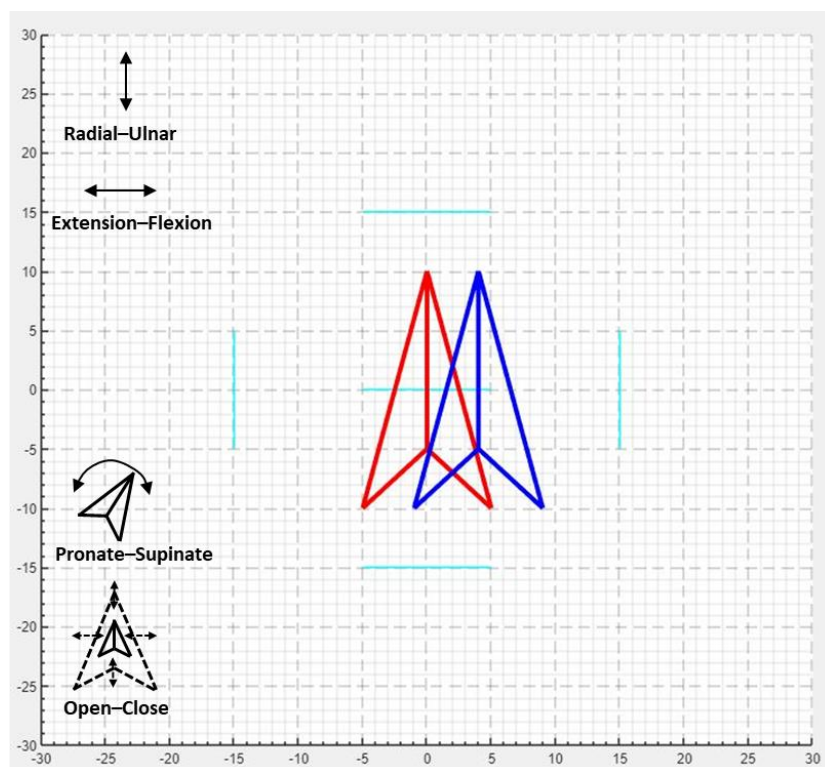
Fig. 2.2 MATLAB real time EMG electrodes site selection and training system main display window. Icons at left depict the four arrow movements.

For able-bodied subjects, sixteen bipolar encased EMG electrode-amplifiers (case dimensions: 32 mm long by 12 mm wide by 5 mm thick) were secured along the long axis of the dominant forearm, equally spaced about its circumference, with the midpoints of the bipolar electrode contacts placed 5 cm distal to the elbow crease. The electrodes were 8 mm in diameter, stainless steel, hemispherical contacts separated 1 cm

edge-to-edge (Lee, Rawley et al. 2018). A reference electrode was gelled and taped over the styloid process of the radius on the same side. Each bipolar EMG signal was wired to a custom differential amplifier circuit (18–690 Hz pass band, CMRR > 92 dB over the pass band). Limb-absent subjects had thinner forearms compared to able-bodied subjects. Hence, the above encased electrodes were too wide to fit. Since data were collected on limb-absent subjects after able-bodied subjects, we needed to use an alternative EMG front-end with a set of encased electrodes whose case dimensions were smaller (32 mm long by 8 mm wide by 3 mm thick). These electrodes differed in that they were 5 mm in diameter. The reference electrode was secured just proximal to the row of active electrodes, as might occur within a prosthesis socket. These electrodes had been designed for use with a commercial amplifier circuit (Liberating Technologies, Inc. BE328 amplifier; 30–500 Hz pass band, CMRR > 100 dB over the pass band). Both amplifier systems retained information over the relevant EMG frequency band (Merletti 1999, Gallina, Disselhorst-Klug et al. 2022). For all subjects, all EMG channels were sampled at 2000 Hz with 16-bit resolution, and target movement was recorded at 100 Hz. Both electrode system inputs were connected to a PC-based real-time EMG electrode site selection and training system implemented in MATLABTM (The MathWorks, Natick, MA, USA) (Boyd 2018).

2.2.2 Methods of Data Calibration, Processing and Control

Two, simultaneous 2-DoF control methods were tested: Rad-Uln & Ext-Flx tracking target x-y location (Intuitive control); and Pro-Sup & Opn-Cls tracking target rotation-size (Mapping control). Additionally, Sequential control was tested tracking target x-y location, only (so as to limit experimental duration).

1) *Calibration data*: The experimenter instructed each subject to complete the necessary calibration tasks. Initially, all limb-absent subjects completed 10–20 minutes of mirror-box training for both 1- and 2-DoF contractions to support a better sense of muscle contraction [see (Zhu, Li et al. 2022) for details]. Preliminary testing indicated that performing MVC contractions helped subjects better estimate the contraction level needed for a 30% MVC (needed for our calibrations), even though feedback was not provided. In the absence of MVCs, subjects seemed to substantially over-estimate the force level corresponding to 30% MVC. After a warm-up period, subjects performed dominant/affected-side MVC trials for each of actual/phantom wrist radial and ulnar deviation, wrist pronation and supination, wrist extension and flexion, and hand close and open. Subjects took ~3–5 s to ramp up to their MVC effort, then maintained this effort for 5 s. Lastly, rest trials were recorded for noise level evaluation. A minimum two-minute rest interval was provided between trials to limit muscle fatigue.

Then, prior to each of the two calibration contraction sets (Intuitive control, followed by Mapping control), all subjects practiced the eight constituent contractions (Fig. 2.3) for 30 s, without feedback. Next, each 90 s calibration trial was recorded, consisting of one 10 s rest and eight distinct 10 s contractions (4, 1-

DoF contractions and 4 combined 2-DoF contractions, depending on the 2-DoF controller being calibrated), as queued by Fig. 3. Contiguous constant-posture constant-force contractions were requested. Subjects were asked to maintain 30% maximum voluntary contraction (MVC) effort for each contraction, as best as possible, without any feedback provided, since force feedback is not available for prosthesis users. These contractions elicit each 1-DoF and each 2-DoF contraction combination. The contraction sequence was not randomized, since a consistent pattern is more easily learned by users who might frequently calibrate a commercial prosthesis based on this approach. The experimenter observed each contraction to assure that the correct contraction sequence and timing occurred. A contraction trial was repeated if, in the subject's (or experimenter's) judgement, an inadequate contraction profile was produced or if inadequate cursor control resulted after calibration (described below). No feedback was provided.

Control	10 s	10 s	10 s	10 s	10 s	10 s	10 s	10 s	10 s
Intuitive Control									
Motions	Rest	Cls	Opn	Sup	Pro	Cls + Sup	Cls + Pro	Opn + Sup	Opn + Pro
Mapping Control									
Motions	Rest	Flx	Ext	Uln	Rad	Flx + Uln	Flx + Rad	Ext + Uln	Ext + Rad

Rest ← → | 1-DoF (30%MVC) | 2-DoF (30%MVC each Dir)

Fig. 2.3 Ninety second calibration trial sequence for each of the two, 2-DoF control methods

2) *EMG pre-processing:* EMG standard deviation (EMGσ) was generated by the following sequential stages applied to each raw EMG channel (per trial): 60 Hz notch filter to attenuate powerline noise (second-order IIR with 1 Hz notch bandwidth), 15 Hz highpass filter to reduce motion artifact (fifth-order Butterworth), rectify, then decimate by a factor of 20 to 100 Hz (performed in two stages; second stage 9th order Chebyshev Type I, 16 Hz lowpass filter prior to downsampling). A sample raw and pre-processed EMG channel from a dynamic target tracking trial (see Section 2.2.3 below) is shown in Fig. 2.4. Additional lowpass filtering occurred after EMG-force processing, as described below.
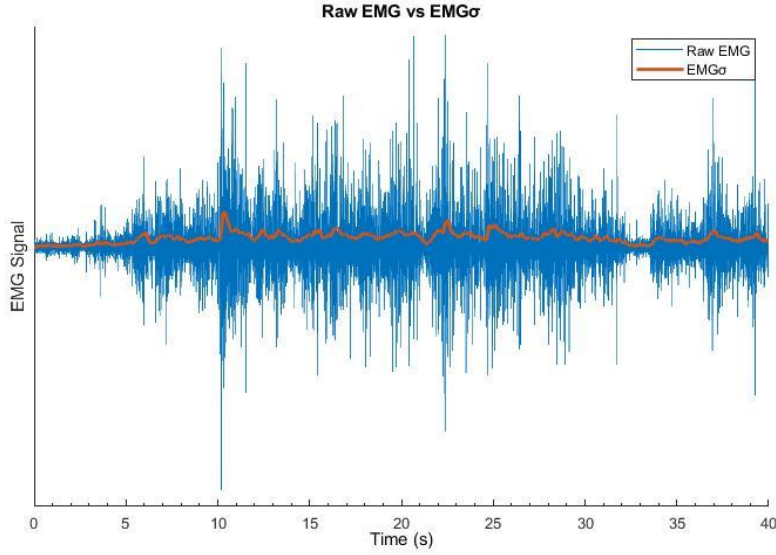
Fig. 2.4 Raw EMG and pre-processed EMGσ from a dynamic target tracking trial.

3) *Calibration of Intuitive and Mapping control:* Each 90 s calibration record consists of 9, ten-second sections, for the 8 contractions and 1 rest period. Within each 10 s segment, the first and last second were removed to avoid contraction transitions. The output force corresponding to each of the eight contractions was assigned as 30% MVC for the respective DoFs and 0% MVC for unused DoFs. This assignment matched the effort levels asked from the subjects during calibration contractions (even though force feedback was not provided.) The output corresponding to the rest period was set to 0 %MVC and this contraction was weighted 8 times (to equal the number of active contractions). A static EMGσ-force model was then formed based on regression. The 2-output model simultaneously solved:

$$F_i[m] = \sum_{e=1}^{E} c_{i,e} EMG\sigma_e[m], \qquad i = 1,2 \qquad (1)$$

where F1, F2 was the force in each DoF (e.g., 1➔ Ext-Flx and 2➔Rad-Uln for Mapping control), m was the decimated discrete-time sample index, E was the number of electrodes used in the fit, and c1,e , c2,e were the fit coefficients for different output DoFs. The linear least squares Moore-Penrose pseudo-inverse method was used for model training, in which singular values of the design matrix were removed if the ratio of that singular value to the largest was less than a tolerance value ($Tol = 0.01$, based on previous study) (Dai, Bardizbanian et al. 2017). Electrode selection used backward stepwise selection. Starting from 16 electrodes, each iteration eliminated the channel whose exclusion gave the lowest RMS error combined across both DoFs on the training data, until the desired number of electrodes was achieved (Clancy, Martinez-Luna et al. 2017, Dai, Zhu et al. 2019). Once the fit coefficients were obtained, force was continuously estimated from the

real-time EMGσ estimates. An additional 1 Hz critically damped lowpass filter (second-order) (Robertson and Dowling 2003) was cascaded with each output DoF to smooth dynamic trials. For fixed targets, the filter cutoff was 0.5 Hz. These cutoff frequencies were established during preliminary testing as a trade-off between sufficient smoothing (achieved with a lower cutoff frequency) vs. short-duration filter lags (achieved with a higher cutoff frequency). The smoothed force estimates were then applied to velocity or position control of the cursor, as described above.

4) *Calibration of Sequential control:* Two electrodes were selected corresponding to the largest "distinct" EMGσ signal when subjects performed Ext or Flx contraction, respectively, where "distinct" accounts for mutual cross-talk/co-activation. When multiple channel option selections existed for limb-absent subjects, we selected sites near their existing prosthesis electrode locations. An additional 1 Hz critically damped lowpass filter (second order) was cascaded with each pre-processed EMG channel during dynamic target tracking. (Sequential control was not used for fixed target tasks.) For each EMG channel, gain was set such that with an approximately 30% MVC effort, the cursor took approximately 1 s to move from the screen center (0,0) to each screen edge (i.e., 30% MVC). Two pairs of EMGσ thresholds and one window size were set as described subsequently. A resting threshold was used to eliminate noise and unintentional movement from each electrode channel. A higher mode switching co-contraction threshold for each electrode channel was used to switch between cursor up-down and left-right movement. Thus, subjects controlled either cursor up-down or left-right at any one time, switching between DoFs by triggering a co-contraction EMG signal. In particular, when both EMGσs were larger than their respective mode switching threshold for a specific, short-duration "window," a co-contraction was detected and a mode switch was performed. The thresholds and window were manually adjusted until subjects could easily and consistently control the cursor and reliably trigger co-contraction. The difference between the two filtered EMGσ signals served as the force estimate for velocity control. This method is the most common for determining velocity in two-site control.

2.2.3 Experimental Protocol

For each of the two tasks described below, we randomized the order of the controller (Intuitive, Mapping, Sequential) and the number of electrodes (6, 12). The subject was always blinded to the number of electrodes in use.

1) Dynamic target tracking tasks: Two, simultaneous 2-DoF control methods were tested: Intuitive control of x-y location and Mapping control of target rotation-size. Additionally, Sequential control tested tracking target x-y location. For each, four repeated tracking trials were acquired for each of two testing conditions (6-electrodes or 12-electrodes) per controller. To limit the duration of the experiment, limb-absent subjects only tested the simpler 6-electrode condition. Each trial was 40 s in

duration. Within the 40 s, successive stationary targets were randomly generated (uniform density for each DoF, ±30 %MVC range for each DoF). Once the subject moved their cursor to match the target location within the desired error (±2 %MVC), the subject cursor color would change from red to green. Once the subject remained within the target location for a 0.5 s duration, a "match" was recorded and the system immediately proceeded to a new random target.

2) Fixed target tasks: Only the simultaneous 2-DoF controllers (Intuitive, Mapping) were used for the fixed target tasks. Sequential control was excluded since it uses velocity control. (Once a target is acquired, a subject using velocity control can rest and the controller's position will lock in place; thus, no effective measure of skill level in maintaining a constant position is available.) Subjects used the 6-electrode controllers, calibrated as in the dynamic tasks, to track a fixed-location target for 20 s using position control. Again, the subject cursor changed color from red to green whenever the subject cursor was within ±2 %MVC of the target. Four distinct co-contraction targets were used for each control method (one per trial), with the contraction level set at 10 %MVC for each DoF. For Intuitive control, the four target combinations were: Cls+Sup, Cls+Pro, Opn+Sup and Opn+Pro. For Mapping control, the four target combinations were: Ext+Uln, Ext+Rad, Flx+Uln and Flx+Rad. These co-contractions were the same as the 2-DoF contractions in the calibration trial, but using 10 %MVC efforts. One trial was recorded per location for each condition.

2.2.4 Methods of Analysis

To quantify performance in dynamic tasks (Igual, Igual et al. 2019), we computed four parameters per trial, each of which was averaged across the four repeated trials per condition. 1. Number of matches. 2. Overshoot rate was the number of times per trial that the cursor and target aligned, but did not remain aligned for 0.5 s (i.e., failed to match). 3. Path efficiency was the ratio of the actual travel path to the shortest path between targets. 4. Throughput (bit/s) represented the ratio of the task difficulty index (bits) for each trial and the completion time (s), as defined by ISO 9241-9 (Soukoreff and MacKenzie 2004). Within our task, the task difficulty index (TDI) was defined as a function of the ratio of target distance (D) from virtual target to the cursor divided by target tolerance (W= ±2 %MVC):

$$TDI = \log_2\left(1 + \frac{D}{W}\right)$$

which is a key real-performance evaluation index in Fitts' law tasks (Fitts 1954, MacKenzie 2015).

For the fixed target task, a fixed target was presented at predefined locations. For each trial, a Similarity Index was computed as the percent of time that the subject cursor remained within ±2 %MVC of the target. Again, this value was averaged across the four distinct trials per condition.

2.2.5 Statistics

The data from each statistical comparison were first tested for normality using the Kolmogorov-Smirnov test. If the data were normally distributed, repeated measures analysis of variance (RANOVA) and post hoc paired t-tests with Bonferroni correction (significance level p = 0.05) were used to test performance differences. Prior to RANOVA, the degree of sphericity (ε) was used to adjust the degrees of freedom by either the method of Greenhouse-Geisser (ε < 0.75) or Hyunh-Feldt (0.75< ε<1). Each RANOVA assessed all possible interactions. These interactions were not significant, unless noted otherwise in the Results. When interactions were found, we proceeded to post hoc pair-wise comparison of all factor combinations, since the number of combinations was small. If the data were not normally distributed, a non-parametric Friedman test was used to test performance differences. If significant, we again proceeded to post hoc paired t-tests with Bonferroni correction.

2.3 Results

2.3.1 Calibration Quality Assessment (Two-DoF controllers, only)
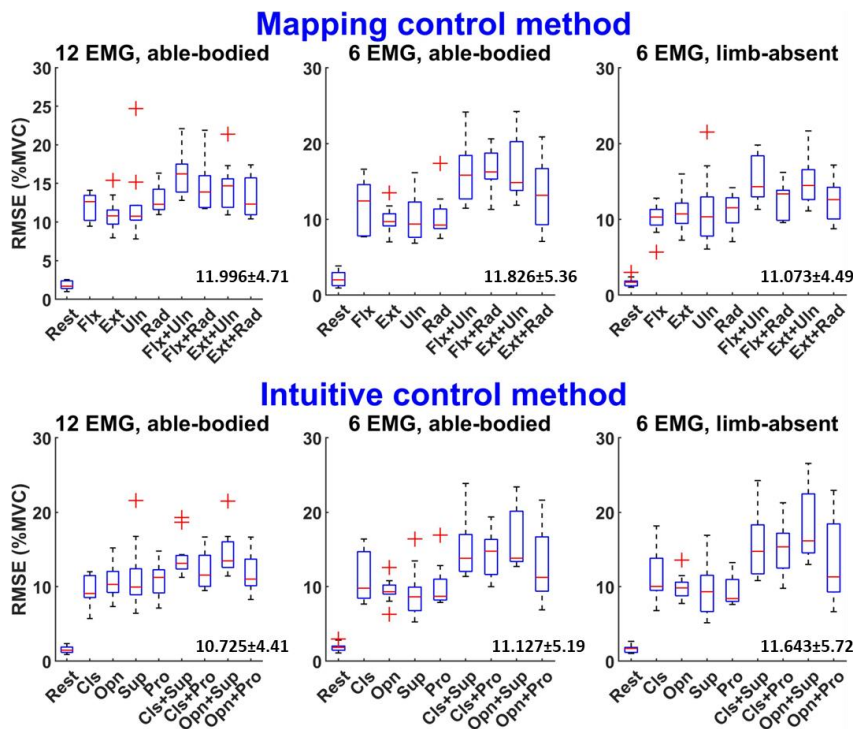
Fig. 2.5 Boxplot RMSE summary results of calibration quality assessment. Overall mean ± standard deviation, for all data from each subplot, listed at bottom right of each subplot.

Fig. 2.5 shows summary RMSE values (%MVC) between EMG-estimated and assigned (i.e. target) force for both 2-DoF calibration methods, separately for able-bodied subjects (using six and 12 electrodes) and limb-absent subjects (six electrodes only), from the calibration trials. For able-bodied subjects, a three-way RANOVA was tested with three factors: control method (Intuitive, Mapping), number of electrodes (6, 12) and calibration type (8 different contractions + rest, i.e., enumerated as listed on the x-axis labels in Fig. 5). A significant interaction was found between control method and calibration type $[F(8,72) = 4.4, p = 0.003]$, while number of electrodes was significant $[F(1,9) = 98, p < 10^{-6}]$. *Post hoc* comparison for the interaction found that for both control methods, rest always had lower RMSE than all other calibration types $(p<10^{-4})$ and pronation had lower RMSE than radial deviation $(p<10^{-4})$. For Intuitive control, Opn had lower RMSE than Cls&Sup $(p = 0.017)$ and Cls&Pro $(p = 0.023)$; Sup had lower RMSE than Cls&Sup $(p = 0.037)$, Cls&Pro $(p = 0.009)$ and Opn&Sup $(p= 0.014)$; and Pro had lower RMSE than Cls&Sup $(p = 0.001)$. For the Mapping method, Flx had lower RMSE than Flx&Uln $(p = 0.021)$; and Ext had lower RMSE than Flx&Uln $(p = 0.045)$. For number of electrodes, 12 electrodes had significantly lower RMSE than 6 electrodes $(p<10^{-4})$.

For limb-absent subjects, a two-way RANOVA with factors control method and calibration type was tested. Control method was not significant $[F(1,8) = 9, p = 0.54]$, while calibration type was significant $[F(8,24) = 21, p = 0.001]$. *Post hoc* comparison for calibration type found that rest always had lower RMSE than all other calibration types $(p<0.01)$.

2.3.2 Dynamic trials, 2-DoF controllers, six vs. twelve Electrodes, Able-bodied subjects
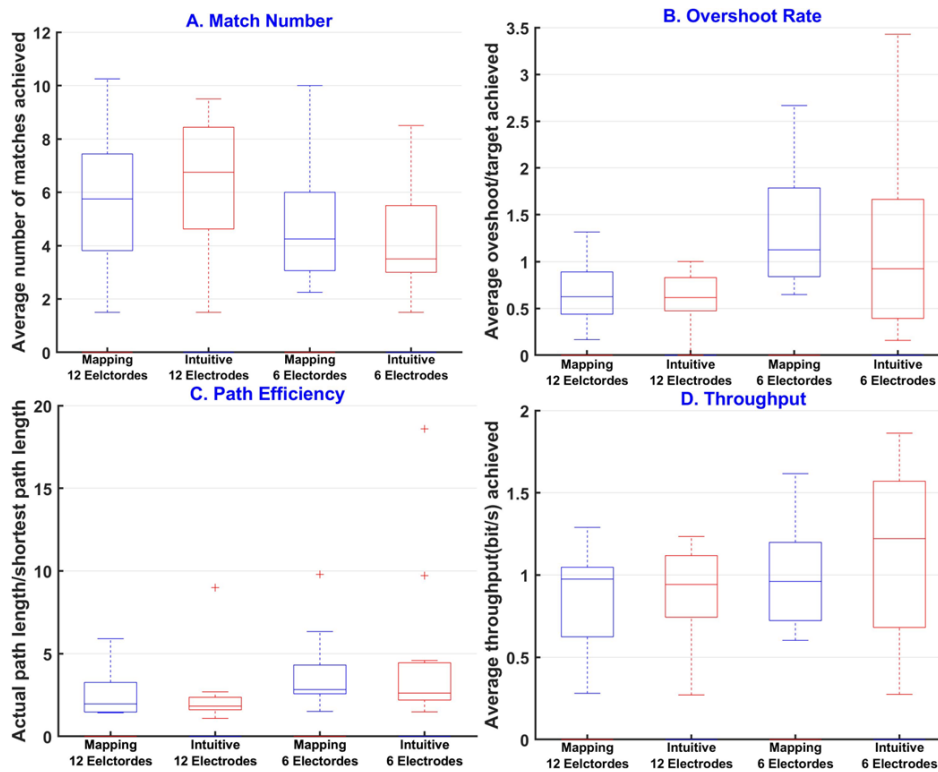
Fig. 2.6 Boxplot summary results of dynamic task performance comparing number of electrodes (6 or 12) and control method (Intuitive, Mapping) for able-bodied subjects.

Fig. 2.6 shows summary dynamic task results comparing number of electrodes and control method for able-bodied subjects. Two-way RANOVAs with factors of control method (Intuitive, Mapping) and number of electrodes (6, 12) for number of matches, overshoot rate and throughput each found no significant difference $[F(1,10) < 4.4, p > 0.06]$. A non-parametric Friedman test with the same factors for path efficiency found no significant difference ($\chi 2(4) = 6.400, p = 0.171$). Due to these results, all further analysis only considered the case of 6 electrodes for the 2-DoF controllers, since fewer electrodes simplify clinical prosthetic systems.

2.3.3 Dynamic Trials, Able-bodied and Limb-absent Subjects
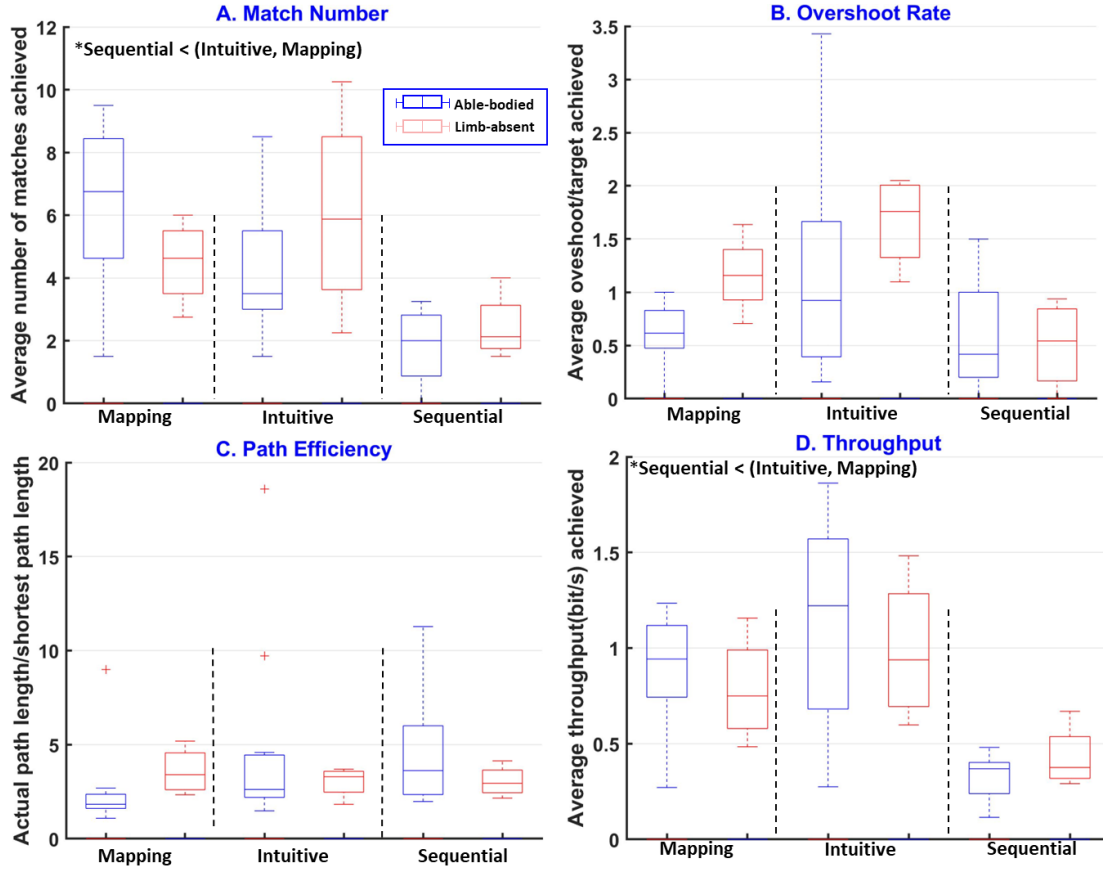
Fig. 7 Boxplot summary results of dynamic tasks for each of able-bodied and limb-absent subjects for each controller (Intuitive, Mapping, Sequential). Intuitive and Mapping control used 6 electrodes, while Sequential control used 2. Embedded text with asterisks list statistically significant differences.

Fig. 2.7 contrasts boxplot summary results of able-bodied and limb-absent subject dynamic tasks for each of the four outcome measures: number of matches, overshoot rate, path efficiency and throughout. Separately for each outcome measure, results were compared using a mixed two-way RANOVA with within-subjects factor of control method (Intuitive, Mapping, Sequential) and between-subjects factor of group (able-bodied, limb-absent).

For number of matches (higher matches represented better performance), only control method was statistically different [$F(2,26) = 12$, $p < 0.001$]. *Post hoc* comparison found that Sequential control had significantly lower number of matches than both Intuitive control ($p = 0.02$) and Mapping control ($p = 0.01$). For overshoot rate (lower overshoot rate represented better performance), no statistical difference was found for either control method [$F(2,26) = 3.4$, $p = 0.050$] or group [$F(1,13) = 0.08$, $p = 0.77$]. For path efficiency (lower path efficiency ratio represented better performance), no statistical difference was found for either control method [$F(2,26) = 0.35$, $p = 0.706$] or group [$F(1,13) = 0.37$, $p = 0.551$]. For throughput (higher

throughput represented better performance), only control strategy was statistically different [F(2,26) = 16, $p <$ 0.001]. *Post hoc* comparison found that Sequential control had significantly lower throughput than both Intuitive ($p < 0.01$) and Mapping control ($p < 0.01$).

2.3.4 Fixed Target Test, Able-bodied and Limb-absent Subjects (Two-DoF controllers, only)
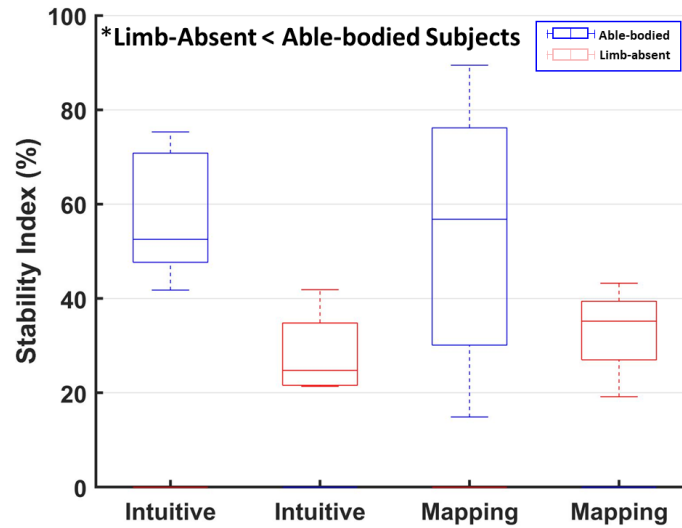
Fig. 2.8 Boxplot summary results of Similarity Index for each of able-bodied and limb-absent subjects. Embedded text with asterisks list statistically significant differences.

Fig. 2.8 contrasts boxplot summary results of able-bodied and limb-absent subject Similarity Index from the fixed target trials (percent time cursor remained within ±2 %MVC of the target). Higher Similarity Index represented better performance. A mixed two-way RANOVA with within-subjects factor of control method (Intuitive, Mapping) and between-subjects factor of group (able-bodied, limb-absent) found only group to be statistically different [F(1,13) = 0.9, $p <$ 0.001]. *Post hoc* comparison found that limb-absent subjects had significantly lower Similarity Index than able-bodied subjects ($p = 0.021$).

2.4 Discussion

2.4.1 Calibration Quality Assessment Results and Number/siting of Electrodes

Our comparative results of RMS calibration errors found that rest periods exhibited lower RMSE than any of the eight active contractions. This result is not surprising, since rest periods do not benefit from force feedback (which was not provided) and active contractions are difficult to maintain, especially without feedback (Johansen-Berg and Matthews 2002, Noble, Eng et al. 2013). Additionally, the variance of EMGσ

is known to increase with activation level (Hogan and Mann 1980), thus EMGσ at 30% MVC should naturally exhibit more variance than EMGσ at rest. Eight of the nine remaining statistical differences found a 2-DoF contraction to have higher error than a 1-DoF contraction. These results may suggest that maintaining a 2-DoF pose is more difficult to perform than maintaining a 1-DoF pose or, in the absence of feedback, might suggest differences in achieved force levels in 1-DoF vs. 2-DoF contractions. A possible manner in which to reduce error would be to feedback the EMGσ values instead of force, e.g. via spider/radar plots (Khushaba, Al-Timemy et al. 2016, Kristoffersen, Franzke et al. 2021). Absolute force would not be available, but relative changes in force would be indicated.

The other main finding from our (offline) calibration quality assessment was that using 12 backward selected electrodes (out of 16 available) produced lower RMSE than using 6. This result is consistent with other EMG-force studies (Clancy, Martinez-Luna et al. 2017, Dai, Zhu et al. 2019, Zhu, Li et al. 2022)—and our quality assessment is essentially EMG-force, since a constant 30% MVC force was assigned as the calibration output. We presumed that lower RMSE corresponded to better calibration of 2-DoF control. However, our offline result was contrary to our online dynamic matching results from able-bodied subjects, showing no difference between using 6 vs. 12 optimally sited electrodes. Indeed, anecdotal comments from subjects—who were blinded to the number of electrodes—consistently described no observable difference in controller performance when comparing 6 vs. 12 electrodes. This contrary result (offline vs. online) has been noticed previously in both pattern recognition- (Simon, Hargrove et al. 2011, Ortiz-Catalan, Rouhani et al. 2015, Roche, Lakey et al. 2019) and regression-based (Zhu, Li et al. 2022) prosthesis control studies. That noted, recent EMG pattern recognition studies have found stronger offline vs. online correlation using alternative performance metrics (Teh and Hargrove 2020) or using combinations of traditional performance metrics (Nawfel, Englehart et al. 2021). Thus, the long-term utility of offline assessment remains a topic of investigation. In any case, it is likely that fewer than 4 electrodes is not compatible with regression-based 2-DoF control (Clancy, Martinez-Luna et al. 2017). Typically, 16 conventional EMG electrodes is the maximum number studied (Hwang, Hahne et al. 2017, Li, Zhang et al. 2020), and our results suggest that a larger number need not be investigated.

We selected a calibration duration of 90 s (10 s for each of nine contractions, including rest) at 30% MVC. Likely, shorter calibration durations would produce similar offline EMG-force RMSE (Clancy and Hogan 1997, Bardizbanian, Zhu et al. 2020), particularly since no dynamics of EMG-force were calibrated. All controller dynamics were pre-determined based on the EMG processing. (When controlling a physical prosthesis, the mechanical dynamics of the end effector would also appear in cascade with those of the EMG processor.) Accordingly, shorter calibration durations might be appropriate for prosthetic control. Online tests of shorter durations would require additional studies. And, other calibration contraction levels might be

investigated. We selected 30% MVC so as to be demonstrably above the noise floor. Note that our calibration procedure also performs optimal electrode site selection, via backward stepwise selection. Since backward selection only produces a local minimum, it is unclear how other site selection methods might perform. Finally, various noise thresholds were manually set for the controllers. A more rigorous, repeatable and automated method for their selection is desired.

2.4.2 Comparison of Controllers

The dynamic matching trials and the fixed target tracking test consistently found no performance difference between the two, 2-DoF controllers (Intuitive, Mapping). This comparison should be considered cautiously, since these two controllers utilized distinct feedback sources. The Intuitive controller (hand Opn-Cls with wrist rotation) used target size and orientation as feedback. Notably, subjects communicated that they struggled to differentiate sizes when the target size was relatively small. In contrast, the Mapping controller (wrist Ext-Flx with Rad-Uln) used target left-right and up-down location as feedback. Hence, a different feedback source. We utilized these more natural feedback sources for this virtual test, recognizing that each controller could be mapped to hand Opn-Cls with wrist rotation in a physical prosthesis. Such mapping can be learned over time (Nazarpour, Barnard et al. 2012, Dyson, Dupan et al. 2020), but such longer term assessments were outside the scope of this study. Overall, these results support use of the Intuitive control algorithm, which should be simpler for prosthesis users to learn.

The dynamic matching trials also found that both 2-DoF controllers performed better than Sequential control on number of matches and throughput. No significant differences were found on the other two measures (overshoot, path efficiency). These results were consistent for able-bodied and limb-absent subjects. Note that the able-bodied subjects did not have experience with the co-contraction technique required to switch modes in Sequential control. Additionally, one of the limb-absent subjects was already expert in Sequential control (queued by co-contraction)—and this subject had the highest number of matches of all subjects when using Sequential control. Thus, our results may be sensitive to the level of experience of the user.

We had expected that path efficiency in the dynamic matching trials would be better using the 2-DoF controllers, but no statistical difference was found. The targets were two dimensional and both dimensions changed for each new target. A 2-DoF controller can move "diagonally" across the plane, while the Sequential controller must move in one dimension at a time (e.g., along paths aligned with the coordinate axes). During 2-DoF control, some subjects noted difficulty in simultaneous control of both DoFs, thus adapting a strategy of only controlling one DoF at a time (albeit without the need for co-contraction mode switching between

them). For these subjects, the ability of the 2-DoF controller to rapidly transition between DoFs may have been more important than simultaneous control of both DoFs.

We did not include the Sequential controller in our fixed target test, since a Sequential controller customarily utilizes velocity control. With velocity control, once a target has been acquired, the user can rest and the controller will remain at its present position indefinitely—hence, no effective measure of a user's ability to maintain a constant contraction occurs. For this reason, our fixed target test utilized position control. However, this consideration points out that certain controllers may be better tuned for certain tasks. For example, using a physical prosthesis with these same three controllers, Zhu et al. (Zhu, Li et al. 2022) found that the Sequential controller performed best on a 1-DoF task (Box and Blocks), while the 2-DoF controllers performed best on 2-DoF tasks. In the 1-DoF task, 2-DoF controllers would occasionally miscue end effector movement in the unused DoF, thus losing time while repositioning that DoF. Adjustments in noise thresholding or other controller algorithm components might help to remove these miscues in the future.

2.4.3 Contrasting Able-bodied and Limb-absent Subject Performance

For the dynamic tracking trials, no statistical differences were found between able-bodied and limb-absent subject performance on any of the four tasks. To their advantage, our limb-absent subjects had prior myoelectric prosthesis control experience. Conversely, our able-bodied subjects, to their advantage, had intact proprioception. In addition, our sample size was modest (11 able-bodied, 4 limb-absent).

However, for the fixed target test, limb-absent subjects held the cursor location within the specified tolerance about half of the amount of time as that of able-bodied subjects. This difference was statistically significant. Holding a constant-force contraction for a long period (20 s for this task) is likely not a task encountered in daily prosthesis usage, and may invoke some amount of localized muscle fatigue. Hence, the prior experience in myoelectric prosthetics was likely not an advantage for this task.

2.4.4 Limitations and Challenges

As noted above, our sample size was modest, with limited statistical power. Low samples size can lead to more non-significant findings. However, large sample populations are uncommon (if found at all) in this field, since the cost, duration and technical requirements to conduct these experiments are high. A better approach may be to support multiple studies of this size, then integrate results across studies (e.g., meta-analysis).

After initial calibration, several subjects could not generate the desired contraction trajectory on their first attempt. However, all such subjects achieved acceptable performance on a second calibration. Most subjects attributed their poor calibration to applying too much force during calibration. Then, during tracking

trials, excessive effort led to uncontrolled contraction efforts. Over time, it is likely that all subjects would become better acquainted with the calibration procedure.

As noted previously, some subjects reported unintentional motion from the unused DoF when using the 2-DoF controllers. Such unintentional motion was often associated with either higher forces or rapid force transients (that likely activate antagonist muscle activity). Such contraction patterns are not present in calibration data. Noise thresholding helps to mitigate these detrimental movements. However, noise thresholding may only be a partial solution, and selecting noise thresholds remains a complicated, multi-factorial process. Resolving these issues seems to be important to the robustness of 2-DoF controllers.

2.5 Conclusion

We studied simultaneous, independent and proportional myoelectric virtual 2-DOF target control of three controllers and optimal selection of 6 vs. 12 electrode sites (from a pool of 16 electrodes). Results from able-bodied and limb-absent subjects found that a relatively brief calibration contraction (90 s), without the use of force feedback, successfully calibrated our 2-DoF regression-based controllers. Shorter calibration durations are likely possible, as no dynamics of the EMG-force relationship are calibrated, only electrode channel gains. Our online results of tracking dynamically located targets found that 6 optimally sited electrodes performed as well as 12. Fewer electrodes are more cost-effective, robust, and easier to fit into a prosthesis socket. Both 2-DoF controllers (Intuitive, Mapping) performed similar to each other, and better than a traditional Sequential controller in the 2-DoF tasks. Overall, we successfully calibrated our controllers with 90 s of data, did so in the absence of force feedback, and found that 6 optimally-sited electrodes performed as well as 12 electrodes. This study shows the potential of the 2-DoF Intuitive and Mapping controllers.

Chapter 3: Application-Layer Time Synchronization and Data Alignment Method for Multichannel Biosignal Sensors Using BLE Protocol

This chapter is in development as a journal paper submission. Jianan Li, Eric Quintin, He Wang, Benjamin E. McDonald, Todd R. Farrell, Ximing Huang and Edward A. Clancy.

Abstract— **Wearable wireless biomedical sensors for health monitoring have emerged as a rapidly growing research field in recent years. For many biomedical signals, e.g. EEG (electroencephalogram), ECG (electrocardiogram) and EMG (electromyography), a single wireless sensor is often not sufficient. Multiple sensors, distributed about the body without local wired connections, are required for most health monitoring applications. However, low cost-high precision time synchronization of acquired data from all peripheral devices to a central node—and ensuring low latency—is a problem. Current solutions include either using custom wireless protocols or using extra hardware for synchronization, solutions which require more power consumption and essentially prohibit migration between commercial microcontrollers. We successfully developed a low latency, Bluetooth Low Energy (BLE)-based time synchronization algorithm and data alignment method, implemented in the BLE application layer, to time synchronize multiple peripheral clocks to a central node and align analog-to-digital conversion data streams from distinct peripherals. The time synchronization method was implemented on two commercial BLE platforms. Our best time synchronization algorithm and data alignment method achieved absolute time differences between two independent peripheral nodes on average 69 ± 71 μs for a TI platform and 477 ± 490 μs for a Nordic platform. The total biosignal latency from end to end would be less than three connection intervals (45 ms for TI ,30 ms for Nordic) with an average of two connection intervals (30 ms for TI and 20 ms for Nordic).**
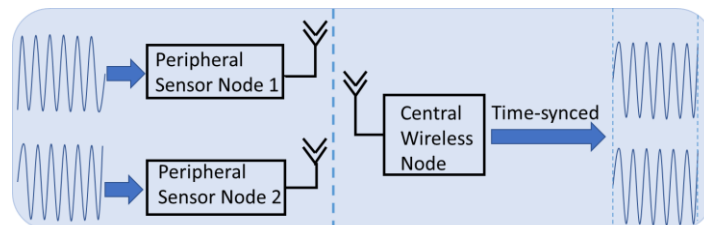
Index Terms— **BLE (Bluetooth Low Energy), biosensor, time synchronization, wireless sensor network, Internet of Things (IoT).**

3.1 Introduction

In recent years, the development of wireless technologies and low power wireless transmission protocols have paved the way for using wireless bio-sensors to continuously monitor human biosignals, benefiting both medical research and personal health care (Cao, Leung et al. 2009, Pantelopoulos and Bourbakis 2010, Lin, Chang et al. 2014, Brunelli, Tadesse et al. 2015, Wang, Chai et al. 2017, Shakya and Sharma 2019, Zhou, Sharma et al. 2021). The use of low power transmission protocols, such as BLE (Bluetooth Low Energy), ZigBee and low power Wi-Fi (IEEE 802.11ah or Wi-Fi HaLow) is increasing rapidly in IoT (internet of things) applications, wearable wireless systems for health monitoring and corresponding research areas (Youn and Kim 2009, Omre and Keeping 2010, Ishak, Ahmad et al. 2017, Fadhlannisa and Basari 2020, Resina 2020, Sharma, Hui et al. 2020). Bio-electric signals, such as EEG (electroencephalogram), ECG (electrocardiogram) and EMG (electromyogram), are frequently used in both medical and biological health applications. These applications require low power consumption, low latency and high accuracy during data transmission. Comparing different low power protocols, BLE has much lower power consumption (~1 mA compared to ~10 mA for low power Wi-Fi), and has a relatively high transmit rate of 2 Mbps physical layer compared to ZigBee's 250 Kbps (Zhang, Xia et al. 2014, Aguilar, Vidal et al. 2017, Tosi, Taffoni et al. 2017, Tosi, Taffoni et al. 2019). Although custom wireless protocols might exceed this performance, they are difficult and expensive to develop and upgrade, whereas improved commercial-off-the-shelf device performance occurs at a rapid pace. Hence, we sought to develop wearable systems based on the standard BLE 5.0 wireless transmission protocol.

Most biosignal applications require multiple signal channels for data analysis (Gravina, Allinia et al. 2017). For example, two EMG channels are typically the minimum required for myoelectric control of a prosthesis. And for these applications, the minimum sampling rate is relatively high, e.g. minimum rates of 1000 Hz for EMG (Battye, Nightingale et al. 1955, Horn 1963, Kwatny, Thomas et al. 1970), as high as 500 Hz for EEG (Weiergraber, Papazoglou et al. 2016) and 250–360 Hz for ECG (Kossmann, Brody et al. 1967, Dixon, Allstot et al. 2012). Currently, most wireless sensor systems either use one combined peripheral data sender hard-wired to multiple sensors (Ganiev, Shin et al. 2016, Javaid, Tiwana et al. 2021) or use custom wireless protocols to achieve high throughput and low latency (Trigno® Research+ System, Delsys Inc, Boston, MA, USA). Combining sensors at a peripheral node does not eliminate wires locally attached across the body (thus, not really wireless) and can make it hard to site all electrodes at their desired positions due to the wires (Brunelli, Farella et al. 2016, Rachim and Chung 2016, Rossi, Khouia et al. 2016). Fully distributed wireless multi-channel peripheral nodes would make it easy to select the best sensor sites. Further, custom

protocols make it hard to migrate from one platform to another, in particular to take advantage of ongoing electronic device improvements. And custom protocols are harder to share within the research community.

Traditionally, wired multi-channel data acquisition systems using a multi-channel analog-to-digital converter (ADC) inherently time synchronize all channels to within one sample period, or better. However, with distinct wireless nodes, each ADC is located on its respective peripheral node, controlled via its local clock. Hence, each ADC operates at a slightly different sampling rate and at unsynchronized sampling phases (Tirado-Andres and Araujo 2019). In addition, each clock rate may drift over time. Thus, a method is needed to synchronize time between the various wireless devices, and then use that time synchronization to align multiplexed data at the central node (Maroti, Kusy et al. 2004, Simeone and Spagnolini 2007, Bruscato, Heimfarth et al. 2017). For the above wireless protocols, native time synchronization methods are not accurate enough for high sample rate biosignals (Sichitiu and Veerarittiphan 2003).

To achieve better time synchronization, several methods have been introduced (Sundararaman, Buy et al. 2005, Lo Bello and Mirabella 2006, Calado, Macciantelli et al. 2020). In BLE, one method is based on Bluetooth beacon role (Bideaux, Zimmermann et al. 2015, Sridhar, Misra et al. 2016, Asgarian and Najafi 2017), in which a central node broadcasts clock information that is received near-simultaneously by all listening peripheral nodes (and with low latency). All peripheral nodes can then synchronize to the central with high precision. Beacon transmissions are repeated to maintain synchronization over time. However, when the central node broadcasts, it cannot receive data from different peripheral nodes in real time. Thus, this beacon role method is not suitable for high throughput, low latency applications. Another method uses extra hardware to detect the onset of antenna activation when transmissions are initiated (Rheinlander and Wehn 2016), achieving high time synchronization precision ($9 \pm 17\mu s$). But, the additional hardware must be designed and produced, extra battery power is always consumed, and such custom hardware is not readily upgradable. For daily health monitoring, less power consumption (and, thus, longer battery life) is desired. For typical wireless nodes with a 20 mAh battery, the additional hardware can preclude a desired battery life of 16 hours (for example). Another recent method used BLE non-connectable non-scannable undirected advertising (BLE "ADV_NONCONN_IND") to reset peripheral clocks to achieve time synchronization (Dian, Yousefi et al. 2017). However, this technique also did not demonstrate a manner in which to maintain synchronization of streaming ADC data from distributed peripheral nodes (Giovanelli, Milosevic et al. 2015).

In this paper, we describe a BLE 5.0 time synchronization and data transmitting system that is programmed at the application layer, demonstrated via two peripherals and one central device, tailored for low-latency high-throughput applications. The method is expandable to more peripheral devices. Two peripherals concurrently transmitted ADC samples at 1000 Hz sampling rate, with latency ≤30 ms. Time synchronization was applied within each peripheral node based on timestamps from the central node These

central timestamps were transmitted to each peripheral using the BLE write-with-response mode. The central node then multiplexes the received data from the peripheral nodes, with proper time alignment. Our method was implemented separately on two common microcontroller platforms (TI and Nordic), demonstrating its portability. No modification of the underlying transmission protocols and no extra hardware was needed.

3.2 Background

3.2.1 Relevant Bluetooth Low Energy Characteristics

IEEE 802.15.1 (Bluetooth) is a wireless technology standard used for short distance applications, utilizing the 2.402 GHz to 2.480 GHz band. Standard Bluetooth has several limitations for our application, including higher power consumption, lower packet size and higher link reestablish time. To improve upon these problems, Bluetooth version 4.0 was introduced as Bluetooth Low Energy (BLE) (Marquess 2010). BLE 4.0 decreased average power consumption from 1 W to 0.01–0.5 W, depending on the use case. And, compared to the standard Bluetooth latency of 100 ms, BLE reduced latency to 6 ms in a non-connection state and even lower in a connection state. Subsequently, BLE 4.2 increased data packet size to 251 bytes plus 4 header bytes per packet (from a prior limit of 27 bytes plus 4 header bytes per packet), facilitating higher data rates (Marquess 2014). BLE 5.0 (used in this research) increased the physical layer transmitting rate from 1 Mbps to 2 Mbps, reducing the transmit duration of each 251-byte packet from 2.12 ms to 1.06 ms. Each of these new BLE 5.0 features benefit our multi-peripheral single-central system (Marquess 2016).

The basic BLE protocol stack that consists of the controller and the host. The stack has two main levels. The controller is the lower level which differs from platform to platform based on different software implementations of the BLE standard. For portability at the application level, we did not want to modify the controller level, which mediates BLE packet sending and receiving. The host level is the application layer which can more easily migrate from one platform to another. Our synchronization and data alignment operated in this level, implemented in "C" code. The Host-Controller Interface (HCI) is used to communicate between the two levels, exchanging packetized data. Within the host level, Generic Access Profile (GAP) controls the transmit-receive state of the device as one of five states: Standby, Advertising, Scanning, Initiating and Connected.

For each BLE device, its GAP layer must run in one of four roles: Broadcaster (the device is an advertiser that is non-connectable), Observer (the device scans for advertisements but cannot initiate connections), Peripheral (the device is an advertiser that is connectable and operates as slave in a single link-layer connection), or Central (the device scans for advertisements and initiates connections and operates as a master in single or multiple link-layer connections). In broadcaster role, the device is continuous transmitting data

on all channels and any nearby device can receive the broadcast, but the amount of data is limited to 37 bytes. Any larger amount of data needs to be transmitted using central role. In our application—because we need to transmit data bi-directionally (timestamp data from central to peripheral; ADC data from peripheral to central)—the central role and peripheral role is required by the central node and each peripheral node.

In BLE peripheral-central role, the central and peripheral node cannot remain continuously connected when multiple peripherals are used. A frequency-hopping, time-division multiplexing (Haartsen 1998) scheme is used to ensure all BLE devices can share the 2.4 GHz band. After a specified time duration selected by the central node (connection interval), the central and designated peripheral node both jump to a new channel, exchange connection parameters to establish a link and initiate data transmission (connection event). Both the central and peripheral nodes maintain a data queue of all data to be transmitted during this connection event. The central node transmits all of its data to the peripheral node, then the peripheral node sends all of its data to the central node. Once data transmission completes, the nodes disconnect from each other and wait for the next connection event. Within each connection interval, each peripheral has a specific "event length" (multiples of 1.25 ms) for data transmission. If no data are to be sent or received, handshaking still occurs so as to maintain the connection. The connection interval ranges from 7.5 ms to 4 s, with a gap of 1.25 ms required between assigned time slots. If multiple peripherals pair with one central, each peripheral node's connection interval is set to their connection setting's least common multiple. For the TI platform, the event length is fixed to 5 ms, requiring our two-peripheral implementation to utilize a connection interval greater than 10 ms (due to the required gap time between assigned time slots). We chose 15 ms. For the Nordic platform, the event length is programmable. We utilized an event length of 3.75 ms and a connection interval of 10 ms, to achieve lower latency.

3.2.2 The TI and Nordic Wireless Microcontrollers

The TI CC2640R2f is a BLE module manufactured by Texas Instruments (TI). It features Bluetooth® 5.0 and a 32-bit 48 MHz ARM Cortex®-M3 processor. The integrated antenna has a maximum transmit (TX) power of +5 dBm and a receiver sensitivity of –97 dBm. Its energy requirement is low, requiring a 5.9 mA receive (RX) current, a 6.1 mA TX current at 0 dBm and 9.1 mA TX current at +5 dBm; all from a 1.8–3.8 V supply. Also, it has a built-in eight-channel 12-bit 200-k samples/s analog-to-digital converter (ADC). However, its 28 KB SRAM was only sufficient in our work when this microcontroller was used as a peripheral node. Hence, our TI-based implementations used a TI CC2642 as the central node. This model has an 80 KB SRAM and slightly higher RX (6.9 mA) and TX current consumption (7.3 mA at 0 dBm and 9. 6mA at +5 dBm), from a 1.8–3.8 V supply. Overall, due to its small size (7 mm × 7 mm), low power

consumption, good RF characteristics and integrated ADC feature, it is an excellent selection for wireless biosensor systems.

To evaluate and demonstrate the ease of migration of our time synchronization methods across platforms, a competitive BLE module was selected. The Nordic Semiconductor nRF52840 also features Bluetooth® 5.0 with a 32-bit 64 MHz ARM Cortex®-M4 processor. Its current consumption is 4.6 mA RX and 4.8 mA TX, from a 1.7–5.5 V supply. It also has a built-in 12-bit 200 k samples/s ADC and is equipped with a large RAM size of 256 KB. With even lower power consumption and similar integrated features, it is also an excellent test platform choice.

3.3 Methods

3.3.1 System Architecture

In this research, we prototyped two BLE wireless biosignal sensor bench-top implementations of our time-synchronization and data transfer method. The first system (Fig. 3.1) is based on a TI BLE development board platform. Variants of these development boards, utilizing the same active hardware, are available in smaller packages for embedded system use. Use of the full size development board facilitated rapid prototyping. Our system is comprised of three parts. The first part is the two peripheral biosensor nodes (one sensor per node), each using TI CC2640R2f boards with built-in 12 bit ADC to sample the biosignals. The second part is the central node using a TI CC2642 development board which receives data from the peripheral
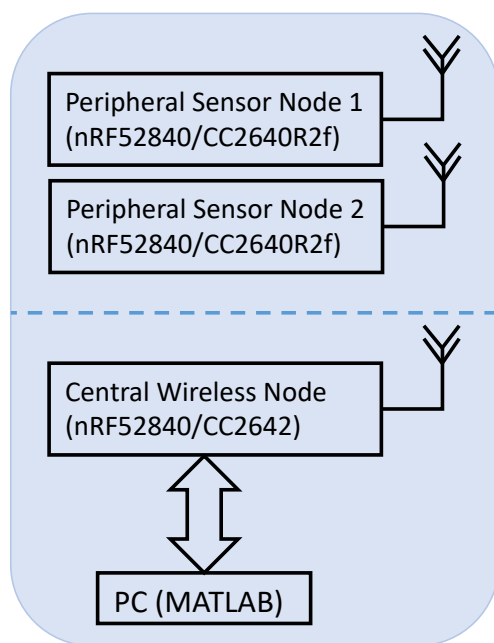
Fig. 3.1. System diagram for both TI and Nordic platforms.

nodes, which are then sent to a PC using its UART port. And the last part is data processing and real time

plotting using MATLAB on a PC. In embedded applications, the PC functions would generally be replaced by other real-time processors.

With only software modifications at the application layer, we implemented the second system (Fig.1) using Nordic BLE development boards. The architecture is similar to that of the TI-based system, except that both peripheral nodes and the central node used the same Nordic development board (nRF52840). And, we combined all PC and MATLAB functions into the central node for a fully embedded implementation. All data were still streamed to the PC for off-line analysis.

The bandwidth of most bioelectric signals is less than 500 Hz, with EMG having the largest range from 10–500 Hz [48]. According to the Nyquist-Shannon theorem, a sampling rate of 1000 Hz is required to correctly reconstruct a signal containing frequencies up to 500 Hz. Hence, we selected a 1000 Hz sampling rate. To achieve continuous transmission of ADC values without delay, a dual buffer structure was used for data collection on a peripheral node. When one buffer is full, an interrupt triggers its transmission, while the second buffer stores the new data without delay. The ADC automatically switches incoming data storage back and forth between these buffers to achieve no missed ADC samples.

On both testing platforms, each peripheral sampled single-channel data at 1000 Hz with 12-bit resolution. The connection interval (and ADC buffer duration) was 15 ms on the TI platform and 10 ms on the Nordic platform, as explained above.

3.3.2 Time Synchronization Method Design

1) Generation of Timestamp Pairs: All newly available ADC samples were transmitted in data packets each connection interval (15 ms for TI; 10 ms for Nordic). Ideally, each connection interval would generate one ADC packet. But, timing variations between a peripheral and central clock can lead, occasionally, to either zero or two packets formed within a connection interval. BLE transmission is not synchronized directly with ADC packet readiness. Rather, the peripheral clock sets the timing of ADC conversion on a peripheral node, whereas the central node schedules BLE transmission. Regardless, as each new ADC packet is generated, it is sent to the peripheral node's BLE transmit buffer for transmission to the central node during the next connection event. Once queued for transmission, the peripheral's application layer software has no further access to the packet. Thus, packet transmission delay times range from near zero up to two connection intervals. Hence, any peripheral clock timestamp that might be loaded with the ADC data has an uncertainty of up to two connection intervals (20–30 ms), which is much too long for many applications. An alternative time synchronization method is necessary.

One alternative is to use beacon transmissions (from the central to all peripherals) at system startup, thereby synchronizing clocks once ("single-shot") (Asgarian and Najafi 2017). Data transmissions would begin thereafter, since they cannot run coincident with beacon transmissions. However, clock drift is not necessarily consistent throughout device operation, i.e., due to changes in temperature, humidity, and other conditions. And, even minute errors in initial synchronization would be amplified progressively over time in devices that operate all day (or longer). As noted previously, repeated/continuous use of beacon transmissions is not consistent with continuous ADC sampling, so is also not a time synchronization option.

In our approach, all data are moved between nodes using BLE notifications. A notification transmission does not receive confirmation, thus it minimizes delay and wireless transmission duration. The basis of our time synchronization method was to generate time-synchronized (paired) central and peripheral timestamps. The more closely paired in time, the better. We found that the most reliable time fiducial occurred on the central node, when it received a peripheral data packet. In particular, if the central node queried its timestamp clock immediately after peripheral data arrival, then added one connection interval to this value, an excellent estimate was produced of the arrival time on that peripheral node of the ensuing central data packet transmission (which is used to instantiate the ensuing connection interval). The central data packet included this central timestamp, denoted $TS_C[m]$, where m indexes the timestamp pairs. Once this central data packet was received on the peripheral, it immediately queried its own timestamp clock (this timestamp being denoted $TS_P[m]$), forming a timestamp pair. The timestamp pair can be used on the peripheral node for data synchronization, or transmitted back to the central node in the next peripheral data packet for synchronization there or on the PC (as done herein). New timestamp pairs were not generated every connection interval (see below). In addition, the ADC clock on the peripheral ran asynchronously from the BLE sub-system. But, when the ADC completed converting data for a packet, a software interrupt was automatically generated at the application layer. Hence, the peripheral immediately queried the timestamp clock again and associated this time with the final ADC sample for that packet. This timestamp was denoted TS_{ADC}.

2) Timestamp Rollover Avoidance: The TI platform generates unsigned 32-bit integer timestamps, which count the number of 10 μs intervals since power-up. Thus, this timestamp rolls over every 11.93 hours. The Nordic platform generates an unsigned 24-bit integer count of the number of 30.1 μs intervals since power-up, rolling over every 8.42 minutes. These rollovers are too short, and would threaten robust real-time synchronization. To avoid rollover effects, we re-stored each timestamp in an unsigned 64-bit integer, accounting for rollover when doing so (i.e., incrementing the 64-bit count through each rollover). The 64-bit timestamps were used thereafter, and rolled over at durations greater than 5 million years.

3) Time Synchronization Model: The N most recent timestamp pairs ($TS_C[m]$ and $TS_P[m]$) were used in a linear least squares clock synchronization method to continuously estimate central clock time. To understand this method, let $TS_P[m], 0 \le m < N$ be the most recent peripheral node clock timestamps and $TS_C[m], 0 \le m < N$ be the paired set of central node clock timestamps. The affine model that estimates central time based on peripheral time is:

$$\widehat{TS}_C[m] = \beta_0 + \beta_1 \cdot TS_P[m] + \epsilon, \qquad (1)$$

where β_0 is the offset parameter, β_1 is the slope parameter, m is the timestamp index and ϵ is a random error term. Since it is assumed that both clocks have reasonable time precision with slightly different drifting rate, it will be the case that the slope parameter β_1 will have a value near 1.0 counts/count. The offset term β_0 could vary over the full range of the timestamp values and can be negative-valued. With N timestamp pairs, we can estimate β_0 and β_1 via linear least squares (Kenney and Keeping 1954) as:

$$\begin{cases} \beta_1 &= \dfrac{N \cdot \Sigma_{PC} - \Sigma_P \cdot \Sigma_C}{N \cdot \Sigma_{PP} - \Sigma_P \cdot \Sigma_P}, \\ \beta_0 &= \dfrac{\Sigma_y - \beta_1 \cdot \Sigma_P}{N} \end{cases} \qquad (2)$$

where $\Sigma_{PC} = \sum_{m=0}^{N-1} TS_P[m] \cdot TS_C[m]$, etc.
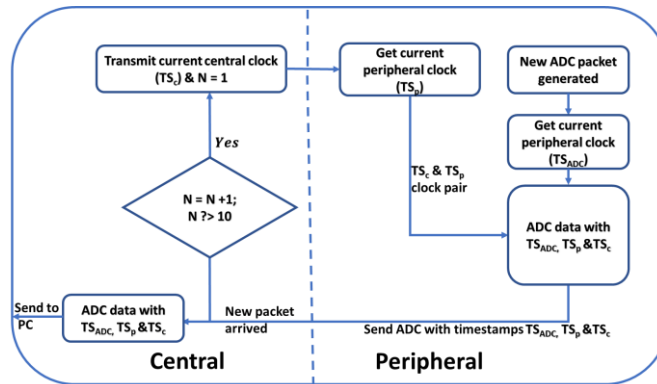
Fig. 3.2. Flow chart of time synchronization method, using $N = 10$ as an example. Variables N, TS$_c$, TS$_p$ and TS$_{ADC}$ defined in the text.

This model is updated as each new timestamp pair is received. For each data packet from the peripheral, the most recent affine model is applied to the ADC timestamp (TS_{ADC}), producing an estimate of the central time corresponding to the last ADC sample. The central time corresponding to earlier samples in the packet is estimated using the sampling period. A flowchart of the time synchronization method is shown in Fig. 3.2.

3.3.3 Data Alignment Algorithm Design

Our data alignment approach is to synchronize each peripheral data stream to the central clock which, in turn, synchronizes them to each other. In addition, even highly accurate clocking on distinct nodes cannot be perfect. That is, the clock rates on distinct nodes will be slightly different. Thus, over time, a peripheral ADC will produce too many or too few samples, relative to time on the central clock. And, if clock rates drift, the relative clock rates will also drift with respect to each other. Hence, a data alignment algorithm was introduced, operating on each peripheral node. This algorithm utilizes the timestamp pairs to detect when the accumulated temporal drift between the central and peripheral clocks is larger than a threshold. If the peripheral clock has been running faster, one data sample is removed from the data stream. If the peripheral clock has been running slower, one data sample is interpolated and added to the data stream. A threshold value that is too small (e.g., under a sampling period) led to excessive corrections in which samples were alternately deleted and interpolated in subsequent packets. A threshold value that was too large (e.g., multiple sample periods) allowed larger time synchronization errors to persist longer in the data stream. We used a threshold value of one sample.
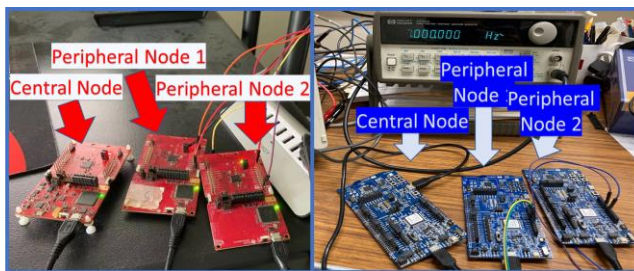
Fig. 3.3. TI Platform (left) and Nordic Platform (right).

3.4 Experimental Methods

The TI- and Nordic-based systems, consisting of two peripheral nodes and one central node, were separately implemented and hardware tested on the benchtop (Fig. 3.3). Both platforms were USB powered. For each platform, a function generator (HP 33120A) simultaneously applied the same input to one ADC channel of each peripheral node. The generator produced a sine wave ranging from 0.5 V to 2.5 V (1.5 V offset, to align with the unipolar ADCs). During a test trial, the signal frequency was varied from 1 Hz to 12

Hz with an increase of 1 Hz every 1 minute. Each testing trial was 12 minutes in duration. Each peripheral node sampled and transmitted these data and the timestamp pairs wirelessly to the central node. For testing, the central node was connected to a PC through a UART port, transferring unsynchronized ADC data packets, their corresponding timestamp pairs and their ADC final sample timestamps from both peripherals directly into MATLAB in real time. These data were then stored to the hard drive for off-line analysis. For each platform, seven trials were collected.

Off-line, each 12-minute recording from both peripherals for a trial were separately time-aligned, using our time synchronization and data alignment method. Each recording was upsampled by a factor of 100 to improve time resolution between samples from 1 ms to 10 µs. We used zero-phase lowpass filtering in the upsampler, thus the first and last 10 s of each recording was discarded, to eliminate filter startup/tail transients. For each 12-minute trial, 700 s of data remained. The data from each trial were then segmented into 1 s duration contiguous epochs (700 segments/trial x 7 trials = 4900 epochs total). For each epoch, we computed the cross-correlation coefficient function between the data from the two peripherals, extracting the location of the maximum correlation and the correlation value at this location. All average correlation values exceeded 0.99. The location of the maximum correlation was an estimate of lag/lead between the peripheral ADC channels. The mean and standard deviation lag/lead of the 4900 epochs was reported and all 4900 values were used for statistical analysis.

The entire process was repeated for all combinations of the number of sequential timestamp pairs used in the affine regression model ($N = 2, 4, 8, 16, 32, 64$ or 128) and the number of connection intervals between timestamp updates (every 10, 20, 50, 100 connection intervals). Smaller N is computationally more expedient, but provides less averaging in the least squares estimate. A small timestamp update period requires more frequent updating of the affine model (thus computationally expensive), whereas an overly long timestamp update period may not adapt quickly enough to true changes in clock rate.

3.5 Results

Fig. 3.4 shows the distribution of inter-channel timing errors for the TI platform, combining results across all different conditions (update interval = 150, 300, 750, 1500 ms; N = 2, 4, 8, 16, 32, 64, 128). Note the large number of times in which the error equals zero lag/lead (a.k.a. count) values (at the upsampled rate). Table I (TI) and Table II (Nordic) show the average and standard deviation signed and absolute time difference errors between the two peripherals as a function of different buffer sizes and timestamp update intervals. The data from each statistical comparison were first tested for normality using the Kolmogorov-Smirnov test. As all data were not normally distributed (p<0.001), a non-parametric Friedman test was used

to test performance differences. If significant, we proceeded to post hoc paired t-tests (Wilcoxon signed-rank test) with Bonferroni-Holm correction.
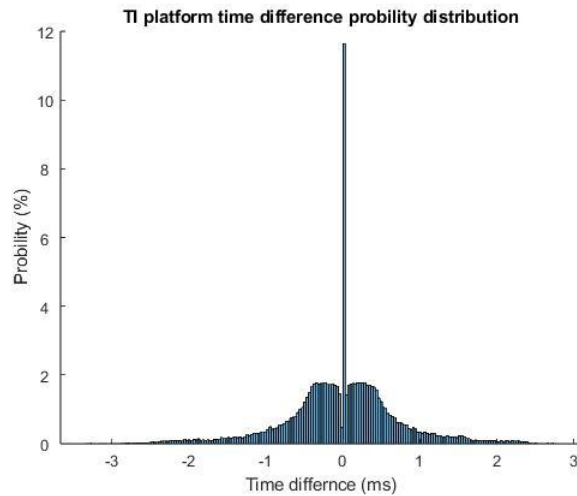
Fig. 3.4. TI platform time difference between two peripherals, combining results from all number of timestamp pairs (N = 2, 4, 8, 16, 32, 64, 128) and update intervals (150, 300, 750 1500 ms)

3.5.1 Texas Instruments (TI) Platform Results

For the TI platform, the Friedman test found a statistically significant difference between different parameter combinations for the signed errors [$\chi2(27)$ = 622, p = 6x10–144]. We began post hoc evaluation by identifying the minimum average error within each update interval (i.e., the best as a function of N), identified in bold red font in Table I. Within the results for each update interval, we pair-wise compared the results of this best value of N to each other value of N. Significant and insignificant results are shown in Table I. In most cases, results within an update interval varied with N. Finally, we compared results from the cell with the overall lowest average error to the best case within each other update interval. This lowest average error of 1 ± 228 µs (N = 8 timestamp pairs, 750 ms timestamp update interval) was significantly lower than each of the others (p<4x10–5).

We repeated this statistical analysis for the absolute errors. The Friedman test found a significant difference [$\chi2(27)$ = 26923, p = 1x10–311]. Post hoc evaluation within each timestamp update interval is shown in Table I. In all cases, results within an update interval varied with N. The cell with the overall lowest average error was a tie for the 750 ms update interval with N = 2 or 64 (error of 69 ± 71 µs). Between-update interval comparisons with the data corresponding to each overall minimum cell found each to be significantly lower than each of the other minimum cells from the other update intervals (p<4x10–13).

TABLE I

SUMMARY RESULTS FOR TI MICROCONTROLLER SYSTEM.
CELLS IN BOLD RED FONT INDICATE RESULT WITH THE MINIMUM MEAN VALUE WITHIN THAT TIMESTAMP UPDATE INTERVAL. "NS" DENOTES THAT THE RESULTS IN THIS CELL ARE NOT SIGNIFICANTLY DIFFERENT FROM THOSE OF THE MINIMUM MEAN VALUE WITHIN THAT TIMESTAMP INTERVAL. MEAN ± STD. DEV. RESULTS ARE EACH FROM 4900 EPOCHS. LAST TWO COLUMNS LIST 90TH AND 95TH PERCENTILE ABSOLUTE ERRORS.

Time-stamp Update Interval (ms)	Number of Time-stamp Pairs (N)	Mean ± Std. Dev. Signed Errors (µs)	|------ Absolute Errors ------|		
			Mean ± Std. Dev. (µs)	90th % (ms)	95th % (ms)
	2	13 ± 508	348 ± 370	0.72	0.91
	4	37 ± 442	318 ± 309	0.70	0.83
	8	26 ± 467	**349 ± 314**	0.75	0.92
150	16	17 ± 502	365 ± 344	0.74	0.91
	32	14 ± 495	366 ± 333	0.85	1.05
	64	33 ± 490	376 ± 316	0.85	1.03
	128	**11 ± 439**	336 ± 283	0.68	0.87
	2	7 ± 483 **NS**	359 ± 323	0.80	0.94
	4	27 ± 517	373 ± 359	0.80	0.91
	8	12 ± 476	346 ± 327	0.75	0.96
300	16	27 ± 458	357 ± 288	0.75	0.91
	32	11 ± 434	322 ± 292	0.74	0.90
	64	9 ± 412 **NS**	317 ± 263	0.63	0.85
	128	**4 ± 412**	**305 ± 277**	0.75	0.90
	2	18 ± 97	**69 ± 71**	0.18	0.19
	4	18 ± 219	114 ± 188	0.22	0.53
	8	**1 ± 228**	115 ± 197	0.22	0.44
750	16	12 ± 267	153 ± 218	0.42	0.59
	32	23 ± 200	120 ± 162	0.22	0.41
	64	18 ± 97	**69 ± 71**	0.18	0.19
	128	8 ± 197	106 ± 166	0.22	0.45
	2	57 ± 413	301 ± 288	0.70	0.85
	4	18 ± 335 **NS**	241 ± 233	0.57	0.70
	8	**7 ± 314**	201 ± 241	0.54	0.74
1500	16	65 ± 361	249 ± 269	0.65	0.76
	32	22 ± 317	196 ± 250	0.53	0.75
	64	27 ± 355	217 ± 282	0.64	0.78
	128	13 ± 282 **NS**	**167 ± 227**	0.46	0.66

TABLE II

SUMMARY RESULTS FOR NORDIC MICROCONTROLLER SYSTEM.
CELLS IN BOLD RED FONT INDICATE RESULT WITH THE MINIMUM MEAN VALUE WITHIN THAT TIMESTAMP UPDATE INTERVAL. "NS" DENOTES THAT THE RESULTS IN THIS CELL ARE NOT SIGNIFICANTLY DIFFERENT FROM THOSE OF THE MINIMUM MEAN VALUE WITHIN THAT TIMESTAMP INTERVAL. MEAN ± STD. DEV. RESULTS ARE EACH FROM 4900 EPOCHS. LAST TWO COLUMNS LIST 90TH AND 95TH PERCENTILE ABSOLUTE ERRORS.

Time-stamp Update Interval (ms)	Number of Time-stamp Pairs (N)	Mean ± Std. Dev. Signed Errors (µs)	|------ Absolute Errors ------|		
			Mean ± Std. Dev. (µs)	90th % (ms)	95th % (ms)
	2	40 ± 731	513 ± 522	1.26	1.66
	4	54 ± 700	491 ± 501 **NS**	1.17	1.57
	8	41 ± 700	**488 ± 504**	1.17	1.54
100	16	53 ± 714	495 ± 517 **NS**	1.20	1.63
	32	13 ± 709	494 ± 509 **NS**	1.20	1.63
	64	**3 ± 716**	502 ± 510 **NS**	1.26	1.63
	128	29 ± 701	491 ± 501 **NS**	1.17	1.60
	2	48 ± 682	**477 ± 490**	1.16	1.57
	4	64 ± 705	491 ± 509 **NS**	1.17	1.57
	8	33 ± 709	488 ± 515 **NS**	1.23	1.63
200	16	**4 ± 714**	498 ± 511 **NS**	1.23	1.63
	32	36 ± 707	492 ± 509 **NS**	1.23	1.60
	64	58 ± 99	493 ± 504 **NS**	1.20	1.54
	128	27 ± 708 **NS**	489 ± 513 **NS**	1.17	1.60
	2	48 ± 700	492 ± 499 **NS**	1.17	1.60
	4	**27 ± 710**	495 ± 509 **NS**	1.20	1.55
	8	55 ± 731	515 ± 522	1.26	1.72
500	16	41 ± 715	491 ± 521 **NS**	1.20	1.63
	32	45 ± 712 **NS**	504 ± 505 **NS**	1.20	1.60
	64	82 ± 712	499 ± 514 **NS**	1.20	1.61
	128	71 ± 696	**486 ± 503**	1.14	1.57
	2	49 ± 699	492 ± 499 **NS**	1.17	1.60
	4	**28 ± 710**	496 ± 509 **NS**	1.20	1.54
	8	56 ± 731	515 ± 522	1.26	1.72
1000	16	42 ± 716	492 ± 522 **NS**	1.20	1.63
	32	44 ± 712 **NS**	504 ± 505 **NS**	1.20	1.60
	64	80 ± 712	499 ± 515 **NS**	1.20	1.63
	128	71 ± 696	**487 ± 502**	1.14	1.57

3.5.2 Nordic Platform Results

For the Nordic platform, the above statistical analysis was repeated. For signed errors, the Friedman test found a statistically significant difference between different parameter combinations [$\chi2(27) = 872$, $p = 3 \times 10{-}166$]. Post hoc evaluation within each timestamp update interval is shown in Table II. In most cases, results within an update interval varied with N. The cell with the overall lowest average error of 3 ± 716 μs (N =64 timestamp pairs, 100 ms timestamp update period) was significantly lower than each of the others (p<0.0012).

For the absolute error, the Friedman test found a significant difference [$\chi2(27) = 108$, $p = 1 \times 10{-}11$]. Post hoc evaluation within each timestamp update interval is shown in Table II. In most cases, results within an update interval did not vary with N. The cell with the overall lowest average error of 477 ± 490 μs (N = 2 timestamp pairs, 200 ms timestamp update period) did not differ significantly from each of the other minima (p>0.179).

3.6 Discussion and Future Direction

3.6.1 Overall Time Synchronization Performance

When independent wireless peripheral nodes are each collecting ADC data, it is imperative to time synchronize these data streams. We did so using a BLE implementation from within the application layer, thereby avoiding the need for custom hardware and facilitating software re-use between microcontroller platforms and versions. Our method synchronizes each peripheral to the central clock, thereby mutually synchronizing multiple peripherals. Our method also avoids timestamp "rollover" errors, so that synchronization remains valid for as long as a device is powered.

We assessed both the signed time synchronization error between two independent peripheral node ADC samples and the absolute error. We tested using input sine wave frequencies spanning 1–12 Hz. The signed error, on average, was quite small, with a best-case mean value of 1 μs for the TI platform (750 ms timestamp update interval, N=8) and 3 μs for the Nordic platform (100 ms timestamp update interval, N=64). However, this error can be misleadingly small if approximately half of the errors cause one peripheral to lead, while the other half cause this same peripheral to lag.

Thus, we also assessed the absolute timing error, which better represents performance. Depending on the timestamp update interval and the number of timestamp pairs (N), the TI platform had mean absolute errors ranging from 69–376 μs and the Nordic platform had mean absolute errors ranging from 477–515 μs. These errors had large standard deviations, typically similar in value to the mean. Thus, we also reported the 90th and 95th percentile errors. The 95th percentile errors were less than ~1 ms for the TI platform and less

than 1.8 ms for the Nordic platform—thus, quite comparable. For many engineering applications, these 95th percentile errors likely provide a better design guideline than the other measures. Surprisingly, these 95th percentile errors did not seem to vary much with timestamp update interval and number of timestamp pairs used in the time synchronization algorithm (see Table I and Table II); although the TI platform may have exhibited somewhat lower 95th percentile errors when using a 750 ms timestamp update interval.

Overall, these errors are quite small when considering biomedical signal acquisition. For ECG and EEG (typical sampling rate below 500 Hz), these errors are less than one sample period. For EMG (typical sampling rates of 1000 or 2000 Hz), these errors are 1–2 sampling periods. Hence, standard comparisons between signals acquired from independent nodes is facilitated.

3.6.2 Robustness of the Timestamps

Synchronization is based entirely on the precision and robustness of the timestamps. When referring to precision, our method relies more on the repeatability of the timestamps, rather than their accuracy. For example, the peripheral TSADC timestamp is created and associated with the final ADC sample in a packet. But, this clock query is completed after the final ADC sample has been acquired and within the resulting ADC software interrupt service routine. In other words, this timestamp always represents a time that is slightly delayed from the actual time at which that last ADC sample is converted. However, this time difference should be small (a few μs). More importantly, this time difference should be very similar on the two peripherals. So long as both peripherals experience the same repeatable delay, their synchronization is preserved.

More concerning is the central timestamp TSC, which is generated by querying the central clock after peripheral data have been received and then adding one connection interval to this value. The precision of this timestamp depends on the reliability of wireless transmission from the peripheral to the central and then (at the next connection interval) from the central to the peripheral. These external delays should be less reliable; hence our use of a synchronization algorithm to average out the timestamp data from several update intervals via regression.

Our laboratory environment happened to have few other active BLE devices, resulting in the Bluetooth 2.4 GHz transmission frequency band experiencing limited use. Thus, we experience limited "blocked" transmissions. A blocked transmission occurs when a given wireless frequency channel is in use; hence the scheduled transmission does not have channel access. When BLE transmission is blocked, BLE will wait an additional connection interval and then re-attempt transmission. This action is not reported to the application-layer software. When a central to peripheral transmission is blocked and delayed by one connection interval, the central clock timestamp becomes stale (incorrect) by one connection interval in our scheme. The

connection interval (10 or 15 ms, depending on the platform) is much longer than our average absolute errors. We anecdotally found much higher absolute errors during the few times in which transmission was blocked. In other laboratory or field settings, this issue may be much more prevalent.

3.6.3 Future Work: Correcting Errors Due to Blocked Central Timestamps

Because blocked central to peripheral transmissions led to large but fixed errors in the central timestamp TSC, they likely can be detected and corrected (by subtracting one connection interval from the timestamp). Doing so on our available dataset was not feasible, since our rate of blocked transmissions was quite small (estimated below 0.001%). Thus, we simulated this condition. Using an update rate of 100 ms, we created one hour's worth of central timestamps at equal timestamp intervals. We then created the matching peripheral timestamps with a time offset error drawn from an independent, random, uniform distribution ranging from 0-1.25 ms. This span is representative of the errors found in our TI and Nordic platforms. Finally, we treated each central timestamp as a Bernoulli trial, adding a 10 ms delay with a selection probability of 0.1%. Hence, on average, one in every thousand central timestamp updates was treated as having been blocked. This blocking rate is artificially high compared to our dataset, but useful in simulation. We then independently analyzed our timestamp pairs to determine if we could detect blocked transmissions. In fact, applying a threshold test to a slope parameter, formed as a ratio of the difference of the last two central timestamps to the difference of the last two peripheral timestamps, led to correct detection of every blocked transmission. Of course, detection is likely more complex in practice. In particular, a transmission can be blocked for several transmit cycles.

3.7 Conclusion

We developed a time synchronization algorithm and data alignment method that operates at the BLE application layer, with low-latency applications. The method is easily transferred from one BLE platform to another and was demonstrated herein on two platforms. The method separately synchronizes each peripheral to the central. As a result, multiple peripherals are mutually synchronized. The 95th percentile absolute errors for both the TI and Nordic platforms were less than 1.8 ms, which is appropriate for use by most ECG, EEG and EMG applications. The 95th percentile results were not particularly sensitive to the timestamp update interval or the number of timestamp pairs used in the time synchronization model. Additional evaluation is warranted in environments in which blocked Bluetooth transmissions are likely. Although the method should scale to systems with many peripheral nodes, evaluation in such systems is an appropriate next step.

Chapter 4: Reducing Electric Power Consumption when Transmitting ECG/EMG/EEG using a Bluetooth Low Energy Microcontroller

This chapter has been published as a conference paper as J. Li, M. Bhuiyan, X. Huang, B. McDonald, T. Farrell and E. A. Clancy *"Reducing Electric Power Consumption when Transmitting ECG/EMG/EEG using a Bluetooth Low Energy Microcontroller," 2018 IEEE Signal Processing in Medicine and Biology Symposium (SPMB), Temple University, Philadelphia, PA, 1 December 2018.* Color versions of one or more of the figures in this paper are available online at https://ieeexplore.ieee.org/document/8615626.

Abstract— **Low-power wearable sensors now have sufficiently high sampling rates and bandwidth to support acquisition of electrophysiologic signals (e.g., ECG/EMG/ EEG) (Cosmanescu, Miller et al. 2006, Belgacem and Bereksi-Reguig 2011, Gomez, Oller et al. 2012). But, these higher sampling rates are associated with higher power consumption, greatly reducing battery life (Kamath and Lindh 2012, Nair, Kulkarni et al. 2015). Thus, we examined average power consumption in a commercial Bluetooth low energy microcontroller (TI CC2640R2 BLE Module) while varying transmission power (maximum vs. minimum available), time interval between transmissions (10 ms to 5 s), sampling frequency (1000 to 4000 Hz), and transmit payload size (all samples vs. one "processed" value per interval); since each of these variants can influence power consumption (Balani 2007, Dementyev, Hodges et al. 2013). Neither sampling rate nor payload size noticeably altered power consumption. Increased transmit power, as expected, increased power consumption. Longer transmit intervals reduced power consumption, with most of this advantage occurring by intervals as small as 50–100 ms. Thus, relatively low latency ($\leq$ 100 ms), low power signal acquisition is supported by these commercial modules, without particular regard to payload size or sampling rate.**

We developed a prototype wireless electrophysiologic acquisition system, applicable to ECG/EMG/EEG signals, comprised of an analog front end and a Bluetooth low energy microcontroller (TI CC2640R2 BLE Module). The front end (see (Neuman 1998)) consisted of an instrumentation amplifier (AD8422), passive band pass filtering, and DC-shifting of the signal into the range of the on-board, unipolar, 12-bit ADC. A set of average electrical current consumption measurements was made while varying all combinations of Bluetooth transmission power (+5 dBm = maximum power, +0 dBm = minimum power), the time interval/latency between transmissions (10, 20, 50, 100 ms), the sampling frequency (fSample =

1000, 2000, 4000 Hz) and the processing-transmission mode (transmit raw two-byte signal vs. transmit one byte per interval—representing on-board signal processing, which greatly reduces channel bandwidth). Average current consumption was measured by inserting a small resistance (1.2 Ω) in series with the 3.3 V battery and then averaging voltage across it for 30 s with a hand-held digital multimeter (RSR MAS830, resolution of 0.1 mV). We separately measured current in the analog front end and in the TI CC2640R2 BLE module.

For all conditions, the analog front end average current consumption was 0.8–0.9 mA. Neither sampling rate nor processor-transmission mode substantively altered this consumption (Table 4.1). These conditions vary the transmit payload, since longer intervals communicate more samples per transmit cycle. Thus, the volume of data transmitted had no practical influence on Bluetooth module power consumption.

However, transmit power and interval had a noticeable influence on average current—larger transmit powers and shorter intervals led to larger currents. We further tested transmit intervals of 500 ms, 1 s, 2 s and 5 s (f_{Sample} = 4000 Hz, Mode = one datum/cycle, lower transmit power). In each case, Bluetooth module average current was 0.8–0.9 mA—essentially its minimum. Thus, Bluetooth module current was maximum at the shortest transmit interval of 10 ms, (2.3 mA) but fell rapidly with increasing interval, quickly approaching its minimum. Overall, power consumption was not substantively influenced by sampling rate or payload size, and transmit intervals above ~50 ms consumed power indistinguishable from minimum power. Transmit power, as expected, directly influenced power consumption. In applications, choice of transmit power level will be influenced by the necessary transmit distance and the ambient environmental electronic noise level (Pahlavan and Krishnamurthy 2009, Pahlavan and Krishnamurthy 2013).

Transmit Power = +5 dBm (Maximum)

	Raw Signal f_{Sample} (Hz)			One Byte/Interval f_{Sample} (Hz)		
Interval	1000	2000	4000	1000	2000	4000
10 ms	3.0	3.0	3.1	3.0	3.0	3.0
20 ms	1.9	1.9	1.9	1.9	1.9	1.9
50 ms	1.2	1.2	NA	1.2	1.2	1.3
100 ms	1.0	NA	NA	1.0	1.1	1.0

Transmit Power = +0 dBm (Minimum)

	Raw Signal f_{Sample} (Hz)			One Byte/Interval f_{Sample} (Hz)		
Interval	1000	2000	4000	1000	2000	4000
10 ms	2.3	2.4	2.4	2.3	2.4	2.3
20 ms	1.6	1.6	1.6	1.7	1.7	1.8
50 ms	1.0	1.0	NA	1.0	0.9	1.0
100 ms	0.9	NA	NA	0.9	NA	NA

Table 4.1. Current consumption (mA) of the TI CC2640R2 BLE Module (excludes analog front end current). "NA" denotes packet size too large or unreliable transmission.

Chapter 5: Myoelectric Control Performance of Two Degrees of Freedom Hand-Wrist Prostheses by Able-Bodied and Limb-Absent Subjects

Abstract— **Recent research has advanced two degree-of-freedom (DoF), simultaneous, independent and proportional control of hand-wrist prostheses using surface electromyogram signals from remnant muscles as the control input. We evaluated two such regression-based controllers, along with conventional, sequential two-site control with co-contraction mode switching (SeqCon), in box-block, refined-clothespin and door-knob tasks, on 10 able-bodied and 4 limb-absent subjects. Subjects operated a commercial hand and wrist using a socket bypass harness. One 2-DoF controller (DirCon) related the intuitive hand actions of open-close and pronation-supination to the associated prosthesis hand-wrist actions, respectively. The other (MapCon) mapped myoelectrically more distinct, but less intuitive, actions of wrist flexion-extension and ulnar-radial deviation. Each 2-DoF controller was calibrated from separate 90 s calibration contractions. SeqCon performed better statistically than MapCon in the predominantly 1-DoF box-block task (>20 blocks/minute vs. 8–18 blocks/minute, on average). In this task, SeqCon likely benefited from an ability to easily focus on 1-DoF and not inadvertently trigger co-contraction for mode switching. The remaining two tasks require 2-DoFs, and both 2-DoF controllers each performed better (factor of 2–4) than SeqCon. We also compared the use of 12 vs. 6 optimally-selected EMG electrodes as inputs, finding no statistical difference. Overall, we provide further evidence of the benefits of regression-based EMG prosthesis control of 2-DoFs in the hand-wrist.**

Index Terms— **Prosthesis control, EMG-force, EMG signal processing, Electromyogram, Myoelectric control.**

5.1 Introduction

More than two million people live with limb absence in the U.S., and this number increases by an average 185,000 each year (McGimpsey and Bradford , Dillingham, Pezzin et al. 2002, Limb Loss Task Force/Amputee Coalition 2012). Trans-radial amputations make up 60% of total wrist and hand amputations, and documented rates of prosthesis use vary from 27–56% for upper-limb amputation (Ziegler-Graham, MacKenzie et al. 2008). The high demand for prostheses, expected to increase by at least 47% by the year 2020, has brought more support from government and growth of the market (Nielsen 2002).

While laboratory-based research on electromyogram (EMG) control has generated new strategies based on machine learning algorithms, most commercial prostheses still use simple two-site control schemes that have been available for decades (Sherman 1964). Typical myoelectric prosthesis sockets are designed with two bipolar electrodes, one each located over extensor and flexor muscles, to control one degree-of-freedom (DoF) prosthesis hand open and close (Opn-Cls), respectively. Kestner (Kestner 2006) found need for a prosthetic wrist, as the fixed angle of a prosthetic hand is not compatible with all daily tasks (e.g., holding flatware for eating, a bottle for drinking). Although some advanced prostheses have a wrist rotator and users can co-contract their muscles to switch between hand open-close and wrist pronation-supination (Pro-Sup) (Lovely 2004, Fougner, Stavdahl et al. 2012), users mostly employ their body and arm/shoulder movement for compensation instead (Ross 2005, MacPhee 2007, Bertels, Schmalz et al. 2009). Prosthesis mode switching, a.k.a. sequential 2-DoF control via co-contraction mode switching, allows users to rotate the wrist with a complex and time-consuming approach (2004). Performance of this technique is highly influenced by a user's residual limb condition, since muscle contraction imbalance or neuron damage impede co-contraction; and users need a long period of time to master this skill, but easily fatigue (Popovic 2003).

Features extracted from myoelectric signals train models to estimate users' intent. Regression modeling is one learning approach used to realize simultaneous, independent and proportional multi-DoF control (Jiang, Englehart et al. 2009, Clancy, Liu et al. 2012, Liu, Liu et al. 2015, Hahne, Markovic et al. 2017, Piazza, Rossi et al. 2020). Compared with classification models, of which numerous varieties have been investigated (Alkan and Gunay 2012, Al-Timemy, Bugmann et al. 2013, Roche, Lakey et al. 2019, Ameri, Akhaee et al. 2020, Teh and Hargrove 2020, Farina, Vujaklija et al. 2021), the continuous outputs of regression estimates may more naturally mimic human movement. Regression models have been found to be more robust to some unpredictable small variations in EMG signals, such as fatigue or poor contact of electrodes, and may generate better performance during untrained conditions compared to classification models (Hahne, Markovic et al. 2017).

Most upper-limb myoelectric control users can easily operate hand open-close via the two-site conventional approach. But for wrist rotation—although most limb-absent users can easily rotate their residual limb repeatedly—the supinator (a wrist rotator) is a deep muscle difficult to record using surface EMG (Gilroy, MacPherson et al. 2008, p. 328–336), and electrodes often shift during forearm rotation. These factors challenge the usability of surface EMG signals. As an alternative, researchers assessed offline other wrist motions of extension-flexion (Ext-Flx) and radial-ulnar deviation (Rad-Uln), especially since the EMG signal during Rad-Uln has demonstrably distinct patterns compared with the other wrist motions (Rojas-Martinez, Mananas et al. 2012). In the context of proportional control of multiple DoFs, "distinct" patterns are most clearly demonstrated when unique EMG channels record large amplitude EMG when contracting directly along one motion (e.g., radial deviation) and low amplitude EMG when contracting directly along all other motions. These results provide a potential 2-DoF control strategy by a corresponding "motion" mapping/translation.

Some prior lab-based prostheses testing of multiple-DoF control schemes used a large number of electrodes, or matrix electrodes. Such systems are not practical in current commercial prostheses due to cost and issues of electrode shorting/lift-off. Some researchers found that at least 4 electrodes were necessary to realize 2-DoF control, with improvement occurring if the number of electrodes increased (Parker, Englehart et al. 2006, Peerdeman, Boere et al. 2011, Dai, Zhu et al. 2019). A balance can be found between economic benefits and product quality if an optimal number of electrodes and their location were decided (Clancy, Martinez-Luna et al. 2017, Dai, Zhu et al. 2019).

Recent laboratory work studied myoelectric control using a 2-D virtual target tracing task, assessing performance via path efficiency, completion time, and attempt-ratio (Igual, Igual et al. 2019). Others have studied the influence of training protocol (Dyson, Dupan et al. 2020), or of using modeling techniques of myoelectric representation learning (MRL) (Olsson, Malesevic et al. 2021), principle component analysis (PCA) (Dyson, Dupan et al. 2020), and frequency division technique (FDT) (Pradhan, Kuruganti et al. 2020). Real 2-DoF prosthesis control during either laboratory or home study found a potential advantage of regression-based controllers (Hahne, Schweisfurth et al. 2018) and classification-based (Amsuess, Goebel et al. 2015, Kuiken, Miller et al. 2016) in multi-DoF control compared with conventional control strategies.

Different regression-based approaches have been evaluated offline and online (e.g., (Zhu, Martinez-Luna et al. 2020)). Most studies have used commercial prosthesis hardware, with custom controllers. Electrode site selection is usually circumferential around the forearm (for hand-wrist prosthesis) with equal inter-electrode distances, or manually selected based on residual anatomy. The number of electrodes used has varied. A few studies have combined pattern recognition with proportional control (Simon and Hargrove 2011, Scheme, Lock et al. 2014) (as have some commercial products). A fundamental limitation of all of this

work is the limited sample size (often ≤10), which seems necessitated by the complexity and cost of such studies (Barnett, Heinemann et al. 2012, Hafner and Sawers 2016). The aggregate sample size of limb-absent subjects that have tested such systems is even smaller (as small as one limb-absent subject in some studies). Hence, there exists no standard approach to regression-based multi-DoF simultaneous, proportional control of prostheses, particularly in controller calibration, regression method, number of electrodes used, electrode site selection, etc.; nor have its advantages vs. disadvantages with respect to other control approaches been adequately understood.

In this paper, we assessed regression-based simultaneous, independent and proportional 2-DoF (hand-wrist) myoelectric prosthesis control on both able-bodied and limb-absent subjects, comparing three control strategies—Opn-Cls & Pro-Sup direct control, a new Ext-Flx & Rad-Uln mapping control with translation, and conventional two-site sequential control. Six or twelve optimally-sited electrodes (out of 16 total) were tested on a prosthesis to investigate the minimum number of electrodes feasible on commercial prostheses. Bypass brackets were designed separately for able-bodied and limb-absent subjects to carry a hand-wrist prosthesis adjacent to the forearm/residual limb. Each bypass allowed subjects to don the prosthesis without a socket, while allowing access to the limb for electrode placement. The three control strategies were tested with different standard physical tasks—box-block, refined-clothespin relocation and door-knob (the latter two requiring use of 2-DoFs). Six vs. twelve optimally-selected electrodes were tested to explore the minimum number of necessary electrodes for able-bodied subjects. Based on these results, more targeted tasks were conducted on limb-absent subjects.

5.2 Methods

5.2.1 Experimental Apparatus

Experimental data were collected from 10 able-bodied (5 male, 5 female; aged 18–45 years) and 4 trans-radial limb-absent (3 male, 1 female; aged 39–65 years; 2 congenital, 2 traumatic amputee) subjects at Worcester Polytechnic Institute (WPI), as approved by the WPI Institutional Review Board (IRB Protocol 17-155). Able-bodied subjects had no physical limitations of their dominant forearm muscles. Limb-absent subjects had ≥5 cm residual limb length with functional muscle contraction and prior experience with myoelectric-controlled prostheses. Subjects provided written informed consent.
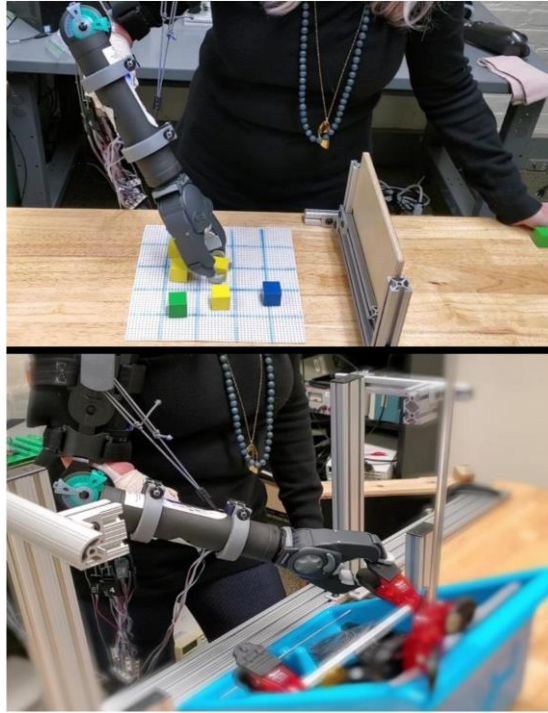
Fig. 5.1. Experimental apparatus for box-block (top) and clothes pin (bottom) tasks, limb-absent subject. The subject was asked to wear a bypass bracket that attached a hand-wrist prosthesis. The forearm could move freely.

Subjects stood at the experimental table, adjusted to hip height (Fig. 5.1). Sixteen bipolar EMG electrodes were secured on the proximal forearm, equally spaced about the forearm's circumference. For able-bodied subjects, electrodes were secured on the dominant side with the midpoint of the bipolar contacts placed 5 cm distal to the elbow crease. For limb-absent subjects, electrodes were secured on the affected side at the level corresponding to that of their own prosthesis. Each bipolar electrode consisted of 5 mm diameter, stainless steel, hemispherical contacts separated 1 cm edge-to-edge, oriented along the forearm's long axis. Each EMG signal was differentially amplified (Liberating Technologies, Inc. BE328 amplifier; 30–500 Hz pass band, CMRR>100 dB over the pass band) and provided selectable gain. All EMG channels were sampled at 2000 Hz on a PC (16-bit resolution).

Then a 3D printed bypass prosthesis bracket was strapped to the shoulder and arm on the same side as the electrodes (Fig. 1). A wrist rotator (Fillauer Motion Control Standard Wrist Rotator, maximum speed 28 rpm) and prosthetic terminal device (System Electric Greifer DMC Plus, proportional speed 8–200 mm/sec) extended from the bypass, providing wrist Pro-Sup and hand Opn-Cls, respectively. The electrodes (input) and the prosthesis control signals (output) were part of a PC-based system programed in MATLAB (The MathWorks, Natick, MA, USA) (Boyd 2018). The main processing loop of this system operated at 100 Hz so as to minimize controller delays.

5.2.2 Prostheses Control System

1) Control Sources: Subjects compared two regression-based 2-DoF simultaneous, independent and proportional velocity control algorithms, and conventional two-site velocity control. Limb-absent subjects controlled the prostheses by attempting to move their phantom limb. The control algorithms were as follows. 1) Direct control (DirCon) in which subjects' Opn-Cls controlled Greifer Opn-Cls, and subjects' Pro-Sup controlled prosthetic wrist rotation. This 2-DoF approach is the most intuitive. 2) Direct control with mapping/translation (MapCon) in which subjects' wrist Ext-Flx controlled Greifer Opn-Cls (Ext corresponded to Opn), and subjects' Rad-Uln controlled prosthetic wrist rotation (Rad corresponded to pronation). Subjects were permitted to invert either/both of these mappings (although none chose to do so). 3) Sequential control (SeqCon) in which subjects controlled either Opn-Cls or Pro-Sup, then switched between them by triggering a co-contraction EMG signal. Co-contraction was defined as a simultaneous contraction of both processed forearm EMGs (processing described below) above set thresholds for a defined time duration (1982, Gribble, Mullin et al. 2003). Each respective threshold was set between the EMG values triggered during a maximum co-contraction and normal hand-wrist tasks, as selected by the subject. The time duration was set between 30–100 ms, again selected by subject preference.

2) Control Calibration and Thresholding: For calibration of DirCon and MapCon (Fig. 5.2), subjects performed a 90 s calibration consisting of 10-s of rest and eight distinct 10-s, contiguous constant-posture constant-force contractions (four 1-DoF and four 2-DoF). Since maximum voluntary contraction (MVC) cannot be measured on the affected side of prosthesis users, all subjects were instructed to maintain, as best as possible, a contraction target effort of 30%—without feedback. MVC was not measured in either the able-bodied or limb-absent subjects. For DirCon, the contraction sequence was: Cls, Opn, Sup, Pro, Cls+Sup, Cls+Pro, Opn+Sup, and Opn+Pro. For MapCon, the contraction sequence was: Flx, Ext, Uln, Rad, Flx+Uln, Flx+Rad, Ext+Uln, and Ext+Rad. Raw EMG signals from all channels were digitally notch filtered (second-order IIR filter at 60 Hz, notch bandwidth of 1 Hz), highpass filtered to attenuate motion artifact (fc=15 Hz, fifth-order Butterworth filter), rectified, lowpass filtered (fc=16 Hz; Chebyshev Type I filter, ninth-order, 0.05 dB peak-to-peak passband ripple) and downsampled from 2000 Hz to 100 Hz. Then, a critically damped
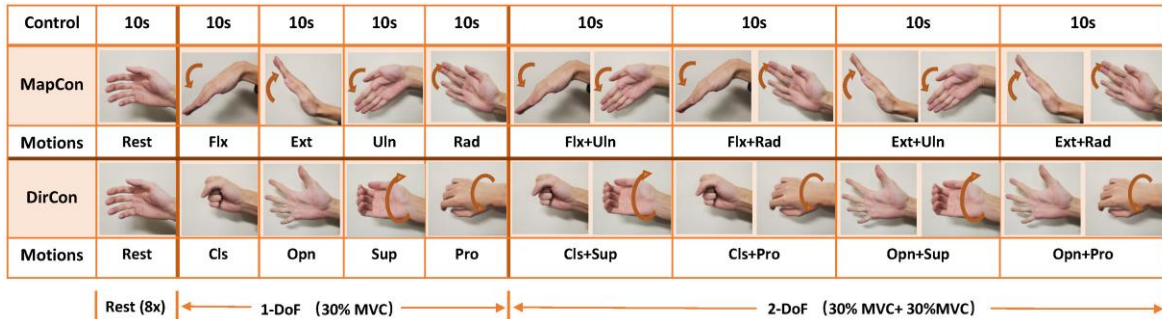
Fig. 5.2. Sequence of calibration contractions. Subjects follow the instructions to perform indicated constant-pose, constant-force contractions over 90 s. The recording was used for coefficient calculation and calibration quality assessment.

lowpass filter (fc=1 Hz, second-order) (Robertson and Dowling 2003) was applied to further smooth the signal and estimate EMG standard deviation (EMGσ, a.k.a. processed EMG). The first and last second of each 10 s contraction was removed to avoid filter and movement transients. Then, each EMGσ from the resting contraction (weighted eight times) and the eight active contractions were used as inputs to a regression-based (2-output) static EMGσ-force model. Re-using one rest contraction balances the weight of the regression fit, without extending its duration. A force of zero was assigned as the output target for unused DoFs during each contraction. Fit coefficients were estimated via the linear least squares pseudo-inverse method, in which singular values of the design matrix were removed if the ratio of that singular value to the largest was less than a tolerance value (Tol=0.01, based on previous study) (Dai, Bardizbanian et al. 2017). Backward stepwise selection was utilized for optimal selection of either 6 or 12 electrodes (out of 16 total). In this manner, only the best channels yielding the lowest RMSE between EMG-force and target force were used, and their gains were calculated for prostheses control. In addition, this RMSE provided an assessment of the calibration quality
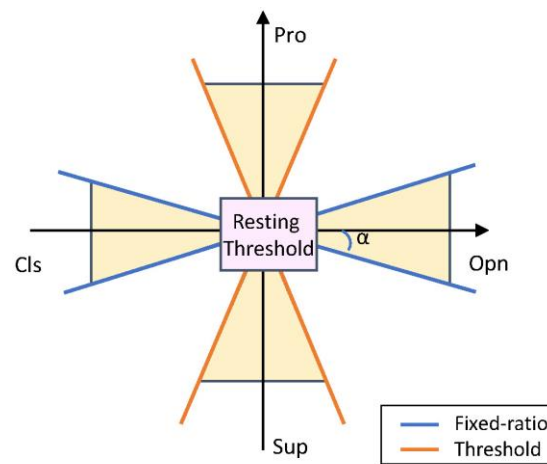
Fig. 5.3. Calibration examples for a) MapCon and b) DirCon. Dashed red line segments show target force level. Wavy blue lines show model-estimated force.

During experimental trials using DirCon and MapCon, EMG-force was computed in real-time, then two thresholding methods were applied. First, a resting threshold was applied to each direction of the two individual DoFs (total of four thresholds) to minimize the impact from noise and unintentional EMGσ signals. Initially, the threshold was set to 10 %MVC for each direction. Then, subjects were asked to rest and to slowly move their arm. If unintentional prosthesis movement resulted, the corresponding threshold was slightly increased until no movement occurred. Second, a fixed-ratio co-activation thresholding method was applied to attenuate the risk of inadvertent activation of another DoF (Fig. 5.3). When the ratio of the larger force (in %MVC) to the smaller force (from the two DoFs) was less than a threshold, only the DoF with the larger force was actuated. If the two forces are drawn in the x-y plane, a default threshold angle of α=25

degrees (Fougner, Stavdahl et al. 2014) was used. This angle could be changed during setup as desired by the subject.

For SeqCon, the two channels which produced the most distinct EMGσ (based on channel amplitudes) when subjects performed Ext and Flx calibration, respectively, were manually chosen. For limb-absent subjects, we selected EMG sites near the location of the sites used by their existing two-site prosthesis controller, whenever multiple distinct channel options existed. Each channel gain was set to correspond to 30% MVC. The estimated force was calculated as the algebraic difference of the forces estimated by each channel. A resting threshold was applied to each channel to reduce the influence of noise and small unintentional activation. For switching between the 2 DoFs, a fixed window size (30–100 ms) and a co-contraction threshold were set to detect a co-contraction. All the channels and coefficients were manually calibrated until subjects could easily control the prostheses and trigger co-contraction.

3) Hardware Control: The estimated hand and wrist force levels, in %MVC, were linearly mapped to hand and wrist velocity (speed and direction), with 50% MVC in each corresponding to maximum speed. Built-in hardware thresholds were essentially disabled by matching the software thresholds to them. Thus, all thresholding was set in our custom software.

5.2.3 Experimental Protocol

Subjects stood for all tasks, but otherwise their posture was not constrained (Fig. 5.1). To prevent cumulative muscle fatigue, at least two minutes rest after calibration and one minute rest between trials were provided. All limb-absent subjects completed 10–20 minutes of mirror-box training before the trials to help rebuild their phantom limb control sensation. The two traumatic amputees had prior mirror-box training experience.

To assess controller performance, three tasks were chosen from widely-used outcome measures described in the literature. 1) The box-block task (Mathiowetz, Volland et al. 1985) was a 1-DoF assessment mainly testing hand Opn-Cls. Subjects grasp (hand Cls) a block and then drop it (hand Opn) after traversing over a partition. They return back over the partition and repeat. We did not lock the prostheses into 1-DoF control during this task. The number of transferred blocks in 60 s and number of drops were measured in each trial. 2) The refined-clothespin relocation task (Hussaini and Kyberd 2017) was a 2-DoF assessment. Subjects perform hand Cls to grasp a clothespin (2 lbs. resistance) from a horizontal rod, rotate the clothespin 90o (wrist Pro or Sup), then place and release (hand Opn) the clothespin onto a vertical rod. Once complete, subjects rotate their wrist back to its original orientation and attempt to relocate another clothespin. Subjects were allowed to use arm or body movement for compensation. If the clothespin dropped, subjects moved on to the next clothespin. The time required to complete three successful moves (maximum of 120 s) and number

of drops were measured in each trial. 3) The doorknob task was a 2-DoF assessment. Opening a door is a common but important task that most people face every day. Compared with the SHAP door-handle test (Light, Chappell et al. 2002), our task used a round knob so as to require actuation of both the wrist and hand—more appropriate for 2-DoF assessment. During each task cycle, subjects grasped the round knob of the door (hand Cls), rotated the knob (wrist Pro or Sup), pulled the door open, and then released the knob (hand Opn). Subjects then shut the door to ready for the next trial. The time required to complete three successful door openings (maximum of 120 s) was measured in each trial.

Three control strategies (DirCon, MapCon, SeqCon) were tested on all subjects. Subjects initially performed calibration, then used all 16 electrodes to test all motions and their combinations. Thresholds were adjusted, based on their feedback, to enhance control robustness and accuracy. If it was still difficult to control the prostheses, all subjects were offered at most three calibrations and chose the best one for the tasks. These calibration steps, combined with subject practice, typically lasted 20–30 minutes per controller. Additional time was provided, as needed, until each subject confirmed that they were comfortable controlling the prosthesis. Then for control tasks, able-bodied subjects used DirCon and MapCon with either 6 or 12 electrodes (backward selected). Limb-absent subjects only used 6 electrodes for DirCon and MapCon, to shorten the experiment length to prevent fatigue. All subjects used SeqCon with 2 electrodes (manually selected, as described above). The three control strategies, number of electrodes used (only varied for able-bodied subjects) and three tasks were randomized during the experiment. Subjects were blinded to the number of electrodes in use. Three trials of data were collected for each condition.

5.2.4 Statistics

1) Calibration Quality Assessment: The RMSEs from the calibration quality assessment satisfied the normality assumption. Thus, repeated measures analysis of variance (RANOVA) and post hoc paired t-tests with Bonferroni correction (significance level p = 0.05) were used to test for RMSE differences. Prior to RANOVA, the degree of sphericity (ε) was used to adjust the degrees of freedom by either the method of Greenhouse-Geisser (ε < 0.75) or Hyunh-Feldt (0.75< ε <1). Each RANOVA assessed all possible interactions. These interactions were not significant, unless noted otherwise in the Results. When interactions were found, we proceeded to post hoc pair-wise comparison of all factor combinations, since the number of combinations was small.

2) Task Outcomes Involving Able-Bodied Subjects: (including comparisons between able-bodied and limb-absent subject results): We separately averaged each outcome measure (number of box-block transfers, time per clothespin transfer, and time per door open and close cycle) across the three trials per condition. Prior to each statistical test, we evaluated the normality assumption of the test data. The number of drops per

trial in box-block and clothespin tasks failed the normality test, thus a non-parametric Friedman test was used to test performance differences. All other outcome measures satisfied the normality assumption. Thus, RANOVA and post hoc paired t-tests with Bonferroni correction were used to test performance differences. Adjustments for degrees of freedom and treatment of interactions were performed as described above.

3) Task Outcomes Involving Only Limb-Absent Subjects: When comparing performance within a task for the limb-absent subjects, our subject pool was quite heterogeneous (2 congenital and 2 traumatic limb loss; distinct remnant musculature for each; distinct past experience with myocontrol for each), thus performance differences were tested using "n-of-1" statistical analysis (i.e., separate statistical analysis for each subject). The n-of-1 approach has been used before in prosthesis control research (Hahne, Schweisfurth et al. 2018) and is well suited for heterogeneous subject pools with chronic conditions (Duan, Kravitz et al. 2013). Thus, we separately conducted RANOVA (after confirming data normality) and post hoc t-tests with Bonferroni correction for each subject, without averaging the three trials per condition. Adjustments for degrees of freedom and treatment of interactions were performed as described above.

5.3 Results

5.3.1 Calibration Quality Assessment

Fig. 5.4 shows example target force levels and EMG-estimated forces for a set of calibration trials. Fig. 5.5 summarizes across subjects the RMSE between the target %MVC and that estimated from EMGσ of each calibration contraction type, separately for able-bodied and limb-absent subjects, and number of electrodes retained after backward stepwise selection. Both hand and wrist errors always contributed to the RMSE, even during 1-DoF tasks. This assessment describes how well subjects can produce the desired calibration contraction, which forms the basis of the 2-DoF control algorithms.
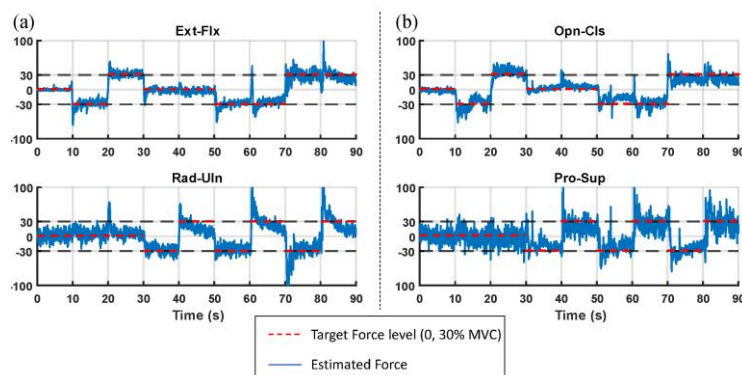
Fig. 5.4. Thresholding methods for 2-DoF control including resting (inner square) and fixed-ratio thresholding (blue and red lines emanating from inner square). Based on method of Fougner *et al.* (Fougner, Stavdahl et al. 2014).

For able-bodied subjects, a three-way RANOVA of RMSE was computed with factors: control strategy (DirCon, MapCon), number of electrodes (6, 12) and calibration contraction type (9 values, see Fig. 5.5). A significant interaction was found between control strategy and number of electrodes [F(1,9)=16.0,p=0.002],

while calibration contraction type was significant [$F(8,72)=43.2, p<10^{-6}$]. Post hoc comparison of the interacting factors found that for both DirCon and MapCon, 12 electrodes had lower RMSE than 6 electrodes ($p \leqslant 10^{-4}$). For contraction type, rest always had lower RMSE than all other types ($p<10^{-4}$), Cls / Flx exhibited lower RMSE than Pro / Rad (p=0.005), Cls+Sup / Flx+Uln (p=0.003), Cls+Pro / Flx+Rad (p=0.006) and Opn+Sup / Ext+Rad ($p=10^{-4}$); Opn / Ext had lower RMSE than Opn+Sup / Ext+Rad (p=0.004); and Sup / Uln had lower RMSE than Cls+Pro / Flx+Rad (p=0.012) and Opn+Sup / Ext+Rad (p=0.026).
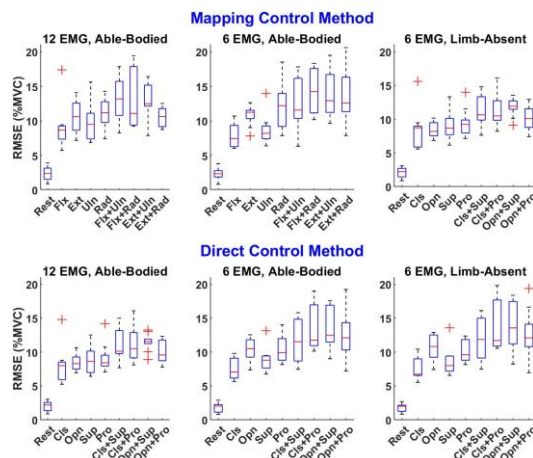
Fig. 5.5. Calibration quality assessment boxplots. RMSE for each contraction type under different control methods (MapCon, DirCon) and number of EMG electrodes (6, 12) for both able-bodied and limb-absent subjects.

For limb-absent subjects, a two-way RANOVA with factors control strategy and segment found only segments was significant [$F(1.5,4.5) = 19.1, p_{GG} = 0.007$]. Post hoc comparison only found rest motion had lower RMSE than all others ($p < 0.04$).

5.3.2 Box-block Task

For able-bodied subjects (see Fig. 5.6 for summary results), the number of transfers in one minute, where more transfers represented better performance, was compared between 2-DoF control strategies (MapCon, DirCon) and number of electrodes (6, 12) via a two -way RANOVA. No statistical differences were found.

Next, we limited analysis of the 2-DoF control strategies to trials using 6 electrodes, available for both able-bodied and limb-absent subjects (see Fig. 5.6 for summary results). For number of transfers, a mixed two-way RANOVA with within-subjects factor of control strategy (DirCon + 6 electrodes, MapCon + 6 electrodes, SeqCon + 2 electrodes) and between-subjects factor of group (able-bodied, limb-absent) found control strategy to be statistically different [$F(2,24)=21.62, p<0.00001$], but group was not [$F(1,12)=3.285, p=0.095$]. Post hoc comparison found that SeqCon transferred significantly more blocks than both MapCon (p<0.001) and DirCon (p=0.004). Note that while using SeqCon on this task, mode switching was not disabled. Nonetheless, the task was completed predominantly using only the hand DoF, and

body/elbow/shoulder movement. Separately, a Friedman test on number of drops per trial (able-bodied subjects only) found no significant difference between the three control strategies.
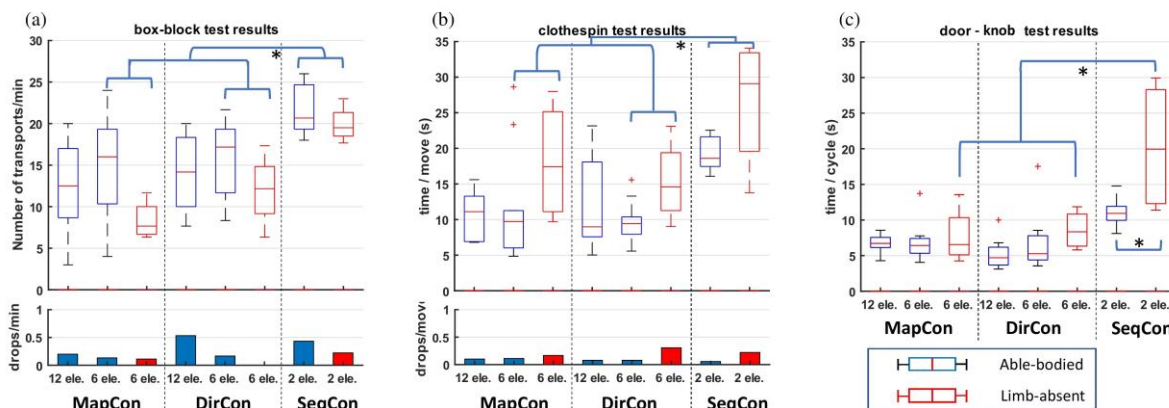
Fig. 5.6. Boxplot results for a) box-block task (number of transfers per minute, drops per minute), b) clothespin task (time per move, drops per successful move), c) door-knob task (time per open/close cycle).

Additionally for each limb-absent subject, the number of transfers in one minute (see Fig. 5.7) was compared between three different control strategies (MapCon+6 electrodes, DirCon+6 electrodes, SeqCon) via a one-way RANOVA, with post hoc comparison made when a significant difference was found. The three trials per condition were not averaged. For three of the four subjects, the RANOVA was significant $[F(2,6)>27, p \leq 0.001]$, with post hoc comparison showing that SeqCon transferred more blocks (by a factor of 2–4) than either MapCon or DirCon ($p < 0.038$). For two of the associated post hoc evaluations, DirCon also transferred more blocks than MapCon ($p < 0.038$).

5.3.3 Refined Clothespin Relocation Task

For able-bodied subjects (Fig. 5.6), the time per move, where shorter time represented better performance, was compared between 2-DoF control strategies (MapCon, DirCon) and number of electrodes (6, 12) via a two-way RANOVA. No statistical differences were found.

Next, we limited analysis of the 2-DoF control strategies to trials using 6 electrodes, available for both able-bodied and limb-absent subjects (Fig. 5.6). For time per move, a mixed two-way RANOVA with within-subjects factor of control strategy (DirCon + 6 electrodes, MapCon + 6 electrodes, SeqCon + 2 electrodes) and between-subjects factor of group (able-bodied, limb-absent) found control strategy to be statistically different $[F(1.27,15.24)=16.97, p_{GG}<0.0001]$, but group was not $[F(1,12)=0.007, p=0.93]$. Post hoc comparison found that SeqCon took significantly longer time than both MapCon ($p=0.003$) and DirCon ($p=10^{-5}$)). Separately, a Friedman test on number of drops per successful move (able-bodied subjects only) found no significant difference between the three different control strategies.

Additionally, for each limb-absent subject, time per move (Fig. 5.7) was compared between three different control strategies (MapCon+6 electrodes, DirCon+6 electrodes, SeqCon) via a one-way RANOVA,
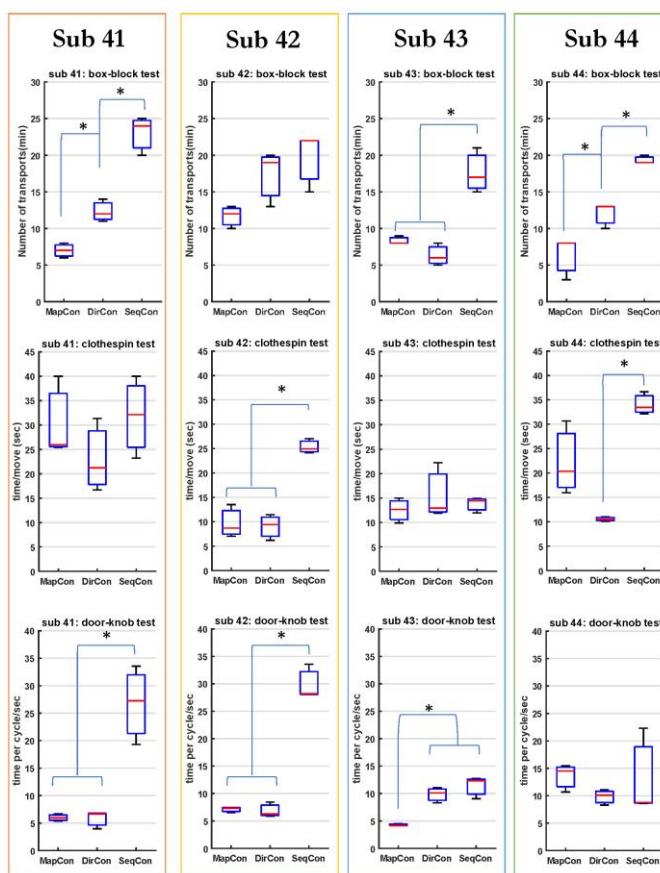
Fig. 5.7. Boxplot results for each limb-absent subject for the box-block task (top row), clothespin task (middle row), and door-knob task (bottom row).

with post hoc comparison made when a significant difference was found. The three trials per condition were not averaged. For two of the four subjects, the RANOVA was significant [$F_{(2,6)}=11, p\leq0.009$], with post hoc comparison in both showing that SeqCon required more time (poorer performance) than DirCon ($p \leq 0.01$). For one of these subjects, SeqCon also required more time than MapCon ($p = 0.001$).

5.3.4 Door-Knob Task

For able-bodied subjects (Fig. 5.6), the time per door-open-close cycle, where shorter time represented better performance, was compared between 2-DoF control strategies (MapCon, DirCon) and number of electrodes (6, 12) via a two -way RANOVA. No statistical differences were found.

Next, we limited analysis of the 2-DoF control strategies to trials using 6 electrodes, available for both able-bodied and limb-absent subjects. For time per cycle, a mixed two-way RANOVA with within-subjects factor of control strategy (DirCon + 6 electrodes, MapCon + 6 electrodes, SeqCon + 2 electrodes) and between-subjects factor of group (able-bodied, limb-absent) found significant interaction between these two factors [$F_{(2,24)}=3.8, p_{GG}=0.037$]. We proceeded to paired post hoc comparisons, finding that with the SeqCon control strategy, limb-absent subjects required more time than able-bodied subjects ($p=0.008$); and with the limb-absent subject group, SeqCon required more time than both MapCon ($p=0.005$) and DirCon ($p=0.01$).

Additionally, for each limb-absent subject, time per cycle was compared between three different control strategies (MapCon+6 electrodes, DirCon+6 electrodes, SeqCon) via a one-way RANOVA, with post hoc comparison made when a significant difference was found. The three trials per condition were not averaged. For two of the four subjects, the RANOVA was significant $[F(2,6)>24, p \leq 0.001]$, with post hoc comparison finding that SeqCon required more time than either of MapCon ($p \leq 0.003$) or DirCon ($p \leq 0.003$). For one other subject, the RANOVA was significant $[F(2,6)=20.72, p=0.002]$, with post hoc comparison finding that SeqCon and DirCon each required more time than MapCon ($p \leq 0.009$).

5.4 Discussion

This research assessed the performance of regression-based 2-DoF simultaneous, independent and proportional myoelectric prosthesis control with different control strategies (DirCon, MapCon) and number of optimally-sited electrodes (6, 12), as compared to conventional sequential control (SeqCon). Evaluation was tested on standard box-block task (1-DoF assessment), refined-clothespin relocation task (2-DoF assessment) and a door-knob task (2-DoF assessment). The overall results showed no significant difference between 6 and 12 electrodes. When tested on limb-absent subjects with only 6 electrodes, all subjects successfully controlled the prostheses to complete the tasks. Both MapCon and the more intuitive DirCon exhibited good performance, indicating they could be potential approaches for 2-DoF control.

5.4.1 Calibration Quality Assessment

In this study, subjects were offered up to three calibration trials, and could self-select the "best" trial after being given ample time to become comfortable with controlling the prosthesis. We presumed that a calibration with low EMG-force RMSE facilitates successful 2-DoF control, and vice versa. Hence, we assessed EMG-force performance of the accepted trial. The principal findings were that RMSE was lower during rest contractions and that 12 electrodes provided better EMG-force estimation than 6. The rest result is likely due to the fact that subjects can easily maintain a reproducible rest contraction, even in the absence of force feedback. But, it is difficult to accurately maintain a fixed active force level in the absence of feedback (Johansen-Berg and Matthews 2002, Noble, Eng et al. 2013), leading to poor tracking of the target force. One possible future solution is to feedback EMGσ in real time, which still avoids the need for measurement of force.

The finding that offline EMG-force estimation improved with 12 electrodes vs. 6 has been noted previously (Clancy, Martinez-Luna et al. 2017, Dai, Zhu et al. 2019). Anecdotally, however, we found that subjects were not necessarily choosing the calibration trial with the lowest RMSE. In fact, some low RMSE calibration trials produced control models in which subjects could not actuate in one of the directions (i.e.,

no movement achievable). These calibrations were not selected. Nonetheless, a better metric might be the worst-case error out of the various control directions within a calibration trial, or some other metric that insures robust performance in all movement directions. This issue of strong offline EMG-force estimation not correlating to strong online prosthetic control has been noted by past studies. But, it is postulated that subjects can learn and adapt to the forward dynamics of the prosthesis in regression-based proportional control processors, perhaps reducing the requirement for highly accurate forward dynamics (Jiang, Vujaklija et al. 2014). Similarly, some studies of classification-based myocontrol of prostheses have found that high offline classification accuracy does not necessarily lead to high online performance (Simon, Hargrove et al. 2011, Ortiz-Catalan, Rouhani et al. 2015). These observations are disconcerting, since online performance evaluation is far more expensive and time-consuming than offline (in which many different processing schemes can be evaluated, with many parameter variations), which likely slows the advancement of control algorithms. To combat this problem, recent investigation found that a combination of offline performance metrics (Nawfel, Englehart et al. 2021), or alternative metrics (Teh and Hargrove 2020), better correlated with online performance in classification-based controllers. Thus, a path may still exist for classification-based offline prosthesis control algorithm development, which would be a welcomed efficiency. Perhaps similar metrics can be developed for proportional control algorithms. In any case, further investigation is warranted to develop a self-assessment of calibration quality.

We calibrated using 10 s contractions at 30% MVC effort. It is likely that shorter durations would yield similar EMG-force performance, and thus be more convenient (Clancy and Hogan 1997, Bardizbanian, Zhu et al. 2020). Other effort levels might also be more appropriate, and could be investigated in the future. In fact, it is not clear that the same effort level should be prescribed for each movement direction. What is most important seems to be controllability. Additional gain (or gain attenuation) could be applied to each movement direction by the controller. Further, selection of the various noise floor thresholds also could strongly influence controller performance.

5.4.2 Sequential Control with Co-Contraction Trended Better for 1-DoF Task

Considering trials using 6 electrodes, SeqCon had (statistically significant) higher number of transports per minute on the 1-DoF box-block task than each of MapCon and DirCon. Because we didn't lock wrist rotation during this task, 2-DoF control had the risk of unwanted wrist rotation, after which subjects lost time realigning the wrist to grasp the next block (e.g., similar to (Ameri, Kamavuako et al. 2014)). Subjects reliably contracted flexor muscles, then extensor muscles to grasp and release blocks, respectively. Therefore, an

option to switch temporarily to 2-site SeqCon may be necessary within advanced prostheses controllers as an alternative scheme during activities when only Opn-Cls (1-DoF) contractions are required.

5.4.3 Two-DoF Control was Best for 2-DoF Task

Sequential control is a complicated approach for 2-DoF control. None of our able-bodied subjects had prior experience using co-contraction for mode switching, thus required a relatively long training time. One limb-absent subject had used a prosthesis with EMG co-contraction mode switching for several years, so achieved complete calibration in less than 5 minutes. The remaining limb-absent subjects struggled to learn the skill. Their imbalanced contraction between flexion and extension muscles made co-contraction difficult. EMGσ from one channel often increased faster than the other, thus the difference between the two channels caused prosthesis movement prior to triggering the desired co-contraction. We mitigated this issue by rigorous selection of thresholds, but could not completely avoid it. Furthermore, frequent co-contraction is likely to cause fatigue.

Multi-DoF control is the trend for future prostheses development. Several virtual studies utilizing classification tests (Soares, Andrade et al. 2003, Xing, Yang et al. 2014) and/or target tracking (Igual, Igual et al. 2019, Zhu, Martinez-Luna et al. 2020) have shown that limb-absent subjects can control a virtual 2-dimensional movement task with high precision. Using a physical prosthesis, all our limb-absent subjects had no difficulty realizing simultaneous, independent and proportional 2-DoF control, without prior experience doing so. Some prior research has found poorer performance when using Pro-Sup inputs, perhaps due to electrode shift over muscle during Pro-Sup rotation or because key active muscles (e.g., supinator) are found deeper within the forearm and may not have EMG that is as identifiable at the skin surface. In contrast, summarizing our results across the 2-DoF tasks found that DirCon (Pro-Sup queued wrist rotation) performed similar to MapCon (Rad-Uln queued wrist rotation), and these two control strategies performed noticeably better than SeqCon.

To realize 2-DoF control, four distinct patterns/dimensions of EMG signals should be generated and then distinguished by the controller. For MapCon, which utilized more distinct wrist actions (Ext-Flx and Rad-Uln), subjects found little difficulty in separately controlling prosthesis open, close, pronate, supinate, or their combinations. But, for DirCon, which utilized less distinct wrist actions (Opn-Cls and Pro-Sup), some subjects inadvertently produced wrist supination when attempting to trigger hand open. To reduce these errors, some subjects slowly opened the prosthesis hand, or triggered prosthesis hand open by simultaneously activating native/phantom hand open with low-effort pronation. We largely mitigated this problem by setting higher Sup thresholds, reducing the sensitivity of rotation. Subjects seemed to prefer this higher threshold,

since they seemed to prioritize hand open/close performance, achieving small hand rotations through body posture and shoulder movement.

Another principle to realize 2-DoF control is the ability of subjects to reproduce the same EMG patterns as during calibration. For able-bodied subjects, reproducibility is facilitated by feedback from their real hand and wrist to produce the same motions. Limb-absent subjects do not have this advantage. In fact, congenital limb-absent subjects will never have experienced these feedback sensations. These differences may explain, in part, why the able-bodied subjects performed better than the limb-absent subjects on the 2-DoF door-knob task. Accordingly, congenital limb-absent subjects may be more amenable to MapCon, since they would be mapping "motions" which they have never experienced in the first place. If novel motor patterns are to be learned, selection of patterns that are more distinguishable from surface EMG are likely to be beneficial.

Traditionally, multi-DoF control is assumed to best be facilitated by selecting intuitive control strategies/phantom limb contractions (Hudgins, Parker et al. 1993, Ison and Artemiadis 2015, Mendez, Iberite et al. 2021). Indeed, limb-absent subjects have also opined this assumption (Franzke, Kristoffersen et al. 2019). However, recent evidence suggests that, with multiday training, feedback can be used to habituate non-intuitive muscle synergies that might be more advantageous for prosthesis control (Nazarpour, Barnard et al. 2012, Dyson, Barnes et al. 2018). Hence, multiday studies, which are more reflective of actual prosthesis use, may be necessary to best contrast the advantages of intuitive contractions vs. those which may be less intuitive but perhaps better for prosthesis control (after training).

5.4.4 Number of Electrodes and Channel Selections

Six or 12 optimally-sited electrodes demonstrated no significant difference when subjects controlled the prostheses for any of the tasks, even though 12 electrodes provided better EMG-force estimation during calibration of both DirCon and MapCon. The tasks and conditions were randomized and subjects were blinded to the number of active EMG channels in use. Most subjects could recognize the difference between 12 vs. 6 channels due to different channel selection and different coefficients, but they could not tell which option provided better control. Six electrodes are reasonable to apply on a commercial prostheses considering cost, complexity and required microcontroller computation speed. When 6 electrodes were applied on limb-absent subjects, they could easily control the prosthesis after practice. Since adjacent EMG signals are highly correlated, a further increase in EMG channels introduces more redundant information, along with increased risk of electrode shorting, lift-off, etc. (Clancy and Hogan 1995). It is possible that even fewer than 6 electrodes might be acceptable, although not likely less than 4 for simultaneous, proportional and independent 2-DoF operation. We used backward stepwise selection from 16 candidate electrodes to reduce the number of electrodes to 12 or 6. In practice, this selection step would be part of the prosthesis fitting operation

completed by a prosthetist and, thereafter, the electrode sites would be fixed into their socket. Though different subjects had their own best electrode locations, the selected electrodes were always spread around the limb, not concentrated in one muscle region.

5.4.5 Limb-Absent Subject Performance

Each limb-absent subject had prior myoelectric prosthesis control experience, completed mirror-box training before the experimental trials, and received practice time with each controller. Anecdotally, the mirror-box training was not judged by the subjects to be essential, since their prior myoelectric prosthesis use seemed to guide their perceived contraction pattern preferences. Nonetheless, we anecdotally observed that subjects became more skilled in the use of the prosthesis trial by trial. These learning effects were mitigated in our statistical comparisons because we randomized the testing order for each subject. Hahne et al. (Hahne, Schweisfurth et al. 2018) compared 2-DoF, regression-based hand-wrist prosthesis control performance in five limb-absent subjects across two days, and found some improvement on the second day. They postulated that prosthesis control might benefit from interactive learning; the algorithm learns the EMG signal patterns from the user and generates corresponding coefficients, then the users learn how to use the prosthesis, etc.

The statistical tests using only limb-absent subject data variously found significance for the box-block, clothespin and door-knob tasks, suggesting that different subjects exhibited unique differences in performance. Numerous pre-existing factors—such as muscle contraction ability, length of prosthesis use, limb-loss type and learning ability—should greatly influence task performance. Hence, prosthesis controller implementation for different users must consider their unique needs and characteristics. Of note, all limb-absent subjects used 2-DoF control for the first time in this study, and with only 20¬–30 minutes of practice. Yet, each limb-absent subject performed better on each 2-DoF task using each 2-DoF controller (compared to SeqCon).

5.4.6 Two-DoF Controller Limitations and Challenges

Though each subject could complete each of the three tasks using the 2-DoF controllers, substantial challenges remain. It was obvious that the quality of calibration was essential to a subject's performance. For some subjects, the first calibration did not result in effective prosthesis control, perhaps because these subjects may have focused more on achieving the instructed calibration contraction profile and not on contraction efforts that would be easy for them to reproduce during real tasks. For these subjects, the second or third calibration usually led to a dramatic improvement in control. A more objective measure of calibration "success" is desired to inform the user if they need to re-calibrate for better control. Assessment of overall RMSE between target force and EMG-estimated force may be dubious. Analyzing the error from each

individual motion direction after calibration might better help the user gradually develop the best patterns for everyday calibration.

Another issue was unintentional movement from another DoF. We manually applied two thresholding methods to reduce the impact from unintentional movement. However, a more reproducible, automated method for threshold selection should be developed. The unintentional movement usually happened in two cases. First, it occurred when subjects had a fast change from one motion to another. In this situation, EMG in most channels would spike, producing EMGσ values much higher than normal contraction. These contractions usually triggered a correct movement of the desired DoF, but also generated unexpected movement from another DoF. Second, unintentional movement was sometimes produced when subjects used very high force levels to control the prostheses, likely due to antagonist muscle co-contraction. In both of these cases, the contraction patterns are not present in the calibration data. It is hard to completely avoid unintentional movement during control, but effective threshold selection and lower muscular efforts can reduce the sensitivity of our current approaches. In this way, users can focus on one DoF with accurate and robust control and use an additional DoF when needed.

5.4.7 Primary Results and Contributions of this Work

The primary results and contributions of this work include:

- The work adds to the body of evidence on the successful use of regression-based EMGσ-force models for simultaneous, independent and proportional myoelectric control of 2 DoFs in a hand-wrist prosthesis. A small number of literature studies/subjects exist in which online performance has been evaluated, processing methods vary for each, and the aggregate sample size of limb-absent subjects in these studies is even smaller. Our studies with limb-absent subjects, therefore, add substantively to the literature. We have shown that our regularization method (Moore-Penrose pseudo-inverse) can provide useful online myocontrol of a physical prosthesis.

- One-DoF controllers demonstrated some advantages in 1-DoF tasks, while 2-DoF controllers performed better in 2-DoF tasks. Prosthesis control algorithms should consider providing a mechanism for users to volitionally toggle between such controllers, in order to select the best controller for the task.

- Determining optimal locations to site EMG electrodes for prosthesis control has historically been more of an art than a science (Cavanaugh, Clancy et al. 1983). We previously introduced applying several electrodes about the limb, then selecting offline a minimum number of optimal electrodes via backward stepwise selection in an EMGσ-force model (Clancy, Martinez-Luna et al. 2017, Dai, Zhu et al. 2019). In the current work, this method was evaluated with online tasks using a physical prosthesis, with both able-bodied and limb-absent subjects. We demonstrated that offline EMGσ-force estimation benefited from 12

electrodes, but online myocontrol performed no different with 6 optimally-sited electrodes (out of 16 total). In practice, electrode site selection would be performed during prosthesis fitting and used to select permanent electrode sites. No automated methods for site selection are available in commercial devices. Our backward selection method could provide such a method.

- This work provided considerable methods detail and discussion on the pivotal role of noise threshold selection in myocontrollers. These parameters and how they are used in the prosthesis controller tend to receive far less attention. But, most muscle effort occurs at low contraction, wherein measurement noise has a disproportionate influence (Wang, Rajotte et al. 2021). Future work could look at more formal methods of noise attenuation, along with automated and reproducible selection of algorithm parameters/thresholds.

- Our work found statistical differences when comparing performance within limb-absent subjects, but these differences were not uniform. Some of these distinctions may simply reflect statistical variation. But, others may be a reminder of the unique anatomical and physiologic characteristics of each prosthesis user. That is, a "one-size fits all" solution may not be best for the limb-absent population.

5.5 Conclusion

This laboratory study evaluated two regression-based 2-DoF prosthesis control methods, compared with conventional co-contraction sequential control in box-block, refined-clothespin, and door-knob tasks on both able-bodied and limb-absent subjects. We found that in the box-block task that focused on 1-DoF performance, conventional SeqCon performed better than MapCon and DirCon. In 2-DoF tasks (clothespin, door-knob), both MapCon and the more intuitive DirCon performed better than SeqCon, with faster and more robust performance. Six optimally-sited electrodes (out of 16 total) had overall similar performance with 12 electrodes and are more feasible for commercial prosthesis applications. More algorithm and hardware design to improve control comfort and robustness are appropriate next steps.

Chapter 6: Comparison of EMG-Force Calibration Protocols for Myoelectric Control of Prostheses

This chapter has been published as: Z. Zhu, J. Li, C. Dai, B. McDonald, T. Farrell, X. Huang, E. A. Clancy, "*Comparison of EMG-Force Calibration Protocols for Myoelectric Control of Prostheses,*" 2019 *IEEE Signal Processing in Medicine and Biology Symposium (SPMB)*, 7 Dec. 2019. Color versions of one or more of the figures in this paper are available online at https://ieeexplore.ieee.org/abstract/document/9037835.

The surface electromyogram (EMG) is used as a control source for limb prostheses. When developing hand-wrist prostheses control schemes with able-bodied subjects, it is common to relate forearm EMG to hand-wrist forces/moments using supervised models. However, subjects with unilateral limb absence cannot produce such forces. Thus, we contrasted use of "output" alternatives from the force generated by the sound side in "mirror" movements (Muceli, Jiang et al. 2010, Nielsen, Holmgaard et al. 2011), or directly using a target followed with their limb-absent side (Ameri, Kamavuako et al. 2014, Ameri, Scheme et al. 2014).

Data were collected at 2048 Hz from 12 able-bodied subjects (6 male, 6 female). Bipolar EMG electrodes (16) were secured around their dominant distal forearm. Each wrist was secured to a separate three-axis load cell to measure wrist force/moment. Each hand was secured to a separate one-DoF load cell to measure handgrip force. Subjects performed constant-posture, 1-degree-of-freedom (DoF) random force target [0.75 Hz, white, bandlimited, 40 s, –30 to 30% maximum voluntary contraction (MVC)] tracking trials of: a) wrist radial-ulnar deviation (Rad-Uln), b) wrist pronation-supination (Pro-Sup) or c) hand open-close (Opn-Cls). Different modes of real-time visual feedback were studied: 1) subjects tracked the target only using real-time force feedback from their dominant limb (EMG-ForceDom); 2) subjects tracked the target with only their dominant limb, with no feedback provided (EMG-TargetDom); 3) subjects tracked a pair of symmetrical targets (one per side), with force feedback from the non-dominant side shown in both displays (mirror visual feedback: EMG-ForceND); 4) EMG data from the prior mode was re-used off-line and related to the target (EMG-TargetMVF). Each trial combination (a–c vs. 1–3) was repeated twice.

Raw EMG were highpass filtered (5th-order Butterworth, fc=15 Hz) to remove motion artifact, notch filtered at the power-line frequency (2nd-order IIR at 60 Hz, notch bandwidth of 1 Hz) and rectified. Hand/wrist force/moment was normalized to MVC. Then, all signals were decimated (lowpass filter: fc=16 Hz, Chebyshev Type I, 9th-order, 0.05 dB peak-to-peak passband ripple) to 40.96 Hz. Since feedback-based force tracking incurs a time latency of up to approximately 200–300 ms, this alignment latency (k samples)

was estimated by maximum cross-correlation between Force-Force (or Force-Target). Then, EMG-Force/Target was modeled as below, where Q=20 was the order of the linear dynamic model, E=16 was the number of electrodes, m was the decimated sample index, and EMGσ were the processed EMG:

$$Force[m] = \sum_{q=0}^{Q}\sum_{e=1}^{E} c_{e,q} EMG\sigma_e[m - q - k].$$

The first trial trained coefficients via the linear least squares pseudo-inverse method (Tol = 0.1), and the second trial tested RMSE between estimated and measured force/target. Then the two trials were flipped for cross-validation and their average was reported.

A two-way repeated measure analysis of variance (RANOVA) was computed with the factors of feedback (EMG-Force$_{Dom}$, EMG-Force$_{ND}$, EMG-Target$_{Dom}$, EMG-Target$_{MVF}$) and DoF (Rad-Uln, Pro-Sup, Opn-Cls). Only feedback was significant (F(3,33) = 14.9, p <10^{-3}), without interaction. Post hoc pairwise comparison t-tests with Bonferroni correction found that conventional EMG-Force$_{Dom}$ had significantly lower RMSE than EMG-Target$_{Dom}$ (p = 0.008) and EMG-Target$_{MVF}$ (p = 0.001); and EMG-Force$_{ND}$ had significantly lower RMSE than EMG-Target$_{MVF}$ ($p < 10^{-3}$).
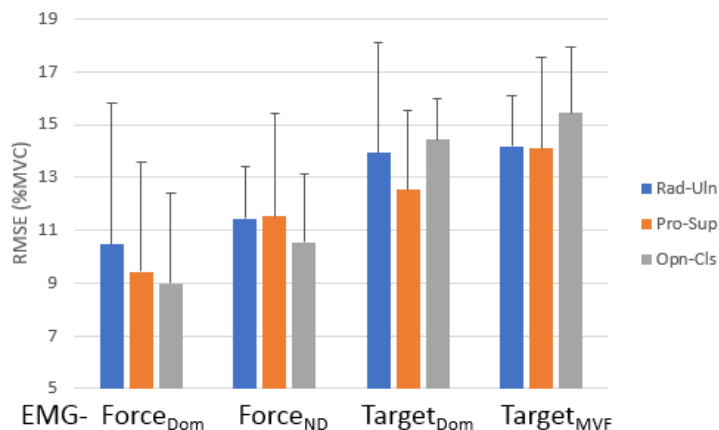
Fig. 6.1. Example 2-DoF EMG-force time-series results, limb-absent subject 21, Rad-Uln & Opn-Cls when using (a) no feedback, (b) contralateral feedback and (c) mirror feedback. EMG acquired from the affected side. Both true force and EMG-estimated force are shown in each plot.

In this experiment, able-bodied subjects simulated limb-absent conditions. Using the contralateral limb for force feedback had similar performance as using conventional ipsilateral limb feedback, and much better performance than using no feedback. Mirror movement did not enhance target estimation. Symmetry is an intrinsic human characteristic (Swinnen 2002), but target tracking is a highly demanding task which needs practice. However, for limb-absent subjects, either congenital or traumatic amputation leads to amyotrophy or neuron damage and may influence the symmetric movement. Thus, further testing on limb-absent subjects is necessary to evaluate the performance of different EMG-force calibration protocols.

Chapter 7: EMG-Force and EMG-Target Models During Force-Varying Bilateral Hand-Wrist Contraction in Able-Bodied and Limb-Absent Subjects

Abstract—**System identification models relating forearm electromyogram (EMG) signals to phantom wrist radial-ulnar deviation force, pronation-supination moment and/or hand open-close force (EMG-force) are hampered by lack of supervised force/moment output signals in limb-absent subjects. In 12 able-bodied and 7 unilateral trans-radial limb-absent subjects, we studied three alternative supervised output sources in one degree of freedom (DoF) and 2-DoF target tracking tasks: (1) bilateral tracking with force feedback from the contralateral side (non-dominant for able-bodied/ sound for limb-absent subjects) with the contralateral force as the output, (2) bilateral tracking with force feedback from the contralateral side with the target as the output, and (3) dominant/limb-absent side unilateral target tracking without feedback and the target used as the output. "Best-case" EMG-force errors averaged ~ 10% of maximum voluntary contraction (MVC) when able-bodied subjects' dominant limb produced unilateral force/moment with feedback. When either bilateral tracking source was used as the model output, statistically larger errors of 12-16 %MVC resulted. The no-feedback alternative produced errors of 25-30 %MVC, which was nearly half the tested force range of ±30 %MVC. Therefore, the no-feedback model output was not acceptable. We found little performance variation between DoFs. Many subjects struggled to perform 2-DoF target tracking.**

7.1 Introduction

Limb-absent subjects can generate motor commands that are communicated to remnant muscle tissue, which contracts and provides a measurable electromyogram (EMG) (Ramachandran and Rogers-Ramachandran 1996, Reilly, Mercier et al. 2006). This remnant muscle EMG is used to command myoelectric prostheses (Parker, Englehart et al. 2006). Proportional myoelectric control of one degree of freedom (DoF) prosthesis tasks has been available commercially for decades—including systems which support sequential switching between distinct DoFs (Mann 1981). So-called seamless sequential control has been achieved via pattern recognition (Hudgins, Parker et al. 1993) and recently commercialized. Simultaneous, independent and proportional control of multiple DoFs is mostly found in research systems and is primarily limited to 2-DoFs. Such control has typically been facilitated via multiple EMG sites (Kuiken, Li et al. 2009) or advanced machine learning algorithms (Hahne, Wilke et al. 2020). Our research described herein is applicable to simultaneous, independent and proportional 2-DoF hand-wrist prosthesis control.

In able-bodied subjects, biomedical signal processing and modelling methods have been used to map EMG to force (Buchanan, Lloyd et al. 2004, Parker, Englehart et al. 2006, Jiang, Englehart et al. 2009, Staudenmann, Roeleveld et al. 2010, Clancy, Liu et al. 2012, Liu, Liu et al. 2015), and to mechanical impedance about a joint (Abul-Haj and Hogan 1990, Popat, Drebs et al. 1993, Kawase, Kambara et al. 2012, Golkar, Tehrani et al. 2017, Dai, Zhu et al. 2019). Historically, such modeling has a goal of improving myoelectric prosthesis control (Abul-Haj and Hogan 1990, Popat, Drebs et al. 1993, Parker, Englehart et al. 2006). Numerous supervised system identification methods have been used to model the EMG-force (or, EMG-kinematics) relationship (see (Buchanan, Lloyd et al. 2004, Staudenmann, Roeleveld et al. 2010) for reviews). All methods use an estimate of the EMG standard deviation (EMGσ, a.k.a. processed EMG) as input (Hogan and Mann 1980, Clancy and Farry 2000), and may use other features extracted from the EMG signal, such as zero crossing rate, slope sign change rate and waveform length (Hudgins, Parker et al. 1993, Dai, Bardizbanian et al. 2017). Regression approaches have been common, with studies using standard (un-regularized) linear regression to fit the model (Messier, Duffy et al. 1971, Smith, Kuiken et al. 2016). Recent work has used various forms or regularized regression, such as ridge (Clancy, Liu et al. 2012), Moore-Penrose pseudo-inverse (Clancy, Liu et al. 2012) and support vector (Ameri, Kamavuako et al. 2014) regression approaches, to improve robustness of the model and reduce its error. Non-linear models have also been shown to reduce error somewhat, from implementations of the EMGσ-force power law observation reported by Vredenbregt and Rau (Vredenbregt and Rau 1973, Dai, Bardizbanian et al. 2017), to neural networks (Liu, Herzog et al. 1999, Luh, Gwo-Ching et al. 1999), to parallel cascade structures (Hashemi, Morin et al. 2012), amongst many others. Some modeling approaches that require limited supervision are also emerging,

including nonnegative matrix factorization (Jiang, Rehbaum et al. 2014, Lin, Wang et al. 2018) and population-based assignment of dynamics (Buchanan, Lloyd et al. 2004, Bardizbanian, Zhu et al. 2020). Of course, a classic approach with limited supervision is to insert dynamics in the form of a conventional linear lowpass filter (e.g., 2nd-order with cut-off frequency ~1.5 Hz) (Winter 2009, pp. 250–280, Koirala, Dasog et al. 2015). Note that each of these less-supervised approaches still must calibrate a gain to each EMG channel.

A fundamental challenge for developing EMG-force models in limb-absent subjects is that end-effector force is not available as the output of supervised model training. As one alternative, EMG from remnant muscles of the absent limb are used to estimate the force (or kinematics) from the contralateral limb when performing bilateral symmetric (mirror) contractions (Muceli, Jiang et al. 2010, Nielsen, Holmgaard et al. 2011, Muceli and Farina 2012). This model is then used as the EMG-force relationship in the absent limb. Mirror-provided optical reflection of contralateral-side movement creates a visual illusion that builds awareness of phantom limb movement (and may relieve phantom limb pain) (Ramachandran and Rogers-Ramachandran 1996, Mercier, Reilly et al. 2006, Chan, Witt et al. 2007, Andison 2011). Bilateral symmetric mirror tracking experiments on able-bodied subjects have found that relating dominant-limb EMG to contralateral hand position is slightly worse than relating it to dominant hand position (Muceli and Farina 2012). However, experiments on amputees led to different results, as they had overall poorer performance than able-bodied subjects, but equal or better performance for some specific motions and their combinations (Jiang, Vest-Nielsen et al. 2012). The individual differences within limb-absent subjects was another important factor, as different kinds of limb-absence (i.e., congenital, traumatic), residual-limb length, or other conditions (e.g., neuron damage, contraction imbalance) may affect performance. Accordingly, some researchers prefer to individualize control methods for each specific subject (Jiang, Vest-Nielsen et al. 2012).

An alternative approach is for limb-absent subjects to directly activate their phantom limb to track a target on a computer screen, then relate EMG to this target (Ameri, Kamavuako et al. 2014, Ameri, Scheme et al. 2014). This solution avoids the need for a physical feedback source (also applicable to those with bilateral limb-absence). However, this approach provides no physical measure of actual achieved remnant muscle force and always produces some amount of tracking error. For example, visual tracking incurs a pure reaction time delay between the target and the produced force (i.e., an average delay of 0.268 s (Luce 1986, p. 209–210)).

Our research extends prior EMG-force study in several manners. First, in able-bodied subjects, we compare and contrast different visual feedbacks within one study: dominant limb force, contralateral limb force with mirror feedback, and no force feedback. Second, in limb-absent subjects, the feedbacks studied

were: contralateral[1] side using mirror feedback and no force feedback. Third, our novel methods include instrumenting hand open-close (Opn-Cls) forces *as well as* wrist forces/moments, and doing so simultaneously on *both sides* of able-bodied subjects. We are not aware of any previous applicable studies that have simultaneously measured hand-wrist forces on *both* sides of able-bodied subjects. This instrumentation provided unique insights into evaluation of EMG-force models, including a direct measure as to how well forces in the contralateral limb are representative of forces in the dominant limb of able-bodied subjects. Our results have important implications for the calibration of myoelectric control algorithms, in particular the extent to which these measures can serve as surrogate supervised output sources for limb-absent subjects.

7.2 Methods

7.2.1 Experimental Apparatus

Experimental data were collected from 12 able-bodied subjects (6 males, 6 females; aged 18–55 years) and 7 trans-radial unilateral limb-absent subjects (4 males, 3 females; aged 27–61 years; see Table 2.1) at Worcester Polytechnic Institute (WPI) and approved by the WPI Institutional Review Board (IRB Protocol #17-155). All limb-absent subjects routinely use myoelectric-controlled upper-limb prostheses and all, except subject 27, were known to have previously participated as subjects in upper-limb myoelectric control studies. All subjects provided written informed consent. Able-bodied subjects had no deficits involving their upper limbs or vision and were right-hand dominant. Limb-absent subjects had no deficits involving their contralateral limb or vision, and the residual limb on the affected side was at least 5 cm in length with

Fig. 7.1. Experimental apparatus. Subjects (limb-absent subject shown) sat in a chair with each able hand secured into force measurement devices, facing the computer screen which displayed a target and real-time force/moment feedback.
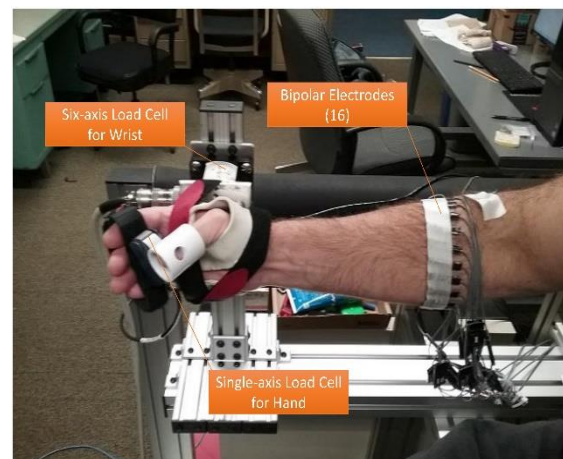
Fig. 7.2. Experimental apparatus at the hand-wrist. Each able hand was separately secured via Velcro to a thermo-formable plastic glove that was bolted to a six-axis load cell to measure the moment at the wrist. Fingers were secured to a single-axis load cell to measure hand grip force. Sixteen EMG electrodes were secured around the dominant/limb-absent forearm.

[1] The term "contralateral" will be used to refer to the non-dominant side of able-bodied subjects and the sound side of limb-absent subjects.

functional muscle contraction. One additional limb-absent subject was excluded due to neural damage on the limb-absent side.

Subjects were seated at the experimental apparatus (Fig. 7.1). The palm of each hand (sound side only for limb-absent subjects) was separately aligned and secured via Velcro straps to a thermo-formable plastic mold which was rigidly connected to a six-DoF load cell (MC3A-100 transducer, Gen 5 signal conditioner, AMTI, Watertown, MA) to measure radial-ulnar deviation (Rad-Uln) force

TABLE 7.1
TRANS-RADIAL LIMB-LOSS SUBJECT INFORMATION.

Sub. Num.	Sex	Age (years)	Type of Limb-Loss	Side	Time Limb Absent (years)	Residual Length (cm)	Circ. (cm)
21	F	61	Congenital	R	61	5.5	19
22	M	27	Congenital	L	27	15	24
23	M	30	Congenital	L	30	13.5	25.5
25	F	49	Traumatic	R	32	10.5	22
26	M	54	Traumatic	R	37	14	20.8
27	F	58	Traumatic	R	33	13	19.6

along one force axis and pronation-supination (Pro-Sup) moment along one moment axis. Rad-Uln force was measured directly. However, this force is not produced at the axis origin of the load cell (which exists within the body of the load cell, approximately 6.3 cm from the center of mass of the palm). Hence, Rad-Uln forces also produced an artifactual Pro-Sup moment. Thus, Pro-Sup moment was computed as the moment measured by the load cell, less the product of the Rad-Uln force times the 6.3 cm moment arm. To measure hand grip force during attempted hand Opn-Cls, each hand (sound side only for limb-absent subjects) additionally gripped a single-axis load cell (LCR-150 with DMD-465WB amplifier, Omega Engineering, Inc., Stamford, CT) while the thumb was secured via a rigid tube and, separately, the proximal aspects of the four fingers were secured by Velcro on the opposing side of the cell. The palms of the hands were oriented perpendicular to the plane of the floor, facing inwards; the wrists were relaxed in a neutral position; and the shoulders were in the anatomical position (Fig. 7.2).

During unilateral tasks (Fig. 7.3, Tasks 1 and 2), a computer-controlled target guided the subject to complete different experimental tasks via a blue arrowhead on the computer screen in front of the subject, with up-down movement displaying wrist radial-ulnar deviation, rotation displaying Pro-Sup moment and arrowhead size displaying hand Opn-Cls force. (Wrist extension-flexion force was considered as an additional contraction dimension, but discarded due to the overall experimental protocol duration and its proximity to muscles used in hand Opn-Cls.) When desired, another red arrowhead displayed real-time force/moment feedback from both load cells on the dominant/affected or contralateral side, depending on the task being performed. During bilateral tasks (Fig. 7.3, Task 3), these displays were mirrored in two display panels on the screen.

One array of 16 bipolar EMG electrodes was secured to a subject's forearm (dominant side for able-bodied subjects, affected side for limb-absent subjects). Electrode gel was applied to a subject's forearm and the electrodes were equally spaced about its circumference, with the midpoints of the bipolar contacts placed

5 cm distal to the elbow crease. Each electrode pair consisted of 5 mm diameter, stainless steel, hemispherical contacts separated 1 cm edge-to-edge, oriented along the forearm's long axis. A reference electrode was gelled and secured on the forearm, just proximal to the active electrodes. Each bipolar EMG signal was differentially amplified (Liberating Technologies, Inc. BE328 amplifier; 30–500 Hz pass band, CMRR>100 dB over the pass band) and then selectable gain was applied. All EMG channels and load cell signals were sampled at 2048 Hz with 16-bit resolution, and target movement was recorded at 800 Hz.

7.2.2 Experimental Protocol

All trials were constant-posture. To prevent cumulative fatigue, the interval between trials was at least two minutes. All limb-absent subjects were offered mirror-box training, using methods designed by a consulting occupational therapist, before tracking trials to help build a better sense of muscle contraction for the different tasks.

1) *MVC Trials*: After a warm-up period during which each task was introduced, able-bodied subjects performed bilateral maximum voluntary contraction (MVC) trials for each of wrist radial and ulnar deviation, wrist pronation and supination, and hand close and open. Limb-absent subjects only performed MVC trials for the sound side. All subjects took 2–3 seconds to ramp up to their MVC effort and then maintained this effort for 2–3 seconds. The plateau force/moment during the maintained period was recorded as the MVC. Lastly, rest trials with all muscles fully relaxed were recorded for EMG noise level evaluation.

2) *Force-Varying Target Tracking Trials*: Next, subjects performed force-varying target tracking Tasks 1, 2 and 3 (explained below) separately for 1-DoF Rad-Uln, Pro-Sup and Opn-Cls; and 2-DoF Rad-Uln & Opn-Cls and, separately, Pro-Sup & Opn-Cls. The 2-DoF tasks always included Opn-Cls, as this function is fundamental to a hand-wrist prosthesis. Only the utilized motions were enabled for visualization in the screen display (i.e., the remaining DoFs were locked out). The target was a 0.75 Hz band-limited, white and uniform random process [16] between ±30% MVC (independently generated for each DoF) corresponding to the utilized task. This bandwidth was the widest for which subjects could maintain target tracking for these tasks during preliminary testing. The order of presentation of DoFs, unilateral/bilateral and visual feedback condition (see below) was randomized and the subjects were told which side was controlling the feedback. Each trial was 40 s in duration and conducted twice per task. Before each trial, subjects were instructed about the range of target movements and allowed practice until they were comfortable. Unilateral and bilateral tasks were completed as described subsequently.

Task 1—Tracking with Dominant-Limb Force Feedback (Fig. 7.3a): Only able-bodied subjects performed these force-varying tracking tasks, using their dominant limb (with EMG electrodes). Feedback of dominant force/moment was provided for target tracking. The contralateral limb was fully at rest and not secured to the load cells. Off-line, EMG (which was acquired only from the dominant side) was related to force/moment on the dominant side. This task provides the best-case scenario for supervised learning of EMG-force models since EMG is recorded directly from the muscles producing the measured force/moment and, thus, represents the benchmark. Limb-absent subjects did not complete this task.

Task 2—Unilateral Tracking with No Visual Feedback (Fig. 7.3c, d): Able-bodied subjects used their dominant limb (with electrodes) to track the target, with no real-time feedback provided. Only the target was shown on the screen. Limb-absent subjects used the limb-absent side (the only side with electrodes) to track the target, with no real-time feedback provided. For all subjects, the contralateral limb was fully at rest (not secured to the load cells). Off-line, EMG was related to the target. This task represents the no-feedback condition in which a dominant/limb-absent side model is built without feedback.

Fig. 7.3. Experiment Protocol. Blue arrowhead is target and red arrowhead is visual feedback. a) Task 1: able-bodied subjects tracked target with their dominant limb given real-time visual feedback of their dominant limb force (F_D); c, d) Task 2: subjects tracked the target with their dominant/limb-absent side with no visual feedback (NVF); e, f) Task 3: subjects tracked the target with both limbs given real-time feedback from their contralateral side and with mirror visual feedback (MVF).

Task 3—Bilateral Tracking with Mirror Visual Feedback (Fig. 7.3e, f): Able-bodied subjects used both limbs to simultaneously track the target. Limb-absent subjects used their sound and phantom limbs to simultaneously track the target. For all subjects, feedback consisted only of the force produced by the contralateral-side limb. This force and its mirror force were simultaneously displayed, producing mirror visual feedback. Offline, EMG was related to contralateral-side force/moment. This task represents use of the force/moment in the contralateral side in order to build the dominant/limb-absent side model. We also related EMG to the target, for comparison.

7.2.3 Methods of Analysis

1) Data Pre-Processing: Data processing was performed in MATLAB 2018b (Mathworks, Inc., Natick, MA). All filters were implemented using the two-pass, zero-phase method, thus their effective filter orders are twice those listed herein. The forces/moments (Rad-Uln, Opn-Cls, Pro-Sup) were each lowpass filtered (*fc*=16 Hz; Chebyshev Type I filter, ninth-order, 0.05 dB peak-to-peak passband ripple) and then downsampled from 2048 Hz to 40.96 Hz. The wrist Rad-Uln data were normalized by $(|MVC_{Rad}|+|MVC_{Uln}|)/2$, and similar normalization was applied to the Pro-Sup and Opn-Cls data. All target data were identically lowpass filtered, then resampled to 40.96 Hz.

For each of the 16 EMG channels in a trial, an estimate of time-varying EMG standard deviation (*EMGσ[m]*, where *m* was the decimated discrete-time sample index) was computed. The raw EMG were highpass filtered (*fc*=15 Hz, fifth-order Butterworth filter) to remove motion artifact, then notch filtered (second-order IIR filter at 60 Hz, notch bandwidth of 1 Hz), rectified, lowpass filtered (*fc*=16 Hz, as above) and finally downsampled to 40.96 Hz. Note that additional lowpass filtering, typically with *fc*≤1 Hz, is optimized to each subject via the EMGσ-force/target model (Koirala, Dasog et al. 2015). Prior to further analysis, the initial and final 1 s of all signals were removed to avoid filter startup transients.

2) Latency Between Forces/Moments and the Target: For each able-bodied subject and DoF, we computed the cross-correlation coefficient function to estimate the latency between subject force/moment and the target (Azaria and Hertz 1984). For 2-DoF tasks, latency estimates were made independently for each DoF. The time location of the maximum of the cross-correlation coefficient function indicated the time delay (latency) ($\tau=k/F_s$, where *k* is the number of samples, F_s is the sampling frequency) at which the force/moment and the target were best aligned. The corresponding maximum cross-correlation coefficient function value (ρ) is a measure of the linear association of the target tracking, after accounting for the latency. It is invariant to gain and, as such, is a measure of timing accuracy in tracking. As the force will lag behind target movement due to the subject's reaction time, we only searched for the maximum ρ between a delay τ of 0 to 1 s. Note that our pre-processing of the force/moment data did not bias the latency estimates, since pre-processing filters were implemented with zero phase.

3) Dynamic EMGσ-Force/Target Modeling: When *EMGσ[m]* was related to force (EMG-force), or when EMG was related directly to the arrowhead target (EMG-target), during 1-DoF trials, a linear, dynamic, finite impulse response relation was used, of the form:

$$F[m] = \sum_{q=0}^{Q}\sum_{e=1}^{E} c_{e,q}EMG\sigma_e[m-q-k],$$

where *F* was the force/target, m was the decimated discrete-time sample index, *q* and *e* were integer indexes, *Q*=20 was the order of the linear dynamic model, *E* = 16 was the number of electrodes used in the

fit, and $c_{e,q}$ were the fit coefficients (Clancy, Martinez-Luna et al. 2017). Latency (k; in samples) was assigned to zero for EMG-force models (we observed that sufficient latency was provided by the frequency-dependent phase response of the linear models). For EMG-target models of able-bodied subjects, latency was taken from the same trial as the model fit, as this value was assumed to be most accurate; for limb-absent subjects (wherein latency cannot be measured on the limb-absent side), the latency used was the average latency from able-bodied subject trials from the same task and DoF. Fit coefficients were estimated via the linear least squares pseudo-inverse method, in which singular values of the design matrix were removed if the ratio of that singular value to the largest was less than a tolerance value (*Tol*=0.1, based on previous study (Clancy, Liu et al. 2012, Dai, Bardizbanian et al. 2017)). We chose this modeling method for its robustness, simplicity and because linear models capture most of the EMG-force/target relationship. In this manner, we could maintain our focus on the different feedback mechanisms.

Each task consisted of two trials. The first trial was used for coefficient training and the second for testing. Then, the training and testing trials were flipped for two-fold cross-validation and the average of the two RMS errors (RMSEs) reported. All RMSEs were in %MVC (normalized force/moment).

For 2-DoF trials, two EMGσ-force/target models were fit, one per DoF (each with its own coefficients). In this manner, each EMG channel contributed to each DoF. Again, one trial was used for training and one for testing, with two-fold cross-validation.

4) EMG-Force, EMG-Target Models Studied: For each experimental task, both 1- and 2-DoF trials had been performed. Thus, both 1- and 2-DoF EMG-force/target models were studied, respectively. From the Task 1 data, EMGσ was related to force in the dominant arm. These data were only available from the able-bodied subjects and represented the reference ("best-case") task. From the Task 2 data in which there was no visual feedback, EMGσ only was related to the target for all subjects. This analysis represents building models when no feedback is available during training (e.g., when building EMG-force style prosthesis control models for limb-absent subjects). From the Task 3 data that used mirror visual feedback, EMGσ was related to contralateral force (representing use of forces from the sound side to train models in unilateral limb-absent subjects); and EMGσ was related to the target for all subjects (for comparison to results from Task 2). Again, the average RMSEs from two-fold cross-validated results is reported.

7.2.4 Statistics

Our primary evaluation metrics were latency between forces/moments and the target, and maximum cross correlation coefficient/RMSE between measured/EMG-estimated forces/moments. Unless noted otherwise, performance differences were evaluated using repeated measures analysis of variance (RANOVA)

in SPSS 22, using a significance level of p=0.05. Prior to RANOVA, the degree of sphericity (ε) was used to adjust the degrees of freedom by either the method of Greenhouse-Geisser (ε < 0.75) or the method of Hyunh-Feldt (0.75< ε <1). Unless stated otherwise, no interactions were found. Pairwise comparisons (post hoc or stand-alone) were conducted using paired t-tests with Bonferroni correction. We statistically analyzed 1-DoF tasks separately from 2-DoF tasks.

7.3 Results

7.3.1 Latencies Between Force/Moment and Target

Table 7.2 shows the mean ±std. dev. latencies between force/moment and target for each experimental task, for the able-bodied subjects. RMSE between force/moment and target was compared pairwise with vs. without latency adjustment. Pooling all conditions [288 1-DoF trials (12 subjects × 4 feedback types × 3 DoFs × 2 sets) and 384 2-DoF trials (12 subjects × 4 feedback types × 2 DoF pairs × 2 errors per DoF pair × 2 sets], the latency adjusted error was smaller (in 658 of 672 pairs) by an average of 4.60±2.91 %MVC, which was statistically significant ($p < 10^{-6}$, paired sign test). This result formed the basis for our step in the Methods section to latency-adjust all EMG-target models.

7.3.2 RMSE, Dominant Force vs. Target, Able-Bodied Subjects
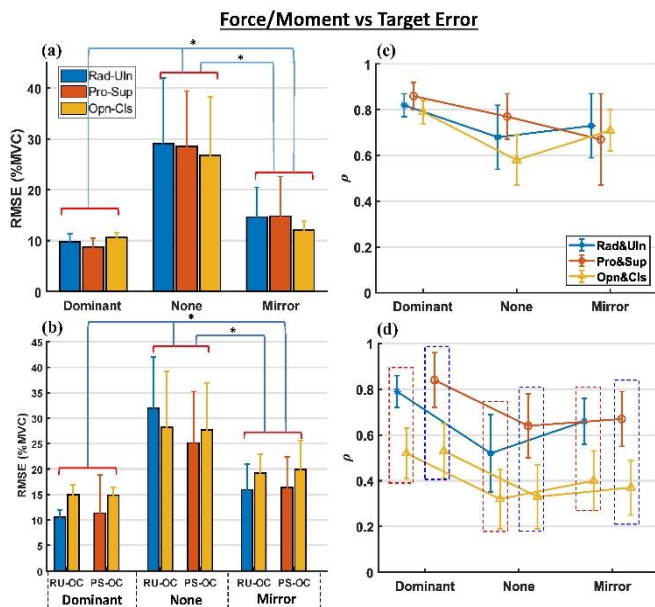
Fig. 7.4. Mean + std. dev. errors between dominant limb force/moment and *target* for able-bodied subjects, after adjusting for time latency. Statistically significant differences between feedback types indicated with "*". RMSE (left) with different feedback conditions [dominant (Task 1), none (Task 2) and mirror (Task 3)] as a function of DoF for 1-DoF tasks (top) and as a function of DoF pairs for 2-DoF tasks (bottom). Maximum cross-correlation coefficients (ρ) shown at right. Dash-line boxes in (d) group DoF pairs.

TABLE 7.2
ABLE-BODIED SUBJECTS, TRACKING LATENCY BETWEEN ACTUAL
FORCE/MOMENT AND TARGET, FOR EACH DoF (MS)

1-DoF:	Rad-Uln	Pro-Sup	Opn-Cls
Task 1, Dominant	268±46	300±68	330±75
Task 2, Dominant	274±100	240±79	234±73
Task 3, Dominant	278±53	349±144	353±88
Contralateral	293±54	349±98	367±102

2-DoF:	Rad-Uln	Opn-Cls	Pro-Sup	Opn-Cls
Task 1, Dominant	242±37	491±90	289±38	485±100
Task 2, Dominant	431±171	458±192	263±72	509±189

Before reporting EMG-force and EMG-target performance (see subsequent sub-sections), we describe the ability of able-bodied subjects to track the random target in Tasks 1–3. Fig. 7.4 shows summary RMSE and ρ of dominant limb force in able-bodied subjects vs. *target* for the different feedback conditions (i.e., tasks),

after adjusting for time latency. RMSE measures tracking error, while ρ provides an error measure that is invariant to gain (and provides our latency values).

In 1-DoF tasks, a two-way RANOVA of RMSE with the factors feedback (dominant, none, mirror) and DoF (Rad-Uln, Pro-Sup, Opn-Cls) found only feedback as significant [$F(1.1, 12.6) = 42$, $p_{GG} = 10^{-5}$. Pairwise comparison found RMSE in dominant feedback was significantly lower than none ($p = 10^{-4}$) and mirror ($p = 0.002$), and mirror had significantly lower error than none ($p = 10^{-4}$).

In 2-DoF tasks, a three-way RANOVA for tracking RMSE with the factors of feedback (dominant, none, mirror), DoF pair (Rad-Uln & Opn-Cls or Pro-Sup & Opn-Cls) and motion-within-DoF (wrist Rad vs. Uln, or Pro vs. Sup; or hand Opn vs. Cls) found only feedback was significant [$F(1.2, 13.0) = 40$, $p_{GG} = 10^{-5}$]. Pairwise comparison found RMSE in dominant feedback was significantly lower than none ($p = 10^{-4}$) and mirror ($p = 10^{-4}$), and RMSE in mirror was significantly lower than none ($p = 0.001$). In both 1-DoF and 2-DoF tasks, the average error when using no feedback is nearly half the contraction range of ±30 %MVC, which seems unacceptable.

Fig. 7.6. Mean + std. dev. errors between dominant limb force/moment and *target* for able-bodied subjects, after adjusting for time latency. Statistically significant differences between feedback types indicated with "*". RMSE (left) with different feedback conditions [dominant (Task 1), none (Task 2) and mirror (Task 3)] as a function of DoF for 1-DoF tasks (top) and as a function of DoF pairs for 2-DoF tasks (bottom). Maximum cross-correlation coefficients (ρ) shown at right. Dash-line boxes in (d) group DoF pairs.

7.3.3 Train EMG-Force, EMG-Target: Test Using Dominant Limb Forces of Able-Bodied Subjects (Tasks 1–3)

Fig. 7.5 shows summary results of EMG-force/target models *trained* with the various indicated signal as the supervised output, but always *tested* using a distinct trial of able-bodied *dominant* limb forces. Thus, regardless as to whether the *training* set used force or target as the output, the model was *tested* using dominant limb force as the output. When *training* did *not* use dominant limb force, then testing on the dominant limb best indicates if the supervised output is an acceptable surrogate for dominant limb force—which, of course, is not available in limb-absent subjects. Note that *training* with dominant force feedback (same side as the electrode array) represents
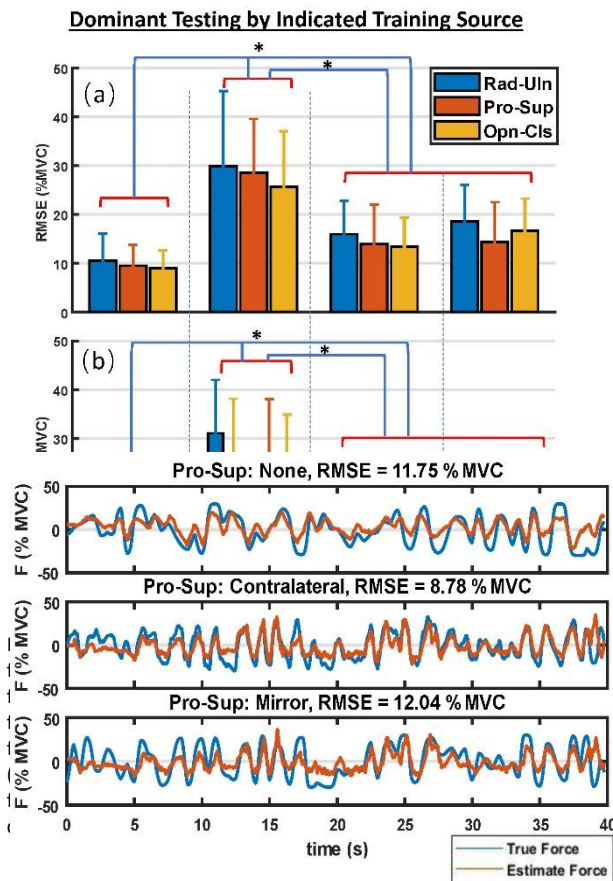
the best-case EMG-force training condition (EMG recorded directly from muscles producing the measured force/moment).

In 1-DoF tasks, a two-way RANOVA with factors: DoF (Rad-Uln, Pro-Sup, Opn-Cls) and feedback (dominant, contralateral, none, mirror) found only feedba ck was significant [$F(1.3, 14) = 45$, $p_{GG} = 10^{-6}$].

Fig. 7.7. Example 2-DoF EMG-force time-series results, limb-absent subject 21, Rad-Uln & Opn-Cls when using (a) no feedback, (b) contralateral feedback and (c) mirror feedback. EMG acquired from the affected side. Both true force and EMG-estimated force are shown in each plot.

Post hoc comparison found that dominant feedback had significantly lower RMSE than the others ($p < 0.002$), contralateral and mirror had no significant difference from each other, and both had lower RMSE than none ($p < 0.001$).

In 2-DoF tasks, a three-way RANOVA with factors: DoF pair (Rad-Uln & Opn-Cls, Pro-Sup & Opn-Cls), feedback (dominant, contralateral, none, mirror) and motion-within-DoF (wrist Rad-Uln vs. hand Opn-Cls, or wrist Pro-Sup vs. hand Opn-Cls) found only feedback was significant [$F(1.4, 16) = 37$, $p_{GG} = 10^{-6}$]. Pairwise comparison found that dominant feedback had significantly lower RMSE than the others ($p < 0.001$), contralateral and mirror had no significant difference from each other, and both had lower RMSE than none ($p < 0.004$).

7.3.4 Train EMG-Force, EMG-Target: Test Using Respective Feedback Signal—All Subjects (Tasks 2, 3)

Fig. 7.6 and Fig. 7.7 show example time-series results. Fig. 7.8 shows summary results of EMG-force/target models when the distinct train and test trials were from the *same* feedback signal *other* than dominant force. These three signals were available for both able-bodied and limb-absent subjects, so provide a more direct means of comparison between these subject populations which is not available from the prior results.

In 1-DoF tasks, a three-way RANOVA for RMSE with two subject-within factors: feedback (contralateral, none, mirror) and DoF (Rad-Uln, Pro-Sup, Opn-Cls); and one subject-between factor: group (able-bodied, limb-absent) found significant interactions. Thus, two-way RANOVAs were computed separately for able-bodied and limb-absent subjects. For able-bodied subjects, the two-way RANOVA found only feedback was significant $[F(2, 22) = 12.5, p = 10^{-4}]$. Pairwise comparison showed that contralateral feedback had significantly lower error than none ($p = 0.04$) and mirror ($p = 10^{-4}$). For limb-absent subjects, the two-way RANOVA found both feedback and DoF significant $[F(2, 22) > 4.0, p < 0.05]$. Pairwise comparison showed that contralateral feedback had significantly lower error than none ($p = 0.035$) and mirror ($p = 0.015$), and that Pro-Sup had better performance than Rad-Uln ($p = 0.021$). Alternatively, we fixed each of the DoFs in the original three-way RANOVA. Of these three two-way RANOVAs, only when Rad-Uln was fixed was a significant difference found in the group factor, with able-bodied subjects exhibiting lower error than limb-absent $[F(1, 17) = 10.8, p = 0.004]$.

Fig. 7.8. Example 2-DoF EMG-force time-series results, limb-absent subject 21, Rad-Uln & Opn-Cls when using (a) no feedback, (b) contralateral feedback and (c) mirror feedback. EMG acquired from the affected side. Both true force and EMG-estimated force are shown in each plot.

In 2-DoF tasks, a four-way RANOVA for RMSE with three subject-within factors: feedback (contralateral, none, mirror), DoF pair (Rad-Uln & Opn-Cls; Pro-Sup & Opn-Cls) and motion-within-DoF (wrist Rad-Uln vs. hand Opn-Cls, or wrist Pro-Sup vs. hand Opn-Cls); and a subject-between factor: group (able-bodied, limb-absent) found DoF to not be significant $[F(1, 17) = 0.3, p = 0.6]$, and the other three factors to interact. Continuing analysis of the three interacting factors, two three-way RANOVAs with factor group fixed were computed. For able-bodied subjects, there was a two-way significant interaction of feedback×motion-within-DoF. Thus, pairwise comparison found that: for both motion-within-DoF wrist Rad-Uln and Pro-Sup, contralateral feedback had significantly lower RMSE than mirror ($p = 0.008$); for motion-within-DoF hand Opn-Cls, contralateral feedback exhibited significantly lower RMSE than both none ($p < 10^{-4}$) and mirror ($p = 0.001$). For limb-absent subjects, the three-way RANOVA found only feedback significant $[F(1.1, 6.4) = 9.4, p = 0.02]$. Pairwise comparison found contralateral feedback had significant lower RMSE than mirror ($p = 0.033$).
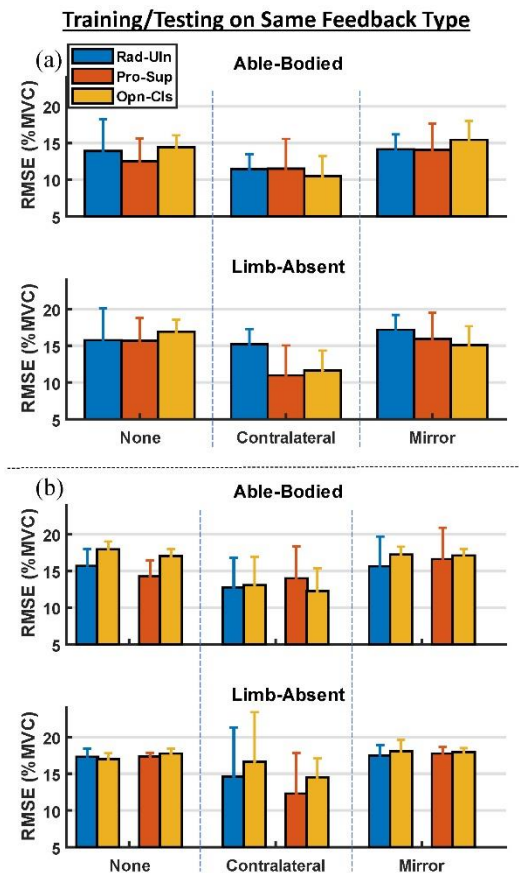
7.4 Discussion

7.4.1 Latencies Between Force/Moment and Target

The 1-DoF latencies between force/moment and target (Table 7.2) are generally consistent with those found in the literature, ranging in average from 234–367 ms (Luce 1986, p. 209–210). When tracking using the contralateral (i.e., non-dominant) limb of able-bodied subjects for feedback, the latencies tended to be longer.

Latencies for our 2-DoF tasks were not readily found within the literature, hence our results for these tasks may be novel. Across Tasks 1–3, the trend was for much larger average latencies (by a factor of ~2) for the Opn-Cls dimension within each 2-DoF task, while the other contraction dimension retained a latency similar to its 1-DoF task. Standard deviations were similar to the 1-DoF results. The only exception was Rad-Uln & Opn-Cls 2-DoF Task 2—in this case both constituent DoFs exhibited the higher average latencies. Anecdotal observation during the trials suggests that subjects struggled to perform the 2-DoF tracking, and may have concentrated their tracking focus on Rad-Uln/Pro-Sup at the expense of Opn-Cls. Additionally, use of arrowhead size as the feedback source for Opn-Cls may have been more challenging compared to the other DoFs. But, this issue is less likely, since no similar performance distinction occurred in 1-DoF. Note that in able-bodied subjects, each subject's latency was available, thus these subject-specific latencies provided the most accurate estimates. For limb-absent subjects, we resorted to using the average value from able-bodied subject trials from the same task and DoF. This approximation was necessary, but likely contributed more error to the limb-absent results.

7.4.2 RMSE, Dominant Force vs. Target, Able-Bodied Subjects

The results in Fig. 7.4 depict the ability of forces/moments in the dominant arm of able-bodied subjects to track the target, as a function of three feedback sources. As expected, when dominant feedback is provided from the dominant limb, errors are statistically lower. Our results then show a hierarchy of performance, with mirror feedback showing the next lowest error and no-feedback providing the highest error. These results are consistent both for 1- and 2-DoF tasks. Notably, the error between the target and the actual force produced by the dominant arm in the no-feedback condition averaged 25–30 %MVC, even though the full force range only spanned ±30 %MVC. Hence, this error was nearly half the available force range, which is quite large; suggesting that the target displayed during the no-feedback condition is quite a poor supervised output source for system identification purposes.

In contrast, the maximum cross-correlation results for all of these tasks are quite high (Fig. 7.4, right). The average value of ρ ranged from ~0.6 to over 0.8 for the 1-DoF tasks. As shown in the time-series plots

of Fig. 7.6 and Fig. 7.7, subjects followed the *timing* of the extrema of target force quite well, but had difficulty in maintaining proper amplitude (especially for 2-DoF tasks).

7.4.3 Train EMG-Force, EMG-Target: Test Using Dominant Limb <u>Forces</u> of Able-Bodied Subjects

Fig. 7.5 shows the principal results of this study. Relating EMG from the dominant limb to forces in that limb, as expected, gives EMG-force models with the lowest errors—since EMG is recorded directly from the muscles producing the measured force/moment. The errors found herein are consistent in magnitude with those found in prior studies (Clancy, Martinez-Luna et al. 2017, Bardizbanian, Zhu et al. 2018). It is also encouraging that the EMG-force errors shown in Fig. 7.5 are similar in amplitude to the force tracking errors shown in Fig. 7.4. Thus, relating EMG to dominant side force has errors that are similar to those between dominant force and the target. But, when dominant limb forces are not available and a surrogate output is needed to train EMG-force for the dominant limb (e.g., limb-absent subjects), our results again found a hierarchy of statistically significant differences: bilateral tracking using contralateral force for training (with or without mirror visual feedback) performed somewhat poorer, while no feedback performed the poorest. Statistically, there was no performance distinction in bilateral tracking between feedback of contralateral force and mirror visual feedback. For both 1- and 2-DoF tasks, the EMG-force/target errors with no feedback were approximately half the available force range. These errors are so large that it is likely that population-based models of EMG-force dynamics (e.g., Hill-style muscle models (Hof and Van den Berg 1981) or generic EMG-force calibrations from a population (Pan, Crouch et al. 2018, Bardizbanian, Zhu et al. 2020), combined with estimation only of one gain parameter per EMG channel, would provide considerably better EMG-force estimation. For example, in a 2-DoF hand-wrist EMG-force task involving nine able-bodied subjects (Bardizbanian, Zhu et al. 2020), we replaced EMG-force dynamics calibrated to each individual with one universal model calibrated across the population. A single gain per EMG channel was still optimally estimated per individual. The population-based model performed nearly identically to those customized to each individual. Of course, optimal gain selection still requires force estimation from the dominant limb. However, prosthetists are familiar with the subtleties of EMG channel gain selection.

Note that EMG-force calibration using contralateral force feedback (with or without mirror feedback) still requires use of a load cell. This option might be reasonable for use in a prosthetist's office, but does not seem reasonable for field calibration of a prosthesis control system.

7.4.4 Train EMG-Force, EMG-Target: Test Using Respective Feedback Signal—All Subjects

Finally, Fig. 7.6 and Fig. 7.7 show results when EMG-force/target models were trained and tested from the same signal source, excluding the previously shown Task 1 results from training using dominant limb force. These models importantly highlight results from the limb-absent subjects (whose anatomy does not permit measurement of affected-side limb forces). The associated statistical results are not as sharply defined, perhaps reflecting the larger result variances and the smaller sample size. Nonetheless, there was still a general trend for lower errors when training EMG-force/target models using contralateral feedback, and unacceptably higher errors when training with no feedback—consistent with results from the able-bodied subjects. Also, there were limited distinctions between the wrist DoFs (although Pro-Sup did have better 1-DoF performance than Rad-Uln). Pro-Sup would be the most intuitive if used to control wrist rotation. And, in limb-absent subjects, it is interesting to note that providing mirror visual feedback was not statistically different from providing no feedback.

7.4.5 General Discussion and Limitations

Our results found a rather clear performance hierarchy, with dominant limb feedback providing the lowest EMG-force error (as would be expected), followed by feedback based on bilateral tracking (using either the forces from the contralateral side, or mirror visual tracking), followed by no feedback. EMG-force models based on bilateral tracking seemed adequate, but require the use of a load cell and would exclude persons with bilateral limb-absence. EMG-target models formed using no feedback seemed inadequate. In such cases, population-based EMG-force models (as least for EMG-force dynamics; one gain per EMG channel is always needed to scale its contribution) might perform better.

In general, we chose to equate the dominant side of able-bodied subjects to the affected side of limb-absent subjects. We did so because prostheses aspire to be a high quality replacement of limb function (which is best represented by the dominant side in able-bodied subjects) and, thus, we wish to advance prosthesis control towards the performance expectations of the dominant limb. In addition, most prior EMG-force modeling has been performed on the dominant side of able-bodied subjects. Nevertheless, the sound side of limb-absent subjects becomes used as the dominant side, regardless of natural handedness—due largely to the limited functionality provided by existing prostheses.

We did not find many substantive differences in performance as a function of DoF. Such changes have been found in the literature (e.g., when relating dominant-limb EMG to hand position in the contralateral hand of able-bodied subjects, during bilateral mirror contractions (Muceli and Farina 2012)) and postulated to be consistent with deeper muscle fibers (which are more poorly represented in surface EMG) that are prime

torque generators for the poorer performing DoFs (Gilroy, MacPherson et al. 2008, p. 328–336). Perhaps if such differences exist, they are subtle enough to be difficult to find with the small sample sizes common in experimental studies in this field. Also, the use of a large number of electrodes, placed about the full extent of the remnant limb (as was done in our work), may help to mitigate these issues (Muceli and Farina 2012).

The tasks tested in this study were relatively novel to both our able-bodied and limb-absent subjects. In particular, 2-DoF target tracking was both novel and challenging. It would be interesting to determine if more tracking practice (or, repeated experimental sessions) would have led to better 2-DoF tracking (Hahne, Schweisfurth et al. 2018, Tabor, Bateman et al. 2018). Note that our force-varying target trajectories were selected for their system identification properties (uniform distribution gives equal weight to each force level; bandlimited and white gives equal weight to each frequency). If subjects are better able to produce the requested forces, the quality of the identified model is likely to improve.

We separated our statistical analyses of 1-DoF tasks from those of 2-DoF tasks, because these tasks are inherently different. Testing for a statistical difference between inherently distinct tasks is, generally, not of scientific value (Clancy, Martinez-Luna et al. 2017, Dai, Zhu et al. 2019). As shown in Table 2.2, Opn-Cls tracking latencies during 2-DoF tasks trended longer than those from 1-DoF tasks. Similarly, Fig. 2.5 and Fig. 2.8 suggest a trend for larger 2-DoF EMG-force RMSEs compared to 1-DoF. These trends are consistent with our anecdotal observation that subjects had more difficulty tracking in 2-DoFs than 1-DoF. Future work might seek to better understand the decrement in performance, if any, in 2-DoF tracking tasks vs. 1-DoF tracking tasks.

It is always important to recognize that the neuromuscular anatomy of limb-absent subjects is both different from that of able-bodied subjects and highly variable. For example, our able-bodied subjects had a mean ± std. dev. forearm circumference of 25.9 ± 3.2 cm compared to 22.2 ± 2.3 cm for the limb-absent subjects. Remnant muscle tissue typically has more neuromuscular damage and may be more prone to fatigue (e.g., (Hahne, Schweisfurth et al. 2018)). And, the sensation of a phantom hand may be more or less expressive in different subjects. Anecdotally, phantom limb sensation may have been more of a limitation in 2-DoF tasks than in 1-DoF tasks. Each of these factors may influence EMG-force performance.

Finally, there is some evidence suggesting that an accurate model of the dynamics between muscular activation (inputs) and kinetic/kinematic outputs is not paramount to control of the existing generation of myoelectrically-controlled prostheses, which provide relatively rudimentary function. If the myoelectric control model is repeatable and largely linear, then prosthesis users are hypothesized to adapt/re-learn the necessary inputs (muscular activations) required to achieve the desired output (Jiang, Vujaklija et al. 2014, Hahne, Markovic et al. 2017, Hahne, Schweisfurth et al. 2018). In fact, existing commercial prosthesis users have been doing so for years, albeit at the cost of additional mental workload (among other limiting factors)

(Williams III 1990). Of course, the higher the fidelity with which future prosthetic devices reproduce the function of intact limbs, the more apparent will become the benefit of accurately identifying models relating muscular activation to kinetics/kinematics. And, unilateral prosthesis users should benefit from more accurate forward-path activation models during, for example, bilaterally symmetric tasks, wherein the central nervous system nominally matches muscular activation between the affected and the sound side.

7.5 Conclusion

The prime goal of this work was to evaluate distinct options for surrogate supervised output sources in hand-wrist EMG-force models for limb-absent subjects. We did so using novel instrumentation in which hand Opn-Cls forces as well as wrist Rad-Uln force and Pro-Sup moment were simultaneously measured on both sides of our able-bodied subjects. This instrumentation allowed us to report novel quantitative results on the latency between force/moment and our random target (Table 7.2); and on the ability of these subjects to perform random target tracking during our various tasks, contrasting RMSE to cross-correlation coefficient (Fig. 7.4).

For EMG-force modeling, our comparison of different feedback approaches found that use of the phantom limb for bilateral tracking (with or without mirror visual feedback) permitted the limb on the sound side to provide a reasonable substitute force measurement. But, this output source is only available to persons with unilateral limb-absence and still requires use of a load cell. As such, it is primarily of use in a prosthetist's office, and not in the field. We found that use of the tracking target without a feedback source (applicable to limb-absent subjects) resulted in an inadequate EMG-force model. In such cases, use of generic models for EMG-force dynamics, combined with simple gain selection for each EMG channel, would likely provide better performance.

Chapter 8: Efficiently Training Two-DoF Hand-Wrist EMG-Force Models

This chapter is published as: Berj Bardizbanian, Ziling Zhu, Jianan Li, Xinming Huang, Chenyun Dai, Carlos Martinez-Luna, Benjamin E. McDonald, Todd R. Farrell, Edward A. Clancy, "Efficiently Training Two-DoF Hand-Wirst, EMG-Force Models," *2020 42nd Annual International Conference of IEEE Engineering in Medicine & Biology Society (EMBC)*, 20–24 July, 2020. Color versions of one or more of the figures in this paper are available online at: https://ieeexplore.ieee.org/abstract/document/9175675.

Abstract— **Single-use EMG-force models (i.e., a new model is trained each time the electrodes are donned) are used in various areas, including ergonomics assessment, clinical biomechanics, and motor control research. For one degree of freedom (1-DoF) tasks, input-output (black box) models are common. Recently, black box models have expanded to 2-DoF tasks. To facilitate efficient training, we examined parameters of black box model training methods in 2-DoF force-varying, constant-posture tasks consisting of hand open-close combined with one wrist DoF. We found that approximately 40–60 s of training data is best, with progressively higher EMG-force errors occurring for progressively shorter training durations. Surprisingly, 2-DoF models in which the dynamics were universal across all subjects (only channel gain was trained to each subject) generally performed 15–21% better than models in which the complete dynamics were trained to each subject. In summary, lower error EMG-force models can be formed through diligent attention to optimization of these factors.**

8.1 Introduction

Over the past several decades, numerous investigators have studied the dynamic system relationship between the conventional surface electromyogram (EMG) and muscle force/joint torque (Buchanan, Lloyd et al. 2004, Staudenmann, Roeleveld et al. 2010). Much of this modeling trains an EMG-force model for single-use (i.e., a new model is trained each time the electrodes are applied), applicable to areas such as ergonomics assessment, clinical biomechanics, scientific studies relating EMG to joint mechanical impedance, and motor control research. Single-use EMG-force calibration is appropriate, as there is evidence of inter-day decrements in performance when an EMG-force model is not re-calibrated (Oskouei, Paulin et al. 2013). Some emerging studies have introduced the use of large, high-density surface EMG arrays (Muceli and Farina 2012, Liu, Brown et al. 2013, Hahne, Biessmann et al. 2014). But, these arrays generally remain rather complex and expensive for biomechanics investigations, and are presently impractical for most commercial applications of EMG.

In one modeling paradigm, EMG-force dynamics are assumed (e.g., length-tension and force-velocity relationships) and only the gains of each EMG channel are optimized (Hof and Van den Berg 1981, Buchanan, Lloyd et al. 2004). This "Hill-style" paradigm is simpler and of particular benefit in multi-joint studies for which training of system dynamics would be a daunting task. Alternatively, the "black box" system identification paradigm trains subject- and muscle-specific EMG-force models (Hof and Van den Berg 1981, Doheny, Lowery et al. 2008, Clancy, Liu et al. 2012, Hashemi, Morin et al. 2012, Hashemi, Morin et al. 2013, Hashemi, Morin et al. 2015, Liu, Liu et al. 2015). Because these models adapt to the specific subject and/or muscle, they would generally be hypothesized to be more accurate than Hill-style models, but require longer training trials (Ljung 1999) and more effort to program. For simplicity, most early work in this area focused on linear models of single-joint systems. Non-linear models, however, have been shown to improve the relationship (Vredenbregt and Rau 1973, Hashemi, Morin et al. 2012, Dai, Bardizbanian et al. 2017).

Recently, there has been increased interest in expanding these black box models to multi-joint applications, for example to two degree of freedom (DoF) systems in the upper limb (Hahne, Biessmann et al. 2014, Clancy, Martinez-Luna et al. 2017, Hahne, Schweisfurth et al. 2018, Dai, Zhu et al. 2019). In doing so, several technical questions related to system identification are encountered. Previously (Dai, Zhu et al. 2019), we studied 2-DoF EMG-force in the hand-wrist, finding lower errors when training sets included both 1-DoF and 2-DoF trials. Further, we studied the required number of conventional electrodes, when placed eqidistant about the circumference of the proximal forearm. Using backward stepwise selection of 16 electrodes, we found that error was optimized with 6 electrodes. Of course, backward selection of electrode sites may have limited utility in single-use EMG-force studies, since all 16 electrodes must still be applied.

These insights narrow the range of system identification methods that need be considered when conducting single-use EMG-force studies. However, other modeling questions remain: determining the necessary duration of training data used to form the EMG-force relationship and choosing the specificity of the model (subject-specific vs. DoF-specific models of dynamics vs. a "universal" Hill-style model of dynamics used for all subjects and muscles). Herein, we examine these questions when relating forearm surface EMG to hand open-close (Opn-Cls) combined with one of three wrist DoFs—either extension-flexion (Ext-Flx) force, radial-ulnar (Rad-Uln) force, or pronation-supination (Pro-Sup) moment.

8.2 Methods

8.2.1 Experimental Data and Apparatus

<u>Data Collection—Setup:</u> The WPI IRB approved reprocessing of previously acquired data from able-bodied subjects (5 males, 4 females; aged 27±9.7 years) (Dai, Zhu et al. 2019). Subjects sat at the

experimental apparatus (see (Dai, Zhu et al. 2019), Figs. 1–3) with their dominant hand cuffed to a 6-DoF load cell, to measure wrist force/torque. Separately, Opn-Cls grip force was measured by a single-axis load cell by securing to the thumb on one side and the distal aspects of the four fingers on the opposite side. The shoulder was flexed 45º forward from the anatomical position along the sagittal plane, the wrist was in a neutral position and the palm of the hand was perpendicular with the plane of the floor. The elbow was supported.

Skin about the forearm was scrubbed with an alcohol wipe and electrode gel was applied. Sixteen bipolar EMG electrodes were applied equidistant and circumferentially about the forearm: their mid-point was located 5 cm distal to the elbow crease. Bipolar electrodes were 5 mm diameter, stainless steel, hemispherical contacts separated 1 cm edge-to-edge, oriented along the forearm's long axis. A gelled reference electrode was secured on the ventral forearm. Each EMG signal was differentially amplified (30–500 Hz pass band, CMRR > 100 dB over the pass band). Load cell force/moment was displayed in real-time as a blue arrowhead on a computer screen. The arrowhead displayed 4 DoFs: x-axis location for Ext-Flx force, y-axis location for Rad-Uln force, rotation for Pro-Sup moment, and size for hand Opn-Cls force. A second red arrowhead displayed a computer-controlled target. Four load cell signals and 16 EMG channels were each sampled at 2048 Hz with 16-bit resolution.

Data Collection—Contractions: All contractions were constant-posture, with a two-minute rest interval between each. After warm-up, maximum voluntary contraction (MVC) was measured separately for both directions of each of the 4 DoFs. Next, subjects produced 5 s constant-force 50% MVC contractions for each direction within a DoF.

Then, subjects completed 1-DoF *dynamic* tracking trials, separately for each DoF (randomized order). Feedback only displayed the specified DoF. For Rad-Uln, the target moved randomly between ±(|30 %MVC Rad| + |30 %MVC Uln|)/2. The random target movement was a 0.75 Hz band-limited, white and uniform random process. Four trials of 40 s duration each were completed. The equivalent trials were completed for the three remaining DoFs (16 trials total); except that the maximum force was reduced to 15 %MVC for Opn-Cls due to excessive hand open fatigue found during preliminary testing.

Lastly, subjects tracked *dynamic* 2-DoF targets: hand Opn-Cls paired with one wrist DOF (Ext-Flx, Rad-Uln or Pro-Sup). The same random target style was used, with independent random instances per DoF. Four trials of 40 s duration were completed for each DoF combination (12 trials total).

8.2.2 Analysis: Signal Pre-Processing

Data analysis was performed offline in MATLAB. Time-varying EMG standard deviation (EMGσ[n], for discrete-time sample n) was estimated for each channel. Raw EMG were highpass filtered (5th-order

Butterworth, f_c=15 Hz), notch filtered to attenuate power-line interference (2nd-order IIR filter at 60 Hz, notch bandwidth of 1 Hz), rectified, lowpass filtered at 16 Hz (Chebyshev Type 1 filter, 9th-order, 0.05 dB peak-to-peak passband ripple), and downsampled to 40.96 Hz (Ljung 1999, Clancy, Bida et al. 2006). Each force/moment signal was normalized by its corresponding MVC level pair. For example, Rad-Uln was normalized by: $(|MVC_{Rad}| + |MVC_{Uln}|)/2$.

8.2.3 Analysis: One-DoF Models

1) Subject-Specific, Full-Duration Model: One-DoF modeling only utilized 1-DoF trials. EMGσ values were related to force/moment—separately for each DoF—via regression (20th- order linear dynamic model (Clancy, Liu et al. 2012, Dai, Zhu et al. 2019); 2 or 16 electrodes used in the fit, where values less than 16 were arrived at using backward stepwise selection (Clancy, Martinez-Luna et al. 2017, Dai, Zhu et al. 2019). Model training used the least squares pseudo-inverse method (Press, Flannery et al. 1994), with singular values of the design matrix removed if the ratio of their magnitude to that of the largest singular value was less than 0.01 (Clancy, Liu et al. 2012). Note that backward selection down to 2 electrodes has previously been shown to perform as well as 16 electrodes for these 1-DoF tasks (Clancy, Martinez-Luna et al. 2017, Dai, Zhu et al. 2019). Two trials were used for training, and two for testing (RMS error between the estimated and measured torques, expressed in %MVC, after discarding the first 2 s of each trial). Training and testing trials were then exchanged (two-fold cross-validation), with the average of these two folds reported.

2) Subject-Specific, Reduced-Duration Model: The above procedure was repeated while utilizing less than the full available training time, thus varying the time duration used for training. In this manner, we could evaluate model performance vs. training duration. For training durations of 14, 22, 30 and 38 s, only the necessary initial portion of the first training trial was used, and the second training trial was ignored. For training durations of 44, 52, 60, 68 and 76 s, equal durations of both training trials were used (half of the training duration derived from each trial). As above, model testing used both full testing trials, with the two-fold cross-validation results averaged.

3) DoF-Specific Model: General dynamic models, one per DoF, were next constructed, using data from 1-DoF trials. Two trials were used to train subject-specific models for each subject. After backward selecting down to the channels preferred for EMG-force estimation, the fit coefficients define a FIR filter, which is inherently lowpass in shape (Inman, Ralston et al. 1952, Hof and Van den Berg 1981, Winter and Yack 1987, Winter 2009, pp. 250–280, Koirala, Dasog et al. 2015, Clancy, Negro et al. 2016). These filters were each normalized to a gain of one at 0 Hz—expressing the EMGσ-force dynamics, absent of the gains for each EMG channel. A total of 36 gain-normalized filters were formed per DoF (nine subjects, two EMG channels

per subject, two cross-validations). The ensemble mean coefficient values of these filters (one filter per DoF) were computed.

This DoF-specific filter was used, in place of the dynamics provided by subject-specific filters by appending them to the EMG pre-processing (after the decimation step). This evaluation assessed if subject-specific, EMG channel-specific calibration of dynamics could be replaced with one dynamic filter per DoF. Once the DoF-specific filters were formed, the training trials were used to calibrate *only* the gains of each EMG channel. Testing was performed on the remaining two trials. Backward stepwise selection from 16 down to 2 electrodes was performed, with only results for 2 and 16 EMG channels reported (with cross-validation). This analysis was completed for each of the DoFs and training durations.

4) Universal Model: This analysis was similar to the prior analysis, except that the 36 DoF-specific filter coefficients were ensemble averaged into one "universal" filter (Fig. 6.1) to assess if one filter shape could capture all dynamics for all DoFs. Again, analysis was completed for all training durations and only the results for 2 and 16 EMG channels are reported.
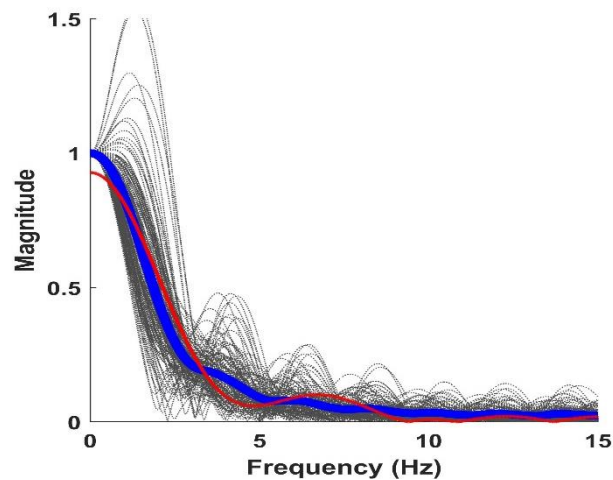
Fig. 8.1. Each of 144 magnitude responses of the 1-DoF models is shown in grey (nine subjects, two EMG channels per subject, two cross-validations, 4 DoFs). Thick blue line is the average and thin red line is the universal FIR filter fit to these responses.

8.2.4 Analysis: Two-DoF Models

Similar 2-DoF EMG-force models were evaluated (with backward stepwise selection to 6 EMG channels and two-fold cross-validation) for each of Opn-Cls paired with one wrist DoF, always estimating 2 DoFs simultaneously. Each EMG channel contributed to both DoFs. Model training always combined both 1-DoF trails and the corresponding 2-DoF trial. Model testing was performed only using the 2-DoF trials. Note that backward selection down to 4–6 electrodes has previously been shown to perform nearly as well as 16 electrodes for these 1-DoF tasks (Clancy, Martinez-Luna et al. 2017, Dai, Zhu et al. 2019).

8.2.5 Statistics

Performance differences were tested statistically with SPSS 25 using multivariate RANOVA. Interactions were not significant, unless noted. When degree of sphericity ε was <0.75, degrees of freedom was adjusted by the method of Greenhouse-Geisser; and when 0.75≤ε<1, by the method of Huynh-Feldt (Girden 1992). When multiple comparisons are summarized, degrees of freedom are reported without adjustment. Tukey *post hoc* comparisons were conducted using Fisher's least significant difference (LSD). A significance level of $p = 0.05$ was used.

8.3 Results

8.3.1 One-DoF Models

Fig. 8.2 shows summary test error results vs. training duration for the 1-DoF models using 2 electrodes. All models experienced lower mean error as training duration increased from 14 s, with less improvement as training duration grew. Using all the results of 1-DoF models, a four-way RANOVA was computed [factors: model (subject-specific, DoF-specific, universal), number of electrodes (2, 16), duration (14, 22, 30, 38, 44, 52, 60, 68, 76 s) and DoF (Flx-Ext, Rad-Uln, Pro-Sup, Opn-Cls)]. Since there was a significant two way interaction term involving model and DoF [$F_{(2.5, 20.0)} = 6.1$, $p_{GG} = 0.006$], three way RANOVA's were implemented fixing each DoF. The main effects were significant for model [$F_{(2,16)} > 77$, $p \leq 0.03$], except for Rad-Uln [$F_{(2,16)} = 3.5$, $p = 0.06$]; significant for duration [$F_{(8,64)} > 5$, $p \leq 0.04$]; but not significant for number of electrodes [$F_{(1,8)} < 6$, $p \geq 0.05$].
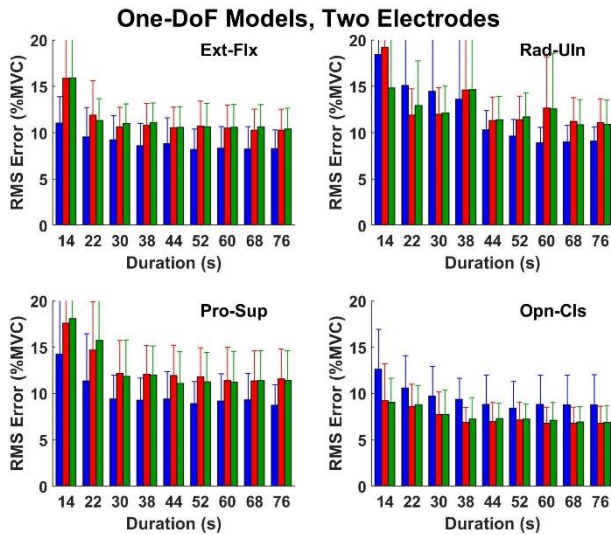
Fig. 8.2. One-DoF summary results for each DoF vs. training duration. Mean error plus one standard deviation shown for 2-electrode models. (Some error bars cropped by *y*-axis scaling.) Subject-specific models in blue, DoF-specific models in red, universal models in green.
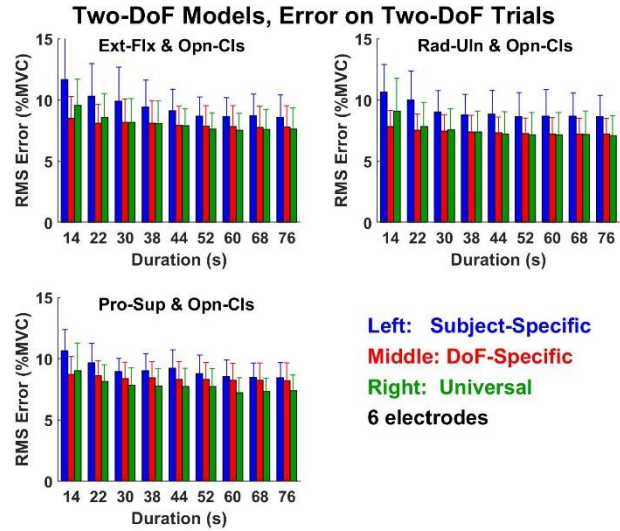
Fig. 8.3. Two-DoF summary results for each DoF pair vs. training duration, when assessing on 2-DoF trials. Mean error plus one standard deviation shown for 6-electrode models.

Tukey *post hoc* comparisons were computed for all significant differences. In summary, when comparing the 1-DoF models, the subject-specific model generally had the lowest errors. There was a clear trend for higher %MVC errors at shorter training durations versus longer durations. For example, training with 14 s always exhibited higher error than $\geq$ 30s and training with 22 s always exhibited higher error than $\geq$ 68s. Performance improvement plateaued at longer durations (e.g. there was no statistically significant improvement for durations beyond 30 s for Rad-Uln and Opn-Cls, or beyond 60 s for Ext-Flx and Pro-Sup). With two backward selected electrodes, a training duration of 60 s and subject specific modeling, average $\pm$ standard deviation errors (% MVC) were: 8.34 $\pm$ 2.32 for Ext-Flx, 8.92 $\pm$ 9.65 for Rad-Uln, 9.2 $\pm$ 2.93 for Pro-Sup and 8.81 $\pm$ 3.18 for Opn-Cls.

8.3.2 Two-DoF Models Assessed on Two-DoF Trials

Fig. 8.3 shows summary test error results vs. training duration for the 2-DoF models using 6 electrodes. All models experienced clearly lower error as training duration increased from 14 s, with less improvement as training duration grew. Using all the results of 2-DoF models, a four-way RANOVA was computed [factors: model (subject-specific, DoF-specific, universal), number of electrodes (6, 16), duration (14, 22, 30, 38, 44, 52, 60, 68, 76 s) and DoF pair (Opn-Cls with Flx-Ext, Opn-Cls with Rad-Uln, Opn-Cls with Pro-Sup). There were significant interactions involving model and duration [$F_{(16,128)}=17$, *p*=0.0001]. Unfortunately, fixing a second factor did not eliminate interactions. Thus, we continued to pursue the non-interacting factors within this four-way RANOVA. These other main effects were significant for number of electrodes [$F_{(1,8)}=16$, *p*=0.004] and not significant for DoF pair [$F_{(2,16)}=0.6$, *p*=0.6]. Tukey *post hoc* comparisons found that using 6 electrodes had a significantly higher mean error than using 16 electrodes.

To examine the model and duration factors, we next performed Tukey pair-wise comparisons for each combination of these factors (with Bonferroni correction). Considering duration: subject-specific models with durations below 38 s always had higher errors than those with durations above 68 s; and DoF-specific and universal models with durations below 30 s always had higher errors than respective models with durations above 68 s. Considering model: subject-specific models always had 15–21% *higher* error than the other two models (except at a duration of 60 s—likely an anomaly), and DOF-specific models did not differ from universal models.

8.4 Discussion

8.4.1 Parameter Selection for Efficient EMG-Force Training

This research focused on two technical details related to forming 2-DoF EMG-force models at the hand-wrist. An ability to time-efficiently and accurately calibrate EMG-force models is of value to several application areas, including ergonomics assessment, clinical biomechanics, scientific studies of muscle tension and joint impedance. First, we examined the duration of training used to form the EMG-force relationship. For single-use applications, it is most useful to be able to train models quickly. With all 1-DoF models, error decreased in an exponential fashion as training duration

increased. These changes were consistently statistically significant at the shorter durations (where the slope of error vs. duration was largest), but less so at the longer training durations (where more statistical power would be required in order to identify the smaller presumed differences). Most of the error reduction occurred with durations up to 40–60 s. These hand-wrist results are consistent with 1-DoF EMG-force results in the elbow (Clancy, Liu et al. 2012), wherein 52 s of training data for similar dynamic models were found to reduce error compared to 26 s. For our 2-DoF models, a similar exponential trend was found (error decaying with increased training duration), but the rate of error decay was not as steep. This difference in rate may reflect that the final error was, on average, larger for the 2-DoF trials. These results are generally consistent with system identification theory, in which the necessary training duration is proportional to the number of fit parameters (2-DoF models have more fit parameters) and that error reduces less than linearly as the training size progressively increases (Ljung 1999).

Second, we researched the specificity of the model (subject-specific vs. DoF-specific vs. universal). A universal model is similar to a Hill model in that the dynamics are pre-assigned. For 1-DoF models, subject-specific models clearly performed best, in general, reducing error by 11–24% compared to universal models. But, for 2-DoF models, universal models actually performed *better* than subject-specific models, in general, by 15–21%. Since model training for 2-DoF models uses twice as many fit parameters, one would expect a

poorer fit (if all other factors are identical). Thus, perhaps it is simply more difficult to identify these more complex models, leading to poorer model fits in the subject-specific models. Additionally, our anecdotal evidence during data collection is that subjects struggled to perform 2-DoF tracking, and may have exhibited greatly reduced tracking accuracy in one of the two DoFs. Thus, the second DoF may have been limited to contractions with a non-uniform distributed range of forces and a colored band-limited spectrum, resulting in poorer per-subject model calibration. However, since the universal model was constructed from 1-DoF trials, it would not suffer from this problem. Note that our universal models were still formed from data specific to our muscles studied, arm pose and training-testing trajectories. Hence, generic models (e.g., Hill style) that are not tuned in this manner (i.e., simply selected, for example, as second-order lowpass dynamics—a common selection) might be expected to perform poorer. Thus, our results do not directly suggest that Hill style models will outperform subject-specific models in all cases.

8.4.2 Limitations and Extensions

First, our sample size was limited and we studied a single joint. Second, we limited our contractions to being constant posture. It is well established that EMG-force varies with joint angle (e.g., the length-tension curve (Rack and Westbury 1969, Vredenbregt and Rau 1973, Doheny, Lowery et al. 2008, Hashemi, Morin et al. 2013, Liu, Liu et al. 2013, Liu, Liu et al. 2015)). Thus, conditions of this work should be extended to varied angle in the future. Third, the method of electrode site selection by backward stepping produces a locally optimum solution, but not necessarily a global optimum. And, this solution is limited by the sites imposed by the original equal-spaced application of the 16 electrodes. Alternative schemes exists, including schemes based on muscle anatomy (Fougner, Stavdahl et al. 2014). Fourth, these results present a conundrum for single-use applications: much fewer than 16 electrodes provide minimum error performance, but the complete set of 16 electrodes must be mounted in order to determine the optimal electrode sites. For single-use applications, it may be as effective to simply use the full 16-channel electrode system and forgo any backward selection of EMG channels. Finally, in order to focus on efficient training of EMG-force models, we limited our models to be linear and did not pre-whiten our EMG data. Non-linear models have been shown to produce better EMG-force relationships (Vredenbregt and Rau 1973, Hashemi, Morin et al. 2012, Dai, Bardizbanian et al. 2017). Further, EMG pre-whitening has been shown to reduce the variance of the EMGσ estimate (Hogan and Mann 1980, Clancy and Hogan 1994), resulting in reduced EMG-force error (Clancy and Hogan 1997, Clancy, Liu et al. 2012, Dai, Bardizbanian et al. 2017). Each of these methods can be incorporated in future work.

8.5 Conclusion

We studied efficient training of 2-DoF EMG-force models using conventional EMG electrodes. We found that EMG-force error reduced as training duration increased, for durations up to 40–60 s. Improvement in performance was greatest at the lower training durations. And, subject-specific models performed best when forming 1-DoF models, but (generally) worst when forming 2-DoF models.

References

(1982). Human Motor Behavior: An Introduction. New York, Psychology Press.

(2004). Powered Upper Limb Prostheses. Berlin, Springer.

Abul-Haj, C. J. and N. Hogan (1990). "Functional assessment of control systems for cybernetic elbow prosthesis—Part I: Description of the technique." IEEE Trans. Biomed. Eng. 37(11): 1025–1036.

Aguilar, S., R. Vidal and C. Gomez (2017). "Opportunistic sensor data collection with Bluetooth low energy." Sensors 17: 159.

Ahmadizadeh, C., M. Khoshnam and C. Menon (2021). "Human-machine interfaces in upper-limb prosthesis control." IEEE Sig. Proc. Mag. 38(4): 12–22.

Ahmadizadeh, C., L.-K. Merhi, B. Pousett, S. Sangha and C. Menon (2017). "Toward intuitive prosthesis control: Solving common issues using force myography, surface electromyography, and pattern recognition in a pilot case study." IEEE Robot. Automat. Mag. 24(4): 102–111.

Al-Timemy, A. H., G. Bugmann, J. Escudero and N. Outram (2013). "Classification of finger movements for the dexterous hand prosthesis control with surface electromyography." IEEE J. Biomed. Health Inform. 17(3): 608–618.

Albrektsson, T. and C. Johansson (2001). "Osteoinduction, osteoconduction and osseointegration." European spine journal 10(2): S96-S101.

Alkan, A. and M. Gunay (2012). "Identification of EMG signals using discriminant analysis and SVM classifier." Exp. Sys. App. 39: 44–47.

Ameri, A., M. A. Akhaee, E. Scheme and K. Englehart (2020). "A deep transfer learning approach to reducing the effect of electrode shift in EMG pattern recognition-based control." IEEE Trans. Neural Sys. Rehabil. Eng. 28(2): 370–379.

Ameri, A., E. N. Kamavuako, E. J. Scheme, K. B. Englehart and P. Parker (2014). "Support vector regression for improved real-time, simultaneous myoelectric control." IEEE Trans. Neural Sys. Rehabil. Eng. 22(6): 1198–1209.

Ameri, A., E. J. Scheme, E. N. Kamavuako, K. B. Englehart and P. A. Parker (2014). "Real-time, simultaneous myoelectric control using force and position-based training paradigms." IEEE Trans. Biomed. Eng. 61(2): 279–287.

Amsuess, S., P. Goebel, B. Graimann and D. Farina (2015). "A multi-class proportional myocontrol algorithm for upper limb prosthesis control: Validation in real-life scenarios in amputees." IEEE Trans. Neural Sys. Rehabil. Eng. 23(5): 827–836.

Andison, C. (2011). EMG-based assessment of active muscle stiffness and co-contraction in muscles with primary and secondary actions at the wrist during piano playing. Master of Applied Science, Carleton University.

Asgarian, F. and K. Najafi (2017). Time synchronizatino in a network of Bluetooth low energy beacons. SIGCOMM.

Azaria, M. and D. Hertz (1984). "Time delay estimation by generalized cross correlation methods." IEEE Trans. Acoust. Speech Sig. Proc. 32(2): 280–285.

Balani, R. (2007). Energy consumption analysis for Bluetooth, WiFi and cellular networks, University of California at Los Angeles (UCLA).

Bardizbanian, B., J. Keating, X. Huang and E. A. Clancy (2020). Estimating Individual and Combined Fingertip Forces From Forearm EMG During Constant-Pose, Force-Varying Tasks. 2020 42nd Annual International Conference of the IEEE Engineering in Medicine & Biology Society (EMBC), IEEE.

Bardizbanian, B., Z. Zhu, J. Li, C. Dai, C. Martinez-Luna, X. Huang, T. Farrell and E. A. Clancy (2018). Calibration of dynamic hand-wrist EMG-force models using a minimum number of electrodes. IEEE SPMB Symp., Philadelphia, PA.

Bardizbanian, B., Z. Zhu, J. Li, X. Huang, C. Dai, C. Martinez-Luna, B. E. McDonald, T. R. Farrell and E. A. Clancy (2020). Efficiently training two-DoF hand-wrist EMG-force models. Ann. Int. Conf. IEEE EMBS, Montreal, Canada.

Barmparas, G., K. Inaba, P. G. Teixeira, J. J. Dubose, M. Criscuoli, P. Talving, D. Plurad, D. Green and D. Demetriades (2010). "Epidemiology of post-traumatic limb amputation: a National Trauma Databank analysis." The American Surgeon 76(11): 1214-1222.

Barnett, S. D., A. W. Heinemann, A. Libin, A. C. Houts, J. Gassaway, S. Sen-Gupta, A. Resch and D. F. Brossart (2012). "Small N designs for rehabilitation research." J. Rehabil. Res. Devel. 49(1): 175–186.

Bates, T., J., J. R. Fergason and S. N. Pierrie (2020). "Technological advances in prosthesis design and rehabilitation following upper extremity limb loss." Curr. Rev. Musculo. Med. 13: 485–493.

Battye, C. K., A. Nightingale and J. Whillis (1955). "The use of myo-electric currents in the operation of prostheses." J. Bone Joint Surg. 37B(3): 506–510.

Belgacem, N. and F. Bereksi-Reguig (2011). "Bluetooth portable device for ECG and patient motion monitoring." Nature Tech.(4): 19–23.

Bertels, T., T. Schmalz and E. Ludwigs (2009). "Objectifying the functional advantages of prosthetic wrist flexion." J. Prosthet. Orthot. 21(2): 74–78.

Biddiss, E., D. Beaton and T. Chau (2007). "Consumer design priorities for upper limb prosthetics." Disab. Rehabil. Assist. Tech. 2(6): 346–357.

Bideaux, A., B. Zimmermann, S. Hey and W. Stork (2015). "Synchronization in wireless biomedical-sensor networks with Bluetooth low energy." Cur. Dir. Biomed. Eng 1: 73–76.

Boyd, W. J. (2018). EMG Site: A MATLAB-Based Application for EMG Data Collection and EMG-Based Prosthetic Control. M.S., Worcester Polytechnic Institutte.

Branemark, P.-I. (1983). "Osseointegration and its experimental background." J prosthet Dent 50: 399-410.

Brunelli, D., E. Farella, D. Giovanelli, B. Milosevic and I. Minakov (2016). "Design considerations for wireless acquisition of multichannel sEMG signals in prosthetic hand control." IEEE Sensors J. 16(23): 8338–8347.

Brunelli, D., A. M. Tadesse, B. Vodermayer, M. Nowak and C. Castellini (2015). Low-cost wearable multichannel surface EMG acquisition for prosthetic hand control. Int. Worksh. Adv. Sensors Interface., Galipoli, Italy.

Bruscato, L. T., T. Heimfarth and E. P. de Freitas (2017). "Enhancing time synchronization support in wireless sensor networks." Sensors 17: 2956.

Buchanan, T. S., D. G. Lloyd, K. Manal and T. F. Besier (2004). "Neuromusculoskeletal modeling: Estimation of muscle forces and joint moments and movements from measurements of neural command." J Appl Biomech 20(4): 367–395.

Burger, H. and G. Vidmar (2016). "A survey of overuse problems in patients with acquired or congenital upper limb deficiency." Prosthet. Orthot. Int. 40(4): 497–502.

Calado, A., G. Macciantelli, V. Errico, E. Gruppioni and G. Saggio (2020). Evaluation of dedicated Bluetooth Low Energy wireless data transfer for an implantable EMG sensor. ACM Sensors Sig. Image Proc., Prague, Czech Republic.

Cao, H., V. Leung, C. Chow and H. Chan (2009). "Enabling technologies for wireless body area networks: A survey and outlook." IEEE Comm. Mag. 47(12): 84–93.

Cavanaugh, K. T., E. A. Clancy, J. A. Natrillo, R. J. Paquette and F. J. Looft (1983). "Optimal site selection for prosthetic control." IEEE 1983 Frontiers Eng. Comput. Health Care: 565–569.

Chan, B. L., R. Witt, A. P. Charrow, A. Magee, R. Howard, P. F. Pasquina, K. M. Heilman and J. W. Tsao (2007). "Mirror therapy for phantom limb pain." New England J. Med. 357(21): 2206–2207.

Cipriani, C., R. Sassu, M. Controzzi and M. C. Carrozza (2011). Influence of weight actions of the hand prosthesis on the performance of pattern recognition based myoelectric control: Preliminary study. 33rd Ann. Int. Conf. IEEE EMBS.

Clancy, E. A. (1991). Stochastic Modeling of the Relationship Between the Surface Electromygram and Muscle Torque, Ph.D Thesis, Massachusetts Institute of Technology, p. 303–352, 449–469.

Clancy, E. A. (2019). Optimal Electromyogram Modeling and Processing During Active Contractions and Rest, Haopeng Wang M.S. Thesis, Worcester Polytechnic Institute: 40–58.

Clancy, E. A., O. Bida and D. Rancourt (2006). "Influence of advanced electromyogram (EMG) amplitude processors on EMG-to-torque estimation during constant-posture, force-varying contractions." J. Biomech. 39: 2690–2698.

Clancy, E. A. and K. A. Farry (2000). "Adaptive whitening of the electromyogram to improve amplitude estimation." IEEE Trans. Biomed. Eng. 47(6): 709–719.

Clancy, E. A. and N. Hogan (1994). "Single site electromyograph amplitude estimation." IEEE Trans. Biomed. Eng. 41(2): 159–167.

Clancy, E. A. and N. Hogan (1995). "Multiple site electromyograph amplitude estimation." IEEE Trans. Biomed. Eng. 42(2): 203–211.

Clancy, E. A. and N. Hogan (1997). "Relating agonist-antagonist electromyograms to joint torque during isometric, quasi-isotonic, non-fatiguing contractions." IEEE Trans. Biomed. Eng. 44(10): 1024–1028.

Clancy, E. A., L. Liu, P. Liu and D. V. Moyer (2012). "Identification of constant-posture EMG-torque relationship about the elbow using nonlinear dynamic models." IEEE Trans. Biomed. Eng. 59(1): 205–212.

Clancy, E. A., C. Martinez-Luna, M. Wartenberg, C. Dai and T. Farrell (2017). "Two degrees of freedom quasi-static EMG-force at the wrist using a minimum number of electrodes." J. Electromyogr. Kinesiol. 34: 24–36.

Clancy, E. A., F. Negro and D. Farina (2016). Single-channel techniques for information extraction from the surface EMG signal. Surface Electromyography: Physiology, Engineering, and Applications. R. Merletti and D. Farina, John Wiley & Sons, Inc.: 91–125.

Connolly, C. (2008). "Prosthetic hands from Touch Bionics." Indust. Robot Int. J. 35(4): 290–293.

Cordella, F., A. L. Ciancio, R. Sacchetti, A. Davalli, A. G. Cutti, E. Guglielmelli and L. Zollo (2016). "Literature review on needs of upper limb prosthesis users." Front. Neurosci. 10: 209.

Cosmanescu, A., B. Miller, T. Magno, A. Ahmed and I. Kremenic (2006). Design and implementation of a wireless (Bluetooth) four channel bio-instrumentation amplifier and digital data acquisition device with user-selectable gain, frequency, and driven reference. 28th IEEE EMBS Annual International Conference.

Dai, C., B. Bardizbanian and E. A. Clancy (2016). "Comparison of constant-posture force-varying EMG-force dynamic models about the elbow." IEEE Transactions on Neural Systems and Rehabilitation Engineering 25(9): 1529-1538.

Dai, C., B. Bardizbanian and E. A. Clancy (2017). "Comparison of constant-posture force-varying EMG-force dynamic models about the elbow." IEEE Trans. Neural Sys. Rehabil. Eng.(9): 1529–1538.

Dai, C., Z. Zhu, C. Martinez-Luna, T. R. Hunt, T. R. Farrell and E. A. Clancy (2019). "Two degrees of freedom, dynamic, hand-wrist EMG-force using a minimum number of electrodes." J. Electromyo. Kinesiol. 47: 10–18.

Dementyev, A., S. Hodges, S. Taylor and J. Smith (2013). Power consumption analysis of Bluetooth low energy, ZigBee and ANT sensor nodes in a cyclic sleep scenario. 2013 IEEE International Wireless Symposium.

Dian, F. J., A. Yousefi and K. Somaratne (2017). A study in accuracy of time synchronization of BLE devices using connection-based event. IEEE IEMCON.

Dillingham, T. R., L. E. Pezzin and E. J. MacKenzie (2002). "Limb Amputation and Limb Deficiency: Epidemiology and Recent Trends in the United States." South. Med. J. 95: 875–883.

Dixon, A. M. R., E. G. Allstot, D. Gangopadhyay and D. J. Allstot (2012). "Compressed sensing system considerations for ECG and EMG wireless biosensors." IEEE Trans. Biomed. Circ. Sys. 6(2): 156–166.

Doheny, E. P., M. M. Lowery, D. P. FitzPatrick and M. J. O'Malley (2008). "Effect of elbow joint angle on force-EMG relationships in human elbow flexor and extensor muscles." J Electromyogr Kinesiol 18: 760–770.

Duan, N., R. L. Kravitz and C. H. Schmid (2013). "Single-patient (n-of-1) trials: A pragmatic clinical decision methodology for patient-centered comparative effectiveness research." J. Clin. Epi. 66: S21–S28.

Dyson, M., J. Barnes and K. Nazarpour (2018). "Myoelectric control with abstract decoders." J. Neural. Eng. 15: 056003.

Dyson, M., S. Dupan, H. Jones and K. Nazarpour (2020). "Learning, gneralization, and scalability of abstract myoelectric control." IEEE Trans. Neural Sys. Rehabil. Eng. 28(7): 1539–1547.

Early, E. J., L. J. Hargrove and T. A. Kuiken (2016). "Dual window pattern recognition classifier for improved partial-hand prosthesis control." Front. Neurosci. 10: 58.

Englehart, K. and B. Hudgins (2003). "A robust, real-time control scheme for multifunction myoelectric control." IEEE Trans. Biomed. Eng. 50(7): 848–854.

Fadhlannisa, N. F. and B. Basari (2020). Design of wireless electromyography (EMG) monitoring system for muscle activity detection on Parkinson disease. IEEE Int. Conf. Smart Tech. Appl.

Farina, D., I. Vujaklija, R. Branemark, A. M. J. Bull, H. Dietl, B. Graimann, L. J. Hargrove, K.-P. Hoffmann, H. H. Huang, T. Ingvarsson, H. B. Janusson, K. Kristjansson, T. Kuiken, S. Micera, T. Stieglitz, A. Sturma, D. Tyler, R. F. f. Weir and O. C. Aszmann (2021). "Toward higher-performance bionic limbs for wider clinical use." Nature Biomed. Eng.

Farina, D., I. Vujaklija, M. Sartori, T. Kapelner, F. Negro, N. Jiang, K. Bergmeister, A. Andalib, J. Principe and O. C. Aszmann (2017). "Man/machine interface based on the discharge timings of spinal motor neurons after targeted muscle reinnervation." Nat. Biomed. Eng. 1: 0025.

Farrell, T. R. (2008). "A comparison of the effects of electrode implantation and targeting on pattern classification accuracy for prosthesis control." IEEE Transactions on Biomedical Engineering 55(9): 2198-2211.

Fitts, P. M. (1954). "The information capacity of the human motor system in controlling the amplitude of movement." J. Exp. Psych. 47(6): 381–391.

Fougner, A., O. Stavdahl, P. J. Kyberd, Y. G. Losier and P. A. Parker (2012). "Control of upper limb prosthesis: Terminology and proportional myoelectric Control—A review." IEEE Trans. Neural Sys. Rehabil. Eng. 20(5): 663–677.

Fougner, A. L., O. Stavdahl and P. J. Kyberd (2014). "System training and assessment in simultaneous proportional myoelectric prosthesis control." J. NeuroEng. Rehabil. 11:75.

Franzke, A. W., M. B. Kristoffersen, R. M. Bongers, A. Murgia, B. Pobatschnig, F. Unglaube and C. K. van der Sluis (2019). "Users' and therapists' perceptions of myoelectric multi-function upper limb prostheses with conventional and pattern recognition control." PLoS ONE 18(8): e0220899.

Gallina, A., C. Disselhorst-Klug, D. Farina, R. Merletti, M. Besomi, A. Holobar, R. M. Enoka, F. Hug, D. Falla and K. Søgaard (2022). "Consensus for experimental design in electromyography (CEDE) project: High-density surface electromyography matrix." Journal of Electromyography and Kinesiology 64: 102656.

Ganiev, A., H.-S. Shin and K.-H. Lee (2016). "Study on virtual control of a robotic arm via a myo armband for the self-manipulation of a hand amputee." Int. J. Appl. Eng. Res. 11(2): 775–782.

Gilroy, A. M., B. R. MacPherson, L. M. Ross, J. Broman and A. Josephson (2008, p. 328–336). Atlas of Anatomy. Germany, Thieme.

Giovanelli, D., B. Milosevic and E. Farella (2015). Bluetooth Low Energy for data streaming: Application-level analysis and recommendation. IEEE Adv. Sensors Interfaces, Gallipoli, Italy.

Girden, E. R. (1992). ANOVA: Repeated Measures, Sage Publications: 21.

Golkar, M. A., E. S. Tehrani and R. E. Kearney (2017). "Linear parametric varying identification of dynamic joint stiffness during time-varying voluntary contractions." Front. Comput. Neurosci. 11: 35.

Gomez, C., J. Oller and J. Paradells (2012). "Overview and evaluation of Bluetooth low energy: An emerging low-power wireless technology." Sensors 12: 11734–11753.

Gravina, R., P. Allinia, H. Ghasemzadeh and G. Fortino (2017). "Multi-sensor fusion in body sensor networks: State-of-the-art and research challenges." Info. Fus. 35: 68–80.

Gribble, P. L., L. I. Mullin, N. Cothros and A. Mattar (2003). "Role of cocontraction in arm movement acuracy." J. Neurophysiol. 89: 2396–2405.

Haartsen, J. (1998). BLUETOOTH—The universal radio interface for ad hoc, wireless connectivity. Ericsson Rev. 3: 110–117.

Hafner, B. J. and A. B. Sawers (2016). "Issues affecting the level of prosthetics research evidence: Secondary analysis of a systematic review." Prosthet. Orthot. Int. 40(1): 31–43.

Hahne, J. M., Biessmann, F., N. Jiang, H. Rehbaum, D. Farina, F. C. Meinecke, K.-R. Muller and L. C. Parra (2014). "Linear and nonlinear regression techniques for simultaneous and proportional myoelectric control." IEEE Trans. Neural Sys. Rehabil. Eng. 22(2): 269–279.

Hahne, J. M., B. Graimann and K.-R. Muller (2012). "Spatial filtering for robust myoelectric control." IEEE Trans. Biomed. Eng. 59(5): 1436–1443.

Hahne, J. M., M. Markovic and D. Farina (2017). "User adaptation in myoelectric man-machine interfaces." Sci. Reports 7: 4437.

Hahne, J. M., M. A. Schweisfurth, M. Koppe and D. Farina (2018). "Simultaneous control of multiple functions of bionic hand prostheses: Performance and robustness in end users." Sci. Robot. 3: eaat3630.

Hahne, J. M., M. A. Wilke, M. Koppe, D. Farina and A. F. Schilling (2020). "Longitudinal case study of regression-based hand prosthesis control in daily life." Front. Neurosci. 14: 600.

Harris, A., K. Katyal, M. Para and J. Thomas (2011). Revolutionizing prosthetics software technology. IEEE Int. Conf. Sys. Man Cyber.

Hashemi, J., E. Morin, P. Mousavi and K. Hashtrudi-Zaad (2013). "Surface EMG force modeling with joint angle based calibration." J Electromyogr Kinesiol 23: 416–424.

Hashemi, J., E. Morin, P. Mousavi and K. Hashtrudi-Zaad (2015). "Enhanced dynamic EMG-force estimation through calibration and PCI modeling." IEEE Trans. Neural Sys. Rehabil. Eng. 23(1): 41–50.

Hashemi, J., E. Morin, P. Mousavi, K. Mountjoy and K. Hashtrudi-Zaad (2012). "EMG-force modeling using parallel cascade identification." J. Electromyogr. Kinesiol. 22: 469–477.

Hasson, S. M., J. Williams, W. Gadberry and T. Henrich (1989). "Viewing low and high wavelength light: Effect on EMG activity and force production during maximal voluntary handgrip contraction." Physiotherapy Canada 41(1): 32-35.

Hirt, B., H. Seyhan, M. Wagner and R. Zumhasch (2017). Hand and Wrist Anatomy and Biomechanics: A Comprehensive Guide. Stuttgart, Germany, Georg Thieme Verlag.

Hof, A. L. and J. Van den Berg (1981). "EMG to force processing I: An electrical analogue of the Hill muscle model." J. Biomech. 14(11): 747–758.

Hogan, N. and R. W. Mann (1980). "Myoelectric signal processing: Optimal estimation applied to electromyography—Part I: Derivation of the optimal myoprocessor." IEEE Trans. Biomed. Eng. 27(7): 382–395.

Hogan, N. and R. W. Mann (1980). "Myoelectric signal processing: Optimal estimation applied to electromyography—Part II: Experimental demonstration of optimal myoprocessor performance." IEEE Trans. Biomed. Eng. 27(7): 396–410.

Horn, G. W. (1963). "Muscle voltage moves artificial hand." Electronics 30(41): 34.

Huang, H., P. Zhou, G. Li and T. A. Kuiken (2008). "An analysis of EMG electrode configuration for targeted muscle reinnervation based neural machine interface." IEEE Trans. Neural Sys. Rehabil. Eng. 16(1): 37–45.

Hudgins, B., P. Parker and R. N. Scott (1993). "A new strategy for multifunction myoelectric control." IEEE Trans. Biomed. Eng. 40(1): 82–94.

Hussaini, A. and P. Kyberd (2017). "Refined clothespin relocation test and assessment of motion." Prosthet. Orthot. Int. 41(3): 294–302.

Hwang, H.-J., J. M. Hahne and K.-R. Muller (2017). "Real-time robustness evaluation of regression based myoelectric control against arm position change and donning/dofing." PLoS ONE 12(11): e0186318.

Igual, C., J. Igual, J. M. Hahne and L. C. Parra (2019). "Adaptive auto-regressive proportional myoelectric control." IEEE Trans. Neural Sys. Rehabil. Eng. 27(2): 314–322.

Inman, V. T., H. J. Ralston, J. B. Saunders, B. Feinstein and E. W. Wright (1952). "Relation of human electromyogram to musculuar tension." EEG Clin. Neurophysiol. 4(2): 187–194.

Iqbal, N. V., K. Subramaniam and S. Asmi P. (2018). "A review on upper-limb myoelectric prosthetic control." IETE J. Res. 64(7): 740–752.

Iqual, C., L. A. Pardo, J. M. Hahne and J. Iqual (2019). "Myoelectric control for upper limb prostheses." Electronics 8: 1244.

Ishak, A. J., S. A. Ahmad, A. C. Soh, N. A. Naraina, R. M. R. Jusoh and W. Chikamme (2017). Design of a wireless surface EMG acquisition system. IEEE Int. Conf. Mechatron. Mach. Vis. Practice.

Ison, M. and P. Artemiadis (2015). "Proportional myoelectric control of robots: Muscle synergy development drives performance enhancement, retainment, and generalization." IEEE Trans. Robotics 31(2): 259–268.

Javaid, H. A., M. I. Tiwana, A. Alsanad, J. Iqbal, M. T. Riaz, S. Ahmad and F. A. Almisned (2021). "Classification of hand movements using MYO armband on an embedded platform." Electronics 10(11): 1322.

Jiang, L., Q. Huang, D. Yang, S. Fan and H. Liu (2018). "A novel hybrid closed-loop control approach for dexterous prosthetic hand based on myoelectric control and electrical stimulation." Indust. Robot Int. J. 45(4): 526–538.

Jiang, N., K. B. Englehart and P. A. Parker (2009). "Extracting simultaneous and proportional neural control information for multiple-DOF prostheses from the surface electromyographic signal." IEEE Trans. Biomed. Eng. 56(4): 1070–1080.

Jiang, N., H. Rehbaum, I. Vujaklija, B. Graimann and D. Farina (2014). "Intuitive, online, simultaneous, and proportional myoelectric control over two degrees-of-freedom in upper limb amputees." IEEE Trans. Neural Sys. Rehabil. Eng. 22(3): 501–510.

Jiang, N., J. L. G. Vest-Nielsen, S. Muceli and D. Farina (2012). "EMG-based simultaneous and proportional estimation of wrist/hand kinematics in uni-lateral trans-radial amputees." J. NeuroEng. Rehabil. 9:42.

Jiang, N., I. Vujaklija, H. Rehbaum, B. Graimann and D. Farina (2014). "Is accurate mapping of EMG signals on kinematics needed for precise online myoelectric control?" IEEE Trans. Neural Sys. Rehabil. Eng. 22(3): 549–558.

Johansen-Berg, H. and P. M. Matthews (2002). "Attention to movement modulates activity in sensori-motor areas, including primary motor cortex." Exp. Brain Res. 142: 13–24.

Jones, L. A. and S. J. Lederman (2006). Human Hand Function. New York, Oxford University Press, Inc.

Jonsson, S., K. Caine-Winterberger and R. Branemark (2011). "Osseointegration amputation prostheses on the upper limb: Methods, prosthetics and rehabilitation." Prosthet. Orthot. Int. 35(2): 190–200.

Kamath, S. and J. Lindh (2012). Measuring Bluetooth low energy power consumption.

Kawase, T., H. Kambara and Y. Koike (2012). "A power assist device based on joint equilibrium point estimation from EMG signals." J. Robot. Mechatron. 24(1): 205–218.

Kendell, C., E. D. Lemaire, Y. Losier, A. Wilson, A. Chan and B. Hudgins (2012). "A novel approch to surface electromyography: An exploratory study of electrode-pair selection based on signal characteristics." J. NeuroEng. Rehabil. 9: 24.

Kenney, J. F. and E. Keeping (1954). Linear regression and correlation. Mathematics of Statistics: 252–285.

Kestner, S. (2006). "Defining the relationship between prosthetic wrist function and its use in performing work tasks and activities of daily living." J. Prosthet. Orthot. 18(3): 80–86.

Khushaba, R. N., A. Al-Timemy, S. Kodagoda and K. Nazarpour (2016). "Combined influence of forearm orientation and muscular contraction on EMG pattern recognition." Exp. Sys. App. 61: 154–161.

Koirala, K., M. Dasog, P. Liu and E. A. Clancy (2015). "Using the electromyogram to anticipate torques about the elbow." IEEE Trans. Neural Sys. Rehabil. Eng. 23(3): 396–402.

Konrad, P. (2005). "The abc of emg." A practical introduction to kinesiological electromyography 1(2005): 30-35.

Kossmann, C. E., D. A. Brody, G. E. Burch, H. H. Hecht, F. D. Johnston, C. Kay, E. Lepeschkin, H. V. Pipberger, G. Baule, A. S. Berson, S. A. Briller, D. B. Geselowitz, L. G. Horan and O. Schmitt (1967). "Recommendations for standardization of leads and of specifications for instruments in electrocardiography and vectorcardiography." Circulation 35: 583–602.

Kristoffersen, M. B., A. W. Franzke, R. M. Bongers, M. Wand, A. Murgia and C. K. Van der Sluis (2021). "User training for maching learning controlled upper limb prosthesis: A serious game approach." J. NeuroEng. Rehabil. 18: 32.

Kuiken, T. A., G. Li, B. A. Lock, R. D. Lipschutz, L. A. Miller, K. A. Stubblefield and K. B. Englehart (2009). "Targeted muscle reinnervation for real-time myoelectric control of multifunction artificial arms." J. Am. Med. Assoc. 301(6): 619–628.

Kuiken, T. A., L. A. Miller, K. Turner and L. J. Hargrove (2016). "A comparisonn of pattern recognition control and direct control of a multiple degree-of-freedom transradial prosthesis." IEEE J. Trans. Eng. Health Med. 4(2100508).

Kwatny, E., D. H. Thomas and H. G. Kwatny (1970). "An application of signal processing techniques to the study of myoelectric signals." IEEE Trans. Biomed. Eng. 17(4): 303–313.

Lee, K., A. Rawley and X. Zhang (2018). Design of a Compact Electromyograph Data Acquisition System, Worcester Polytechnic Institute.

Li, K., J. Zhang, L. Wang, M. Zhang, J. Li and S. Bao (2020). "A review of the key technologies for sEMG-based human-robot interactions systems." Biomed. Sig. Proc. Control 62: 102074.

Light, C. M., P. H. Chappell and P. J. Kyberd (2002). "Establishing a standardized clinical assessment tool of pathologic and prosthetic hand function: Normative data, reliability, and validity." Arch. Phys. Med. Rehabil. 83: 776–783.

Limb Loss Task Force/Amputee Coalition (2012). Roadmap for preventing limb loss in America. Knoxville, TN.

Lin, C., B. Wang, N. Jiang and D. Farina (2018). "Robust extraction of basis functions for simultaneous and proportional myoelectric control via sparse non-negative matrix factorization." J. Neural. Eng. 5: 026017.

Lin, Z.-M., C.-H. Chang, N.-K. Chou and Y.-H. Lin (2014). Bluetooth Low Energy (BLE) based blood pressure monitoring system. IEEE Intell. Green Build. Smart Grid, Taipei, Taiwan.

Linssen, W. H., D. F. Stegeman, E. M. Joosten, R. A. Binkhorst, M. J. Merks, H. J. T. Laak and S. L. Notermans (1991). "Fatigue in type I fiber predominance: a muscle force and surface EMG study on the relative role of type I and type II muscle fibers." Muscle & Nerve: Official Journal of the American Association of Electrodiagnostic Medicine 14(9): 829-837.

Liu, M. M., W. Herzog and H. H. C. M. Savelberg (1999). "Dynamic muscle force predictions from EMG: An artificial neural network approach." J. Electromyo. Kinesiol. 9: 391–400.

Liu, P., D. R. Brown, E. A. Clancy, F. Martel and D. Rancourt (2013). "EMG-force estimation for multiple fingers." IEEE Sig. Proc. Med. Biol. Symp.

Liu, P., L. Liu and E. A. Clancy (2015). "Influence of joint angle on EMG-torque model during constant-posture, torque-varying contractions." IEEE Trans. Neural Sys. Rehabil. Eng. 23(6): 1039–1046.

Liu, P., L. Liu, F. Martel, D. Rancourt and E. A. Clancy (2013). "Influence of joint angle on EMG-torque model during constant-posture quasi-constant-torque contractions." J. Electromyo. Kinesiol. 23: 1020–1028.

Ljung, L. (1999). System Identification: Theory for the User. Upper Saddle River, NJ, Prentice-Hall: 1–8, 408–452, 491–519.

Lo Bello, L. and O. Mirabella (2006). Clock synchronization isues in Bluetooth-based industrial measurements. IEEE. Int. Wk. Factory Comm Sys.

Lovely, D. F. (2004). Signals and Signal Processing for Myoelectric Control. Powered Upper Limb Prostheses. A. Muzumdar. Berlin, Springer.

Luce, R. D. (1986, p. 209–210). Response Times: Their Role in Inferring Elementary Mental Organization, Oxford University Press.

Luh, J.-J., C. Gwo-Ching, C.-K. Cheng, J.-S. Lai and e.-S. Kuo (1999). "Isokinetic elbow joint torques estimation from surface EMG and joint kinematic data: Using an artificial neural network model." J. Electromyo. Kinesiol. 9: 173–183.

MacKenzie, I. S. (2015). Fitts' throughput and the remarkable case of touch-based target selection. Int. Conf. Human-Comp. Interact.: 238–249.

MacPhee, B. J. (2007). Examining the prosthetic function and body behavior of prosthesis users performing activities of daily living. M.S., University of New Brunswick.

Mann, R. W. (1981). "Cybernetic limb prosthesis: The ALZA distinguished lecture." Ann. Biomed. Eng. 9: 1–43.

Mao, Z.-H., H.-N. Lee, R. J. Sclabassi and M. Sun (2009). "Information capacity of the thumb and the index finger in communication." IEEE Trans. Biomed. Eng. 56(5): 1535–1545.

Maroti, M., B. Kusy, G. Simon and A. Ledeczi (2004). The flooding time synchronization protocol. Int. Conf. Embed. Net. Sensor Sys.

Marquess, K. (2010). Bluetooth core specification version 4.0. Specification of the Bluetooth System.

Marquess, K. (2014). Bluetooth core specification version 4.2. Specification of the Bluetooth system.

Marquess, K. (2016). Bluetooth core specification version 5.0. Specification of the Bluetooth system.

Mathiowetz, V., G. Volland, N. Kashman and K. Weber (1985). "Adult norms for the box and block test of manual dexterity." Am. J. Occ. Ther. 39(6): 386–391.

Mavrogenis, A., R. Dimitriou, J. Parvizi and G. C. Babis (2009). "Biology of implant osseointegration." J Musculoskelet Neuronal Interact 9(2): 61-71.

McDonald, C. L., S. Westcott-McCoy, M. R. Weaver, J. Haagsma and D. Kartin (2020). "Global prevalence of traumatic non-fatal limb amputation." Prosthet. Orthot. Int.

McGimpsey, G. and T. C. Bradford Limb prosthetics services and devices, Bioengineering Institute Center for Neuroprosthetics, Worcester Polytechnic Institute, 2008.

Meier, R. H. (2004). "History of arm amputation, prosthetic restoration, and arm amputation rehabilitation." Functional restoration of adults and children with upper extremity amputation: 1-7.

Mendez, V., F. Iberite, S. Shokur and S. Micera (2021). "Current solutions and future trends for robotic prosthetic hands." Annu. Rev. Control Robot. Auton. Sys. 4: 595–627.

Mercier, C., K. T. Reilly, C. D. Vargas, A. Aballea and A. Sirigu (2006). "Mapping phantom movement representations in the motor cortex of amputees." Brain 129(8): 2202–2210.

Merletti, R. (1999). "Standards for reporting EMG data [WWW Document]. J Electromyo Kinesiol. URL https://isek.org/wp-content/uploads/2015/05/Standards-for-Reporting-EMG-Data.pdf."

Messier, R. H., J. Duffy, H. M. Litchman, P. R. Raslay, J. F. Soechting and P. A. Stewart (1971). "The electromyogram as a measure of tension in the human biceps and triceps muscles." Int. J. Mech. Sci. 13: 585–598.

Mozaffarian, D., E. J. Benjamin, A. S. Go, D. K. Arnett, M. J. Blaha, M. Cushman, S. R. Das, S. de Ferranti, J.-P. Després, H. J. Fullerton and e. al. (2016). "Executive summary: Heart disease and stroke statistics—2016 update. A report from the American Heart Association." Circulation 133: 447–454.

Muceli, S. and D. Farina (2012). "Simultaneous and proportional estimation of hand kinematics from EMG during mirrored movements at multiple degrees-of-freedom." IEEE Trans. Neural Sys. Rehabil. Eng. 20(3): 371–378.

Muceli, S., N. Jiang and D. Farina (2010). Multichannel surface EMG based estimation of bilateral hand kinematics during movements at multiple degrees of freedom. Ann. Int. Conf. IEEE EMBS, Buenos Aires, Argentina.

Nair, K., J. Kulkarni, M. Warde, Z. Dave, V. Rawalgaonkar, G. Gore and J. Joshi (2015). Optimizing power consumption in IoT based wireless sensor networks using Bluetooth low energy. 2015 International Conference on Green Computing and Internet of Things (ICGCIoT).

Nawfel, J. L., K. B. Englehart and E. J. Scheme (2021). "A multi-variate approach to predicting myoelectric control usability." IEEE Trans. Neural Sys. Rehabil. Eng. 29: 1312–1327.

Nazarpour, K., A. Barnard and A. Jackson (2012). "Flexible cortical control of task-specific muscle synergies." J. Neurosci. 32(36): 12349–12360.

Neuman, M. R. (1998). Biopotential Amplifiers. Medical Instrumentation: Application and Design, Third Edition. J. G. Webster. New York, John Wiley & Sons, Inc.: 233–286.

Nielsen, C. C. (2002). Issues affecting the future demand for orthotists and prosthetists: Update 2002. Alexandria, VA, National Commission on Orthotic and Prosthetic Education.

Nielsen, J. L., S. Holmgaard, N. Jiang, K. B. Englehart, D. Farina and P. Parker (2011). "Simultaneous and proportional force estimation for multifunction myoelectric prostheses using mirrored bilateral training." IEEE Trans. Biomed. Eng. 58(3): 681–688.

Noble, J. W., J. J. Eng and L. A. Boyd (2013). "Effect of visual feedback on brain activation during motor tasks: An fMRI study." Motor Control 17(3): 298–312.

O'Keeffe, B. (2011). "Prosthetic rehabilitation of the upper limb amputee." Indian Journal of Plastic Surgery 44(02): 246-252.

Olsson, A. E., N. Malesevic, A. Bjorkman and C. Antfolk (2021). "Learning regularized representations of categorically labelled surface EMG enables simultaneous and proportional myoelectric control." J. NeuroEng. Rehabil. 18(35).

Omre, A. H. and S. Keeping (2010). "Bluetooth low energy: Wireless connectivity for medical monitoring." J. Diabetes Sci. Technol. 4(2): 457–463.

Ortiz-Catalan, M., F. Rouhani, R. Branemark and B. Hakansson (2015). Offline accuracy: A potentially misleading metric in myoelectric pattern recognition for prosthetic control. IEEE EMBS Conf. : 1140–1143.

Oskouei, H. A., M. G. Paulin and A. B. Carman (2013). "Intra-session and inter-day reliability of forearm surface EMG during varying hand grip forces." J. Electromyo. Kinesiol. 23: 216–222.

Pahlavan, K. and P. Krishnamurthy (2009). Networking Fundamentals: Wide, Local and Personal Area Communications. Chichester, United Kingdom, John Wiley & Sons, Ltd.: 465–470.

Pahlavan, K. and P. Krishnamurthy (2013). Principles of Wireless Access and Localization. Chichester, United Kingdom, John Wiley & Sons, Ltd.: 100–107.

Pantelopoulos, A. and N. G. Bourbakis (2010). "A survey on wearable sensor-based systems for health monitoring and prognosis." IEEE Trans. Sys. Man Cyber. C 40(1): 1–12.

Parithimarkalaignan, S. and T. Padmanabhan (2013). "Osseointegration: an update." The Journal of Indian Prosthodontic Society 13(1): 2-6.

Parker, P., K. Englehart and B. Hudgins (2006). "Myoelectric signal processing for control of powered limb prostheses." J. Electromyo. Kinesiol. 16: 541–548.

Parker, P. A., J. A. Stuller and R. N. Scott (1977). "Signal processing for the multistate myoelectric channel." Proc. IEEE 65(5): 662–674.

Peerdeman, B., D. Boere, H. Witteveen, R. Huis in 't Veld, H. Hermens, S. Stramigioli, H. Rietman, P. Veltink and S. Misra (2011). "Myoelectric forearm prosthesis: State of the art from a user-centered perspective." J. Rehabil. Res. Devel. 48(6): 719–738.

Petri, R. P. and E. Aguila (2002). "The military upper extremity amputee." Physical Medicine and Rehabilitation Clinics 13(1): 17-43.

Piazza, C., M. Rossi, M. G. Catalano, A. Bicchi and L. J. Hargrove (2020). "Evaluation of a simultaneous myoelectric control strategy for a multi-DoF transradial prosthesis." IEEE Trans. Neural Sys. Rehabil. Eng. 28(10): 2286–2295.

Popat, R. A., D. E. Drebs, J. Mansfield, D. Russell, E. Clancy, K. M. Gill-Body and N. Hogan (1993). "Quantitative assessment of four men using above-elbow prosthetic control." Arch. Phys. Med. Rehabil. 74: 720–729.

Popovic, M. B. (2003). "Control of neural prostheses for grasping and reaching." Med. Eng. Physics 25: 41–50.

Pradhan, A., U. Kuruganti, W. Hill, N. Jiang and V. Chester (2020). Robust simultaneous and proportional myoelectric control scheme for individual with transradial amputations. Ann. Int. Conf. IEEE EMBC.

Prahm, C., A. Schulz, B. PaaBen, J. Schoisswohl, E. Kaniusas, G. Dorffner, B. Hammer and O. Aszmann (2019). "Counteracting electrode shifts in upper-limb prosthesis control via transfer learning." IEEE Trans. Neural Sys. Rehabil. Eng. 27(5): 956–962.

Press, W. H., B. P. Flannery, S. A. Teukolsky and W. T. Vetterling (1994). Numerical Recipies in C. New York, Cambridge Univ. Press: 671–681.

Rachim, V. P. and W.-Y. Chung (2016). "Wearable noncontact armband for mobile ECG monitoring system." IEEE Trans. Biomed. Circ. Sys. 10(6): 1112–1118.

Rack, P. M. H. and D. R. Westbury (1969). "The effects of length and stimulus rate on tension in the isometric cat soleus muscle." J. Physiol. 2014: 443–460.

Ramachandran, V. S. and D. Rogers-Ramachandran (1996). "Synaesthesia in phantom limbs induced with mirrors." Proc. R. Soc. Lond. B 263(1369): 377–386.

Reilly, K. T., C. Mercier, M. H. Schieber and A. Sirigu (2006). "Persistent hand motor commands in the amputees' brain." Brain 129(8): 2211–2223.

Reiter, R. (1948). "Eine neue elektrokunsthand." Grenzgebiete der Medizin 1(4): 133-135.

Resina, E. G. (2020). Design of a Wireless EMG Simulator for the Testing of EMG Acquisition Devices. B.S., Universitat Pompeu Fabra.

Rheinlander, C. C. and N. Wehn (2016). Precise synchronization time stamp generation for Bluetooth low energy. IEEE Sensors.

Richards, M. (2015). Software architecture patterns, O'Reilly Media, Incorporated 1005 Gravenstein Highway North, Sebastopol, CA ….

Robertson, D. G. E., G. E. Caldwell, J. Hamill, G. Kamen and S. Whittlesey (2013). Research methods in biomechanics, Human kinetics.

Robertson, D. G. E. and J. J. Dowling (2003). "Design and responses of Butterworth and critically damped digital filters." J. Electromyo. Kinesiol. 13: 569–573.

Roche, A. D., B. Lakey, I. Mendez, I. Vujaklija, D. Farina and O. C. Aszmann (2019). "Clinical perspectives in upper lmib prostheses: An update." Curr. Surg. Rep. 7(5).

Rojas-Martinez, M., M. A. Mananas and J. F. Alonso (2012). "High-density surface EMG maps from upper-arm and forearm muscles." J. NeuroEng. Rehabil. 9(85).

Ross, M. P. (2005). Development of a quantitative test for prosthetic function using motion analysis and activities of daily living. M.S.

Rossi, M., A. O. Khouia, L. Lorenzelli and D. Brunelli (2016). Energy neutral 32-channel embedded readout system for IoT-ready fitness equipments. IEEE Sensors Appl. Symp., Catania, Italy.

Scheme, E., B. Lock, L. Hargrove, W. Hill, U. Kuruganti and K. Englehart (2014). "Motion normalized proportional control for improved pattern recognition-based myoelectric control." IEEE Trans. Neural Sys. Rehabil. Eng. 22(1): 149–157.

Schieber, M. H. (2001). "Constraints on somatotopic organization in the primary motor cortex." Journal of neurophysiology 86(5): 2125-2143.

Shakya, H. and S. Sharma (2019). Analysis of neck muscle fatigue during cervical traction treatment using wireless EMG sensor. Smart Computational Strategies: Theoretical and Practical Aspects. A. K. Luhach, K. B. G. Hawari, I. C. Mihai, P. A. Hsiung and R. B. Mishra. Singapore, Springer.

Sharma, P., X. Hui, J. Zhou, T. B. Conroy and E. C. Kan (2020). "Wearable radio-frequency sensing of respiratory rate, respiratory volume, and heart rate." Digital Med. 3: 98.

Sherman, E. D. (1964). "A Russian bioelectric-controlled prosthesis: Report of a research team from the Rehabilitation Institute of Montreal." Canad. Med. Ann. J. 91: 1268–1270.

Sichitiu, M. L. and C. Veerarittiphan (2003). Simple, accurate time synchronization for wireless sensor networks. IEEE WCNC.

Simeone, O. and U. Spagnolini (2007). "Distributed time synchronizatin in wireless snesor networks with coupled discrete-time oscillators." EURASIP J. Wire. Comm. Net. 2007: 57054.

Simon, A. M. and L. J. Hargrove (2011). A comparison of the effects of majority vote and a decision-based velocity ramp on real-time pattern recognition control. Ann. Int. Conf. IEEE EMBS.

Simon, A. M., L. J. Hargrove, B. A. Lock and T. A. Kuiken (2011). "Target achievement control test: Evaluating real-time myoelectric pattern-recognition control of multifunctional upper-limb prostheses." J. Rehabil. Res. Devel. 48(6): 619–628.

Smith, L. H., T. A. Kuiken and L. J. Hargrove (2016). "Evaluation of linear regression simultaneous myoelectric control using intramuscular EMG." IEEE Trans. Biomed. Eng. 63(4): 737–746.

Smith, R. J., F. Tenore, D. Huberdeau, R. Etienne-Cummings and N. V. Thakor (2008). "Continuous decoding of finger position from surface EMG signals for the control of powered prostheses." Ann. Int. Conf. IEEE EMBS: 197–200.

Soares, A., A. Andrade, E. Lamounier and R. Carrijo (2003). "The development of a virtual myoelectric prosthesis controlled by an EMG pattern recognition system based on neural networks." J. Intel. Info. Sys. 21(2): 127–141.

Šolić, P., A. Leoni, R. Colella, T. Perković, L. Catarinucci and V. Stornelli (2020). "IoT-ready energy-autonomous parking sensor device." IEEE Internet of Things Journal 8(6): 4830-4840.

Solomonow, M., A. Guzzi, R. Baratta, H. Shoji and R. D'Ambrosia (1986). "EMG-force model of the elbows antagonistic muscle pair." Am. J. Phys. Med. 65(5): 223–244.

Soukoreff, R. W. and I. S. MacKenzie (2004). "Towards a standard for pointing device evaluation, perspectives on 27 years of Fitts' law research in HCI." Int. J. Human-Comp. Studies 61(751–789).

Sridhar, S., P. Misra, G. S. Gill and J. Warrior (2016). "CheepSync: A time synchronization service for resource constrained Bluetooth LE advertisers." IEEE Comm. Mag. 54(1): 136–143.

Staudenmann, D., K. Roeleveld, D. F. Stegeman and J. H. van Dieen (2010). "Methodological aspects of EMG recordings for force estimation—A tutorial and review." J Electromyogr Kinesiol 20: 375–387.

Sturma, A., L. A. Hruby, C. Prahm, J. A. Mayer and O. Aszmann (2018). "Rehabilitation of upper extremity nerve injuries using surface EMG biofeedback: Protocols for clinical application." Front. Neurosci. 12: 906.

Sundararaman, B., U. Buy and A. D. Kshemkalyani (2005). "Clock synchronization for wireless sensor netwoks: A survey." Ad Hoc Net. 3: 281–323.

Swinnen, S. P. (2002). "Intermanual coordination: From behavioral principles to neural-netwok interactions." Nature Rev. 3: 350–361.

Tabor, A., S. Bateman and E. Scheme (2018). "Evaluation of myoelectric control learning using multi-session game-based training." IEEE Trans. Neural Sys. Rehabil. Eng. 26(9): 1680–1688.

Teh, Y. and L. J. Hargrove (2020). Offline repeatability correlates with real-time performance of pattern recognition controllers. Int. Conf. NeuroRehabil.

Teh, Y. and L. J. Hargrove (2020). "Understanding limb position and external load effects on real-time pattern recognition control in amputees." IEEE Trans. Neural Sys. Rehabil. Eng. 28(7): 1605–1613.

Tirado-Andres, F. and A. Araujo (2019). "Performance of clock sources and their influence on time synchronization in wireless sensor networks." Int. J. Distrib. Sens. Net. 15(9).

Toledo-Perez, D. C., J. Rodriguez_Resendiz, R. A. Gomez-Loenzo and J. C. Jauregui-Correa (2019). "Support vector machine-based EMG signal classifcation techniques: A review." Appl. Sci. 9: 4402.

Tosi, J., F. Taffoni, M. Santacatterina, R. Sannino and D. Formica (2017). "Performance evaluation of Bluetooth low energy: A systematic review." Sensors 17: 2898.

Tosi, J., F. Taffoni, M. Santacatterina, R. Sannino and D. Formica (2019). "Throughput analysis of BLE sensor network for motion tracking of human movements." IEEE Sensors J. 19(1): 370–377.

Urbanek, H. and P. van de Smagt (2016). "iEMG: Imaging electromyography." J. Electromyo. Kinesiol. 27: 1–9.

Vidovic, M. M.-C., H.-J. Hwang, S. Amsuss, J. M. Hahne, D. Farina and K.-R. Muller (2016). "Improving the robustness of myoelectric pattern recognition for upper limb prostheses by covariate shift adaptation." IEEE Trans. Neural Sys. Rehabil. Eng. 24(9): 961–970.

Vredenbregt, J. and G. Rau (1973). "Surface electromyography in relation to force, muscle length and endurance." New Developments Electromyogr. Clin. Neurophysiol. 1: 607–622.

Vujaklija, I., D. Farina and O. C. Aszmann (2016). "New developments in prosthetic arm systems." Ortho. Res. Rev. 8: 31–39.

Wang, C., L. Jiang, C. Guo, Q. Huang, B. Yang and H. Liu (2017). sEMG-based estimation of human arm force using regression model. IEEE Int. Conf. Robot. Biomim.

Wang, H., K. J. Rajotte, H. Wang, C. Dai, Z. Zhu, M. Bhuiyan, X. Huang and E. A. Clancy (2019). "Optimal estimation of EMG standard deviation (EMGσ) in additive measurement noise: Model-based derivations and their implications." IEEE Trans. Neural Sys. Rehabil. Eng. 27(12): 2328–2335.

Wang, H., K. J. Rajotte, H. Wang, C. Dai, Z. Zhu, X. huang and E. A. Clancy (2021). "Simplified optimal estimation of time-varying electromyogram standard deviation (EMGσ): Evaluation on two data sets." Sensors 21(15): 5165.

Wang, Q., X. Chai, Y. Wang, D. Liu, M. Chen, Y. Li, X. Liu and O. Bai (2017). A high data rate, multi-nodes wireless personal-area sensor network for real-time data acquisition and control. Elec. Instru. Info. Sys., Harbin, China.

Wang, Z., Y. Fang, D. Zhou, K. Li, C. Cointet and H. Liu (2020). "Ultrasonography and electromyography based hand motion intention recognition for a trans-radial amputee: A case study." Med. Eng. Physics 75: 45–48.

Weiergraber, M., A. Papazoglou, K. Broich and R. Muller (2016). "Sampling rate, signal bandwidth and related pitfalls in EEG analysis." J. Neurosci. Meth. 268: 53–55.

Williams III, T. W. (1990). "Practical methods for controlling powered upper-extremity prostheses." Assist. Technol. 2: 3–18.

Winter, D. A. (2009, pp. 250–280). Biomechanics and Motor Control of Human Movement. New Jersey, John Wiley & Sons, Inc.

Winter, D. A. and H. J. Yack (1987). "EMG profiles during normal human walking: Stride-to-stride and inter-subject variability." Electroenceph Clin Neurophysiol 67: 402–411.

Xing, K., P. Yang, J. Huang, Y. Wang and Q. Zhu (2014). "A real-time EMG pattern recognition method for virtual myoelectric hand control." Neurocomputing 136: 345–355.

Youn, W. and J. Kim (2009). Development of a compact-size and wireless surface EMG measurement system. IEEE ICROS-SICE, Japan.

Zhang, M., W. Xia and L. Shen (2014). Bluetooth Low Energy based motion sensing system. IEEE Wireless Comm. Sig. Proc.

Zhou, J., P. Sharma, X. Hui and E. C. Kan (2021). "A wireless wearable RF sensor for brumation study of chelonians." IEEE J. Electromag. RF Micro. Med. Biol. 5(1): 17–24.

Zhu, Z., J. Li, W. J. Boyd, C. Martinez-Luna, C. Dai, H. Wang, H. Wang, X. Huang, T. R. Farrell and E. A. Clancy (2022). "Myoelectric control performance of two degree of freedom hand-wrist prosthesis by able-bodied and limb-absent subjects." IEEE Trans. Neural Sys. Rehabil. Eng. 30: 893–904.

Zhu, Z., C. Martinez-Luna, J. Li, B. E. McDonald, C. Dai, X. Huang, T. R. Farrell and E. A. Clancy (2020). "EMG-force and EMG-target models during force-varying bilateral hand-wrist contraction in able-bodied and limb-absent subjects." IEEE Trans. Neural Sys. Rehabil. Eng. 28(12): 3040–3050.

Ziegler-Graham, K., E. J. MacKenzie, P. L. Ephraim, T. G. Travison and R. Brookmeyer (2008). "Estimating the prevalence of limb loss in the United States: 2005 to 2050." Arch. Phys. Med. Rehabil. 89: 422–429.

Zuo, K. J. and J. L. Olson (2014). "The evolution of functional hand replacement: From iron prostheses to hand transplantation." Plastic Surgery 22(1): 44-51.